NASA Conference Publication 2502

Joint University Program for Air Transportation Research—1986

Proceedings of a conference held at
Langley Research Center
Hampton, Virginia
January 8-9, 1987

NASA

NASA Conference Publication 2502

Joint University Program for Air Transportation Research—1986

Compiled by
Frederick R. Morrell
Langley Research Center
Hampton, Virginia

Proceedings of a conference sponsored by
the National Aeronautics and Space Administration
and the Federal Aviation Administration and held at
Langley Research Center
January 8–9, 1987

National Aeronautics
and Space Administration

**Scientific and Technical
Information Division**

1988

PREFACE

The Joint University Program for Air Transportation Research is a coordinated set of three grants sponsored by NASA Langley Research Center and the Federal Aviation Administration, one each with Massachusetts Institute of Technology (NGL-22-009-640), Ohio University (NGR-36-009-017), and Princeton University (NGL-31-001-252). The major goal of the Joint University Program is to develop an air transportation system on a national basis. The continued development of the national airspace system requires advanced technology from a variety of disciplines, especially in the areas of computer science, guidance and control theory and practice, aircraft performance, flight dynamics, and applied experimental psychology. Solutions to such large-scale problems can come only when creative, well-trained individuals identify and attempt to solve these problems by using a multidisciplinary approach and when they communicate these results to decision makers. The Joint University Program was created to provide new methods for interdisciplinary education to develop research workers to solve these problems. The research grants that were instituted in 1971 with the Massachusetts Institute of Technology (MIT), Ohio University, and Princeton University build on the strengths of each institution to satisfy aeronautical goals consistent with the interests of both NASA and the Federal Aviation Administration (FAA).

An important feature of this program is the quarterly review held at each of the schools and at a NASA or FAA facility. The 1986 review was held at the NASA Langley Research Center, Hampton, Virginia, January 8 to 9, 1987. At these reviews the program participants, both graduate and undergraduate, have an opportunity to present their research activities to their peers, to professors, and to invited guests from government and industry.

This conference publication represents the seventh in a series of yearly summaries of the program. (The 1985 summary appears in NASA CP-2453.) Most of the material is the effort of the students supported by the research grants.

Three types of contributions are included in this publication. Completed works are represented by full technical papers. Research previously in the open literature (for example, theses or journal articles) is presented in an annotated bibliography. Status reports of ongoing research are represented by copies of viewgraphs augmented with a brief descriptive text.

Use of trade names of manufacturers in this report does not constitute an official endorsement of such products or manufacturers, either expressed or implied, by the National Aeronautics and Space Administration or the Federal Aviation Administration.

Frederick R. Morrell
NASA Langley Research Center

CONTENTS

MASSACHUSETTS INSTITUE OF TECHNOLOGY

INVESTIGATION OF AIR TRANSPORTATION TECHNOLOGY AT MASSACHUSETTS INSTITUTE OF TECHNOLOGY, 1986

Robert W. Simpson
Director, Flight Transportation Laboratory
Cambridge, Massachusetts

INTRODUCTION

There were three areas of research sponsored in the Flight Transportation Laboratory at the Massachusetts Institute of Technology under the Joint University Research Program during 1986. The first was the completion of efforts investigating the possibility of using Loran-C for final approach guidance to a runway; the second is a preliminary exploration of the application of automated speech recognition in Air Traffic Control; the third is a continuation of a series of research topics into aircraft icing problems.

1. APPROACH GUIDANCE TO A RUNWAY USING LORAN-C

This work was aimed at exploring the possibility of flying a pseudo-precision approach using an altimeter-aided display system to provide both cross-track and vertical deviations from the approach centerline and glide path. An experimental flight test system was designed for Grumman Tiger aircraft using a King Radio KEAO-346 electric altimeter to provide data on current altitude and a Micrologic ML-3000 Loran-C receiver to provide (x, y, h_o) data relative to the runway touchdown point. (x = longitudinal distance, y = distance from centerline, h_o = nominal glide slope height at x.) An electronic display system was built to give a cross-pointer display to the pilot given continuous inputs from the Loran-C and the altimeter. Several flight tests were flown (at Hanscom Field, Bedford, Mass.), which unfortunately suffered from a number of deficiencies due to tracking dynamics arising from the slow update rate from the current Loran-C receiver. However, approaches were successfully flown, and the feasibility of using the Loran-C data to define the vertical guidance was demonstrated. Comparative data between the ILS guidance and the Loran-C plus altitude guidance was obtained. A complete description of this work is given in Reference 1 of the Annotated Bibliography.

For the second year in a row, an MIT thesis based on Loran-C research won the W.E. Jackson award for "best student thesis" from the Radio Technical Commission for Aeronautics. This year's thesis was written by Norry Dogan, and is available as MIT FTL Report 86-3 (ref. 1).

2. AUTOMATED SPEECH RECOGNITION IN AIR TRAFFIC CONTROL

The basic goal of this work has been to apply existing ASR technology in an ATC environment in order to explore not only some of the potential benefits and problems arising from the practical application of ASR, but also the features and capabilities desirable in an ASR system to be used in ATC (ref. 2).

This basic goal was accomplished by integrating a VOTAN VPC2000 continuous speech recognition system into an existing ATC simulation to provide a means whereby verbal commands issued by controllers and directed towards aircraft could be entered into the computer directly, thereby eliminating the need for blip drivers or pseudo-pilots.

In general, the potential benefits accrued through the use of ASR in an ATC environment involve the simplification of the controller-computer interface in an environment where the primary means of communication is verbal and the use of and reliance on computers is increasing significantly, both in the air and on the ground.

The major difficulties, however, lie predominantly in the handling of errors. In order to address the problem of recognition errors, the syntax for ATC commands was incorporated into a Speech Input Parser in two basic ways. The first utilized a Finite State Machine approach for syntax specification and required active intervention on the part of the user in order to correct any errors once they were detected. The second, however, used a pattern-matching approach to compare the input command to a list of allowable commands in order to determine the best match, and could hypothesize possible corrections if any errors were detected, as long as these did not critically affect the intelligibility of the commanded action.

The user-based techniques developed for correction of recognition errors consisted of utilizing the verbal channel in order to enter specific keywords that would either delete the last recognized word or delete the entire recognized command so far. These were found to be lacking in terms of speed, flexibility and ease of use, and from the fact that errors could even be made in recognizing these keywords.

The automated techniques developed to correct for recognition errors internally were limited by the capabilities of, and information made available by, the VPC system. In many cases, even though they were successful in hypothesizing the location of these errors, there was no capability to reanalyze the data and validate these hypotheses. As such, these automated techniques were more proof of concept vehicles than implementable strategies (at least with the current configuration of the VPC).

The major drawbacks of the VPC system were its sensitivity to variations in articulation (co-articulation, intonation) and its inability to rewind data in order to reexamine sections of speech data. The former is for the most part inherent in the particular recognition algorithm and technique being used and could not readily be changed. The latter, however, is a result of the actual packaging of the software. This problem has been addressed with a new software package (a library of user-callable C-language subroutines to control the recognition functions) recently made available. There are, however, still some limitations in the capability of the VPC that have not been addressed. In particular, the inability to obtain a ranking, including scores, of how well each of the words in the active vocabulary matched the current input, as well as a pointer to the location in the speech data where each of these words ends and the next word would therefore begin.

This research will be continuing in order to develop a highly reliable method of using voice to communicate to an ATC simulation or a future automated ATC system.

3. AIRCRAFT ICING RESEARCH

The aircraft icing effort over the past year has concentrated on utilizing ultrasonic ice accretion measurement techniques in wind tunnel and flight tests to better understand the ice accretion process, particularly in the glaze (wet) ice regime. Application of the ultrasonic techniques has led to previously unrealizable measurements of heat transfer from ice surfaces during accretion. These measurements have identified fundamental differences in the heat transfer and resulting ice growth, between icing wind tunnel and flight icing conditions. These differences appear to be due to relatively high ambient turbulence levels in ground icing test facilities, which tend to increase the convective heat transfer from the icing surface.

An array of ultrasonic transducers has also been flown on the leading edge of a wing cuff mounted on the NASA Icing Research Aircraft (Twin Otter). The ultrasonic array provided a unique record of the temporal and spatial behavior of the ice accretions. This is important to ice accretion modeling efforts, which rely on time-iterative techniques to generate the predicted ice accretion. In addition, plans exist to test the array-equipped wing cuff in the Icing Research Tunnel to provide a direct comparison between flight, wind tunnel, and analytical aircraft icing test techniques. Two recent papers describing this work in more detail are appended to this report (refs. 3 and 4).

The future efforts in this area will concentrate on the small-scale physics which control the surface roughness, and the resulting convective heat transfer from the ice surface. This area has been clearly identified as the prime region of uncertainty in the current understanding of the ice accretion process. The effort will combine analysis and focused experiments to identify the physical mechanisms which control the microscale roughness on an accreting ice surface.

ANNOTATED BIBLIOGRAPHY

1. Dogan, Norry: Final Approach Guidance Using an Altimeter-Aided Loran-C Display System. MIT FTL Report R86-3, Flight Transportation Laboratory, MIT, Cambridge, MA 02139, May 1986.

2. Trikas, Thanassis: Automated Speech Recognition in Air Traffic Control. MIT FTL Report R87-2, Flight Transportation Laboratory, MIT, Cambridge, MA 02139, May 1987.

3. Kirby, Mark S., and Hansman, R. John: Experimental Measurements of Heat Transfer from an Iced Surface during Artificial and Natural Cloud Icing Conditions. AIAA Paper 87-0178.

4. Hansman, R. John, Kirby, Mark S., McKnight, Robert C., and Haines, Robert L.: In-Flight Measurement of Ice Growth on an Airfoil using an Array of Ultrasonic Transducers, AIAA Paper 86-1352.

IN-FLIGHT MEASUREMENT OF ICE GROWTH ON AN AIRFOIL USING AN ARRAY OF ULTRASONIC TRANSDUCERS#

R. John Hansman, Jr.* and Mark S. Kirby+
Massachusetts Institute of Technology
Cambridge, Mass.

Robert C. McKnight**
NASA Lewis Research Center
Cleveland, Ohio

Robert L. Humes++
Calspan Corporation
Arnold Air Force Station, Tenn.

Abstract

Results of preliminary tests to measure ice growth on an airfoil during flight icing conditions are presented. Ultrasonic pulse-echo measurements of ice thickness are obtained from an array of eight ultrasonic transducers mounted flush with the leading edge of the airfoil. These thickness measurements are used to document the evolution of the ice shape during the encounter in the form of successive ice profiles.

Results from three research flights are presented and discussed. The accuracy of the ultrasonic thickness measurements is found to be within 0.5 mm of mechanical and stereo photograph measurements of the ice accretion. Ultrasonic measurements show that the ice growth rate is typically not constant, but varies during the flight. For dry ice growth, these variations in the ice growth rate are primarily due to fluctuations in the cloud liquid water content. The experimentally measured ice growth profiles are compared with ice growth predicted by an analytical icing code. Discrepancies between these analytical predictions and experimental results highlight the need for a better understanding of the physics of wet ice growth and the effects of varying icing conditions.

Introduction

Aircraft icing is a dynamic process. Ice accreting on a surface alters the aerodynamic flowfield over the surface, changing both the cloud droplet trajectories and the heat transfer from the surface. Since both the cloud droplet trajectories and the local heat transfer control the resulting ice shape, the dynamic nature of the icing process must be considered if accurate icing models and scaling laws are to be developed.

Two distinct icing regimes, "dry" and "wet" ice growth, have been identified. During dry ice growth the impinging droplets freeze on impact, and the ice surface is dry. Dry, or rime ice growth is characteristic of cold cloud temperatures, and low to moderate cloud liquid water contents. If the heat transfer from the accreting surface is insufficient to freeze the impinging cloud droplets, liquid will form locally on the surface, and the ice growth is said to be wet. Wet, or glaze ice growth is typically encountered at warm cloud temperatures close to freezing, and moderate to high cloud liquid water contents.

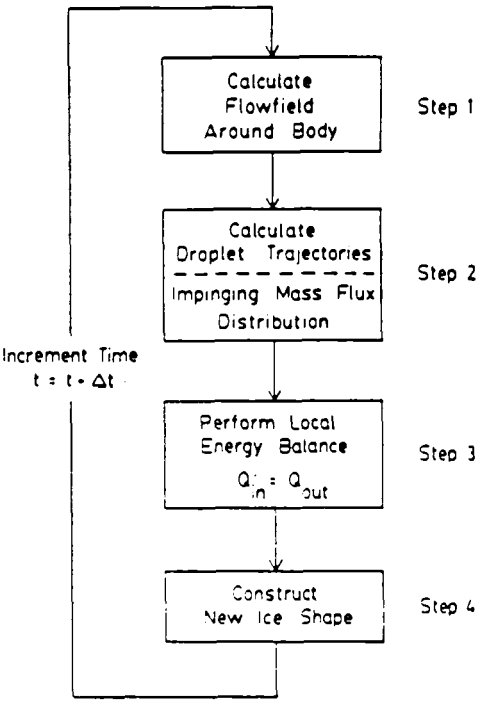

Fig. 1 Schematic breakdown of typical analytical icing model calculations.

Current analytical icing models[1-4] typically divide the icing analysis into four main areas, as shown in the block diagram in figure 1. First, the flowfield around the surface is computed; the droplet trajectories within the flowfield are then calculated by integrating the droplet equations of motion. This second calculation provides the mass flux distribution (due to the droplets) over the body. The third step involves calculating the heat transfer distribution over the surface and then performing a local energy balance to determine the

---

* Assistant Professor, Aeronautics and Astronautics.
\+ Research Assistant, Aeronautics and Astronautics.
** Pilot and Aerospace Engineer.
++ Research Engineer.

AIAA Paper 87-0178.

amount of ice formed. The final step is to construct the new ice shape. By repeating this series of calculations, using the iced geometry for the new flowfield calculation, the dynamic nature of the icing process is analytically simulated.

For dry ice growth conditions, the ice shapes predicted using these analytical models are generally in good agreement with those observed experimentally[1-4]. However for wet or glaze ice conditions, the analytically predicted ice shapes are often in poor agreement with experimental results[1,4]. The reasons for this poor agreement are not certain, although the energy balance used by the analytical models has recently received much attention[5]. A better understanding of the ice accretion process has, however, been hampered by a lack of experimental data on ice growth as a function of time.

Experimentally measured ice shape "histories" would permit a detailed comparison of actual icing behaviour with that predicted analytically. Measurements of ice shape as a function of time would allow the aerodynamic factors involved in the accretion process (i.e. flowfield and droplet trajectories) to be isolated from the more complicated thermodynamic processes involved. For example, by analyzing the flowfield associated with the evolving ice shape, the significance of collection efficiency variation with changes in ice shape could be quantitatively determined. This aerodynamic feedback phenomenon, coupled with changes in the heat transfer distribution over the ice surface, are thought to be the controlling factors in the growth of the "horns" characteristic of glaze ice formations.

In addition to providing insight into the physics of the ice accretion process, experimentally measured ice growth histories would also permit a direct, quantitative comparison of the differences between ice growth in flight and wind tunnel icing tests. A better understanding of these differences is essential for the accurate interpretation and application of icing wind tunnel results[6].

Measurement of ice growth in icing conditions is difficult. Most current ice accretion instruments relate ice growth on an exposed probe to that on the surface of interest. While these probe-type measurements can provide good time resolution of the icing rate, they cannot provide good spatial resolution of the ice accretion on the remote surface (due to differences in the collection efficiencies and heat transfer distributions for the probe and the surface). Alternatively, mechanical or photographic measurements of the ice accretion can be made at the completion of an icing test. While these "end-point" measurements provide excellent spatial resolution of the accretion, they contain no information about the growth of the ice shape prior to the measurement. Since it is not practical to frequently halt an icing encounter in order to make mechanical or photographic measurements, good time resolution of ice growth is not possible with these types of measurements.

Recently developed ultrasonic techniques for ice thickness measurement[7,8] offer the potential for both good time resolution of ice growth as well as good spatial information on the accreted ice shape. The principle of ultrasonic pulse-echo thickness measurement is explained below, and the ultrasonic array approach used to measure ice growth is then outlined.

Ultrasonic Pulse-Echo Thickness Measurement

Ultrasonic pulse-echo measurement of ice thickness on a surface is accomplished by emitting a brief compressive wave, or pulse, from a small ultrasonic transducer mounted flush with the accreting surface (see figure 2). The pulse travels through the ice, is reflected at the ice surface and then returns to the transducer as an echo signal. The time elapsed, T_{p-e}, between the emission of the pulse and the return of the echo from the ice surface can then be used to calculate the ice thickness, D, from the formula:

$$D = C \cdot T_{p-e}/2 \qquad (1)$$

Where C is the speed of propagation of the pulse-echo signal in ice. In a previous study[7], the authors found this speed of propagation to be insensitive to different types of ice (glaze, rime and mixed) formed at typical flight airspeeds. A value of 3.8 mm/μs was used for the speed of sound in ice for all the results presented in this paper.

The ultrasonic pulse-echo technique also allows the presence or absence of liquid water on the ice surface to be uniquely determined by examining the time variations of the echo signals received from the ice surface[8]. This information in turn allows the type of ice growth ocurring, "wet" or "dry", to be discerned.

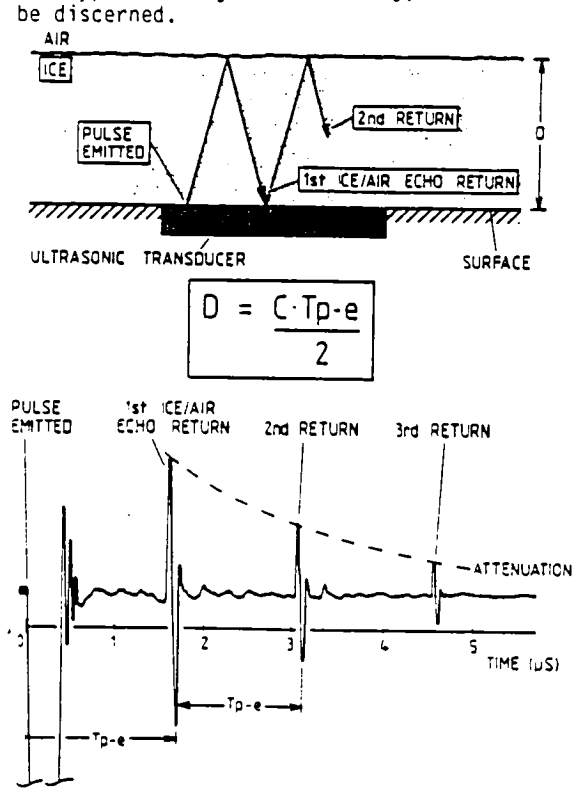

Fig. 2 Ultrasonic pulse-echo thickness measurement and typical ultrasonic pulse-echo signal in ice.

By frequently emitting pulses (typical repetition rates are several KHz), the ultrasonic pulse-echo technique can provide a direct measurement of ice thickness many times a second. If several transducers are grouped in an array, then by interpolating between the individual thickness measurements from each transducer, the ice shape over the array may be measured as a function of time. This paper describes results of preliminary tests using an array of eight ultrasonic transducers to measure ice growth on the leading edge of an airfoil during flight icing conditions. The primary purpose of these tests was to demonstrate the feasibility of using such an array to document ice growth behaviour as a function of time.

Ice growth measurements made with the ultrasonic array during three research flights are presented in this paper. Ice thickness measurements from the array transducers are used to construct profiles of the ice accretion during the icing encounter. These profiles are related to the ambient atmospheric icing conditions and are also compared with ice growth profiles predicted using an analytical icing code.

Experimental Apparatus

NASA Lewis Icing Research Aircraft & Wing Cuff Installation

The aircraft used for flight testing the ultrasonic array was the NASA Lewis Icing Research Aircraft, a De-Havilland DHC-6 Twin Otter. This aircraft is extensively equipped with instrumentation to measure and record the ambient atmospheric icing conditions encountered in flight[9]. The ultrasonic array was installed in a four foot long DHC-6 airfoil section mounted over the starboard wing of the aircraft at approximately the 3/4 span station (see figure 3). This airfoil section, or wing cuff, protruded approximately three inches forward of the main wing. The wing cuff was constructed of aluminum 0.025" thick, and was not equipped with any ice protection system.

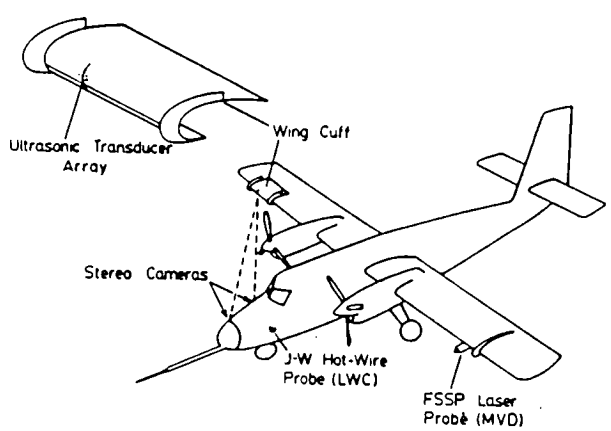

Fig. 3 Wing cuff and ultrasonic array installation on NASA Lewis Icing Research Aircraft (DHC-6 Twin Otter).

Ultrasonic Array

The array consisted of eight identical 5 MHz ultrasonic transducers mounted flush with the wing cuff surface. The transducers were all located within a 90 degree arc around the leading edge of the wing cuff. The transducer positioning was based on previous stereo photograph measurements of ice formations on the leading edge of the research aircraft[10,11]. Due to size constraints only six of the transducers could be placed at the same span station, and two additional transducers were slightly offset (0.75") to provide better ice surface coverage. The eight transducers were of the broadband, heavily damped type, with element diameters of 0.25". The transducers were mechanically supported in the cuff by a thin doubler plate behind the cuff skin.

Multiplexing Pulser/Receiver

A multiplexing pulser/receiver unit was used to sequentially excite each transducer in the array (see figure 4). The pulser/receiver section provided the electrical signals necessary to produce the ultrasonic pulse and amplify the return echo, with the multiplexer controlling the active time for each transducer. Typically, the multiplexing rate was set so that each transducer was active for approximately two seconds; four complete "scans" of the array were thus obtained every minute. Eight 40 foot long co-axial cables carried the electrical signals from the wing cuff array to the multiplexing pulser/receiver in the aircraft cabin.

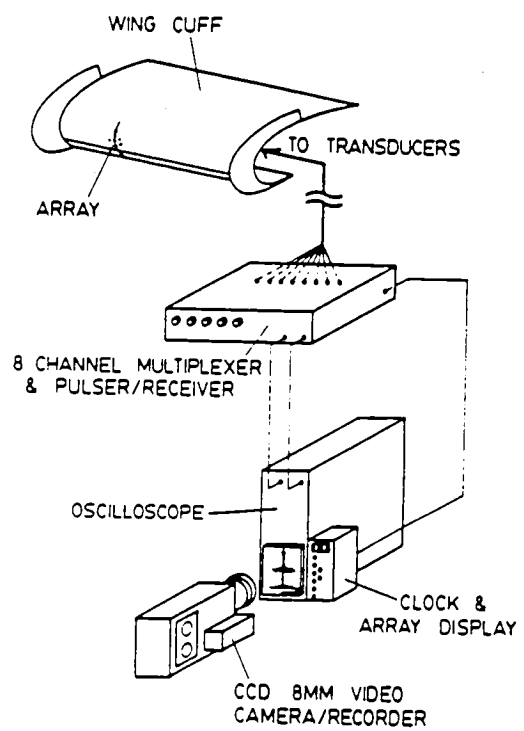

Fig. 4 Schematic of ultrasonic array equipment configuration.

Oscilloscope/Video Camera

A 60 MHz bandwidth oscilloscope was used to display the ultrasonic echo signal from the active transducer. In order to provide a permanent record of these time-dependent echoes, the oscilloscope display was filmed by a video camera (figure 4). Also within the camera's field of view were an electronic clock and an LED display, enabling the exposure time and active transducer to be simultaneously recorded with the pulse-echo trace from the oscilloscope display.

Stereo Camera System

Two 70mm cameras mounted in the nose of the aircraft (see figure 3) were used to photograph the ice accretion on the wing cuff. These photographs were later photogrammetrically analyzed to obtain a profile of the ice shape (a detailed description of the stereo camera system and the associated image analysis is contained in reference 12). The ice surface can typically be resolved to within +/- 0.03 in. from these stereo image pairs. However adequate photographs of the ice accretion can only be obtained when the aircraft is in clear air, and hence the stereo camera system cannot provide ice growth data while the aircraft is in the icing cloud.

Procedure

Since the wing cuff was exposed throughout each flight, the ultrasonic array system was activated from take-off to landing. The multiplexing rate on the pulser/receiver was typically adjusted to allow four complete scans of the array per minute. This multiplexing rate provided frequent ice thickness measurements from each transducer, while still enabling time variations in each echo signal to be observed. As discussed earlier, time variations in the echo signal are used to distinguish the presence of liquid water on the ice surface, and hence to determine if the ice growth is wet or dry.

The ambient icing conditions (temperature, cloud liquid water content, droplet size distribution etc.) were recorded throughout each flight by the aircraft's on-board icing instrumentation. Stereo photograph pairs of the iced wing cuff were also taken during each encounter. However since these photographs could only be obtained outside the icing cloud, the time interval between successive photographs was generally long (10-30 minutes). Typically one or two stereo photograph pairs were taken per encounter.

Since the wing cuff was not de-iced, it was usually possible to mechanically measure the final ice shape (using vernier calipers) after landing. Nine research flights were conducted with the ultrasonic array system between February and March 1986.

Results

Ice growth measurements for three research flights (86-31, 86-32 and 86-33) are presented in this section. Table 1 summarizes the time-averaged icing conditions during each of the three flights.

Flight 86-31

Figure 5 illustrates the final ice shape accreted on the wing cuff at the completion of flight 86-31. Three separate measurements of the final ice profile are shown. The open circles represent thickness readings obtained from the stereo photograph analysis, while the crosses indicate measurements made with vernier calipers after landing. The final ultrasonic ice thickness measurements (from transducers C,D,E and F) are shown as a solid line on the figure. The agreement between all three of these independent measurements is within 0.5 mm, with a final ice thickness of approximately 9 mm indicated. The accretion rate throughout the hour long encounter was low (due to the low cloud liquid water content), and as a result the final accretion is only moderately thick. The relatively large droplet sizes encountered, however, resulted in wide droplet impingement limits and hence the final accretion extends over most of the leading edge.

Due to the cold temperature and low liquid water contents encountered (see Table 1), dry or rime ice growth was observed throughout flight 86-31. Under these conditions, the impinging cloud droplets freeze on impact, and the final ice shape is seen to have a profile similar to that of the leading edge, and does not display the horns characteristic of glaze ice growth. This type of conformal ice shape is typical of moderate thickness rime ice accretions.

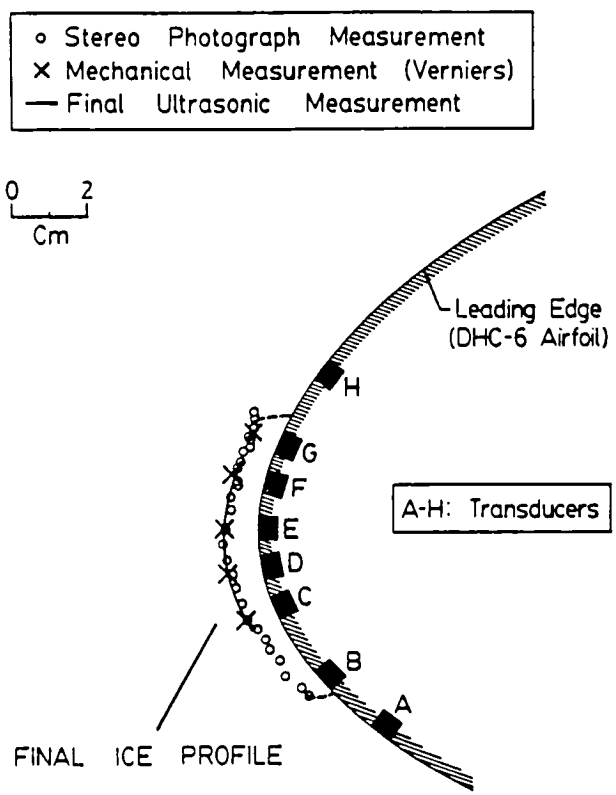

Fig. 5 Final ice profile for flight 86-31.

Flight Number		86-31	86-32	86-33
Flight Duration	(minutes)	66	58	57
Altitude	(feet)	7603	4336	4068
Airspeed	(knots)	138	134	129
Static Temperature	(°C)	-10.0	-6.3	-5.8
Liquid Water Content	(g/m^3)	0.06	0.16	0.26
Median Volume Diameter	(microns)	15.0	14.3	13.0

Table 1 Time-averaged flight and ambient atmospheric icing conditions.

Figure 6 is a plot of ice thickness, measured by the array transducers, versus time during flight 86-31. Each thickness measurement represents the average ice thickness over the transducer beam area, i.e. over a 0.25 in. diameter area. Also shown in the figure is the cloud liquid water content (measured by a Johnson-Williams hot-wire probe) during the flight. From the figure it can be seen that both the cloud liquid water content and the ice growth rate vary during the encounter.

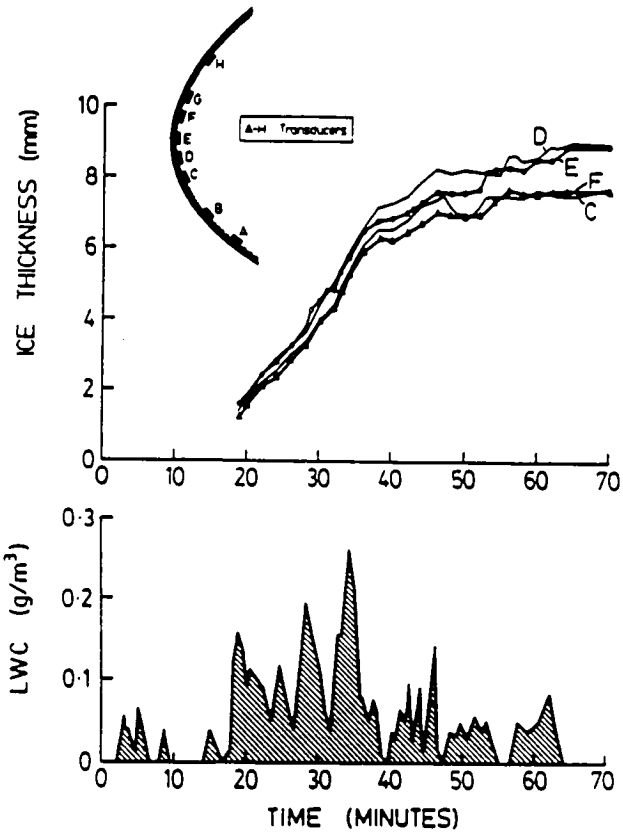

Fig. 6 Ultrasonically measured ice thickness and cloud liquid water content vs. time for flight 86-31.

Since dry ice growth was observed throughout the flight (as indicated by the ultrasonic echo characteristics from the ice surface), tne accretion rate is expected to be proportional to the cloud liquid water content. Therefore fluctuations in the cloud liquid water content will produce similar variations in the ice accretion rate. Figure 6 clearly shows this coupling between cloud liquid water content fluctuations and changes in the ice accretion rate. For example, as a result of the decrease in average liquid water content during the latter part of the flight, the measured growth rates during the last half hour of the flight are significantly lower than those for the first 40 minutes. Shorter time-scale coupling of the cloud liquid water content and ice growth rate is also apparent. For example, the high LWC spike occuring after 35 minutes produces a noticeable increase in the accretion rates at that time.

From figure 6 it can be seen that the ice thickness over the central transducers, D and E, was consistently greater than that over transducers F and C at either side. This spatial variation in ice thickness is due to the higher local collection efficiency near the center of the accretion (transducers D and E), than towards the edges (transducers C and F).

Figure 7 shows the ultrasonically measured ice growth during flight 86-31 in the form of successive ice profiles. These profiles were constructed by fairing a curve through the "point" thickness measurements from the array transducers. A total of six profiles are shown, with six minutes between each profile. The time at which the profiles were measured is indicated on the lower plot of the cloud liquid water content during the flight.

The ultrasonically measured profiles show the ice shape to be relatively conformal to the leading edge throughout the encounter. Thickness measurements from transducers B and G, located near the edges of the accretion, were not possible after the second profile. This was because the slope of the ice surface above these transducers, relative to the airfoil surface, became too large, reflecting the return echo away from the transducer and significantly reducing the received echo strength. Increasing the receiver gain in this situation would alleviate this problem; however, varying the receiver gain between transducers was not practical with the single multiplexed pulser/receiver used for these tests. Since a single "optimum" gain had to be used, this "edge" effect dropout of the echo signal was often unavoidable.

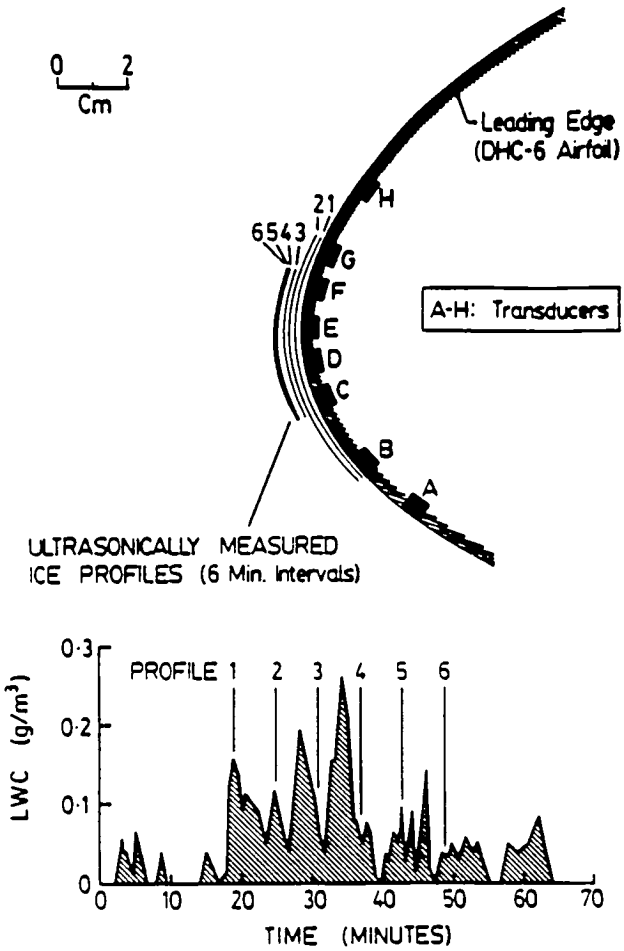

Fig. 7 Ultrasonically measured ice profiles for flight 86-31.

The ice profiles in figure 7 again illustrate the non-uniform growth rate throughout the encounter. The first three profiles all show approximately equal growth, corresponding to the roughly constant average liquid water content during this period. The higher liquid water content in the interval between profiles 3 and 4 results in more growth, as evidenced by the larger profile spacing. Following profile 4 the liquid water content falls, and as a result profiles 5 and 6 show little further growth.

Figure 8 is a comparison of the experimentally measured ice growth during flight 86-31 with that predicted by an analytical icing code (LEWICE)[4]. The time-averaged icing conditions for the flight (see Table 1) were used as input conditions for the code, and ice growth was computed at six minute intervals.

As discussed earlier, the cold cloud temperature and low liquid water contents encountered produced dry ice growth throughout the flight, and the analytical code correctly predicted dry-growth for the duration of the simulation. Because the impinging droplets freeze on impact for dry growth, no local energy balance is required and the analytical code is reduced to a time-stepped calculation of the potential flowfield and local collection efficiency. Both flowfield and droplet trajectory calculations are well understood, and the agreement between the final analytical and experimental ice shapes is good, with both the impingement limits and final thicknesses approximately equal.

The constant icing conditions used by the analytical code do however result in predictions of essentially constant growth rate at each point around the leading edge. Experimentally the growth rate is observed to fluctuate with the varying cloud liquid water content. Since dry ice growth was observed throughout this encounter, these variations in the natural icing conditions affected only the amount of growth between each profile. However, under different ambient conditions, fluctuations in the cloud liquid water content may result in transition between dry and wet ice growth during an encounter[5]. In this case the use of a single, time-averaged liquid water content as input to an analytical code will not accurately model the icing process.

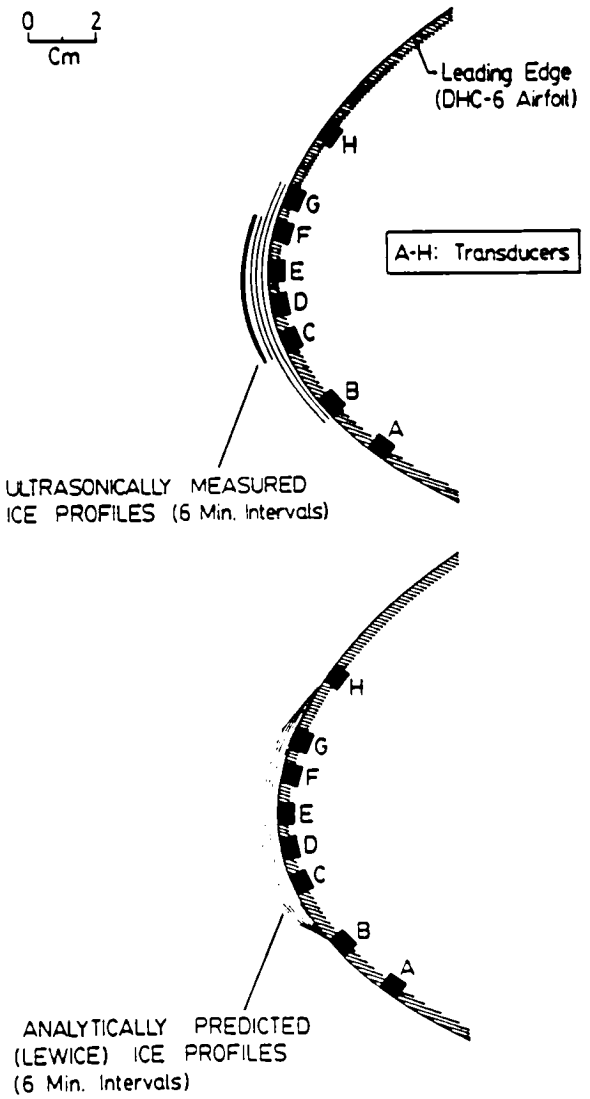

Fig. 8 Comparison of ultrasonically measured ice profiles with analytically predicted (LEWICE) profiles, for flight 86-31.

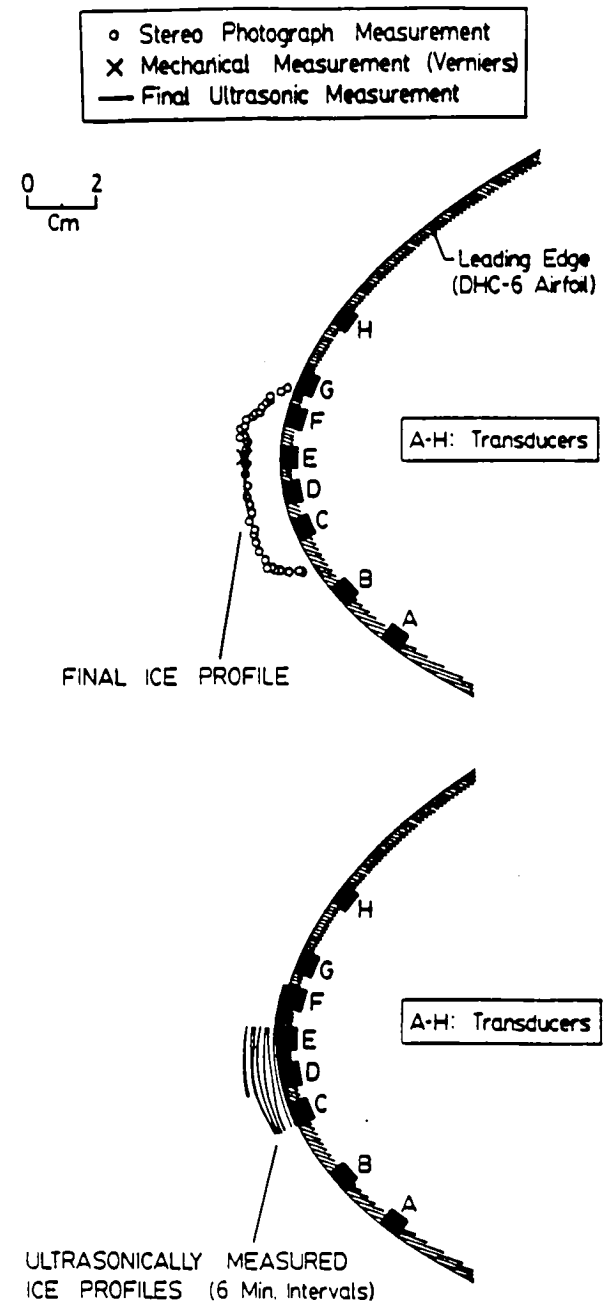

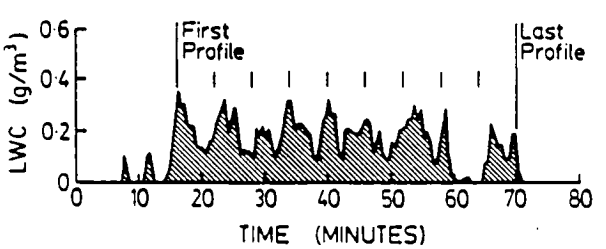

Fig. 9 Final ice profile and ultrasonically measured ice profiles for flight 86-32.

Flight 86-32

Figure 9 summarizes the experimentally measured ice growth for flight 86-32. The final ice shape, obtained from stereo photograph, ultrasonic and vernier caliper measurements, is shown. The agreement between these thickness measurements is again within 0.5 mm. Also shown in the figure are the ultrasonically measured ice growth profiles and the cloud liquid water content during the flight.

Dry ice growth was observed throughout the encounter, and the ice shape is always fairly conformal to the leading edge, as observed for flight 86-31. However, the ice accretion formed during flight 86-32 does not cover as much of the leading edge as the accretion for flight 86-31, due to the smaller droplet sizes encountered during flight 86-32 (see Table 1). Variations in the ice growth rate are clearly illustrated by the profile spacing, and again are due to the varying cloud liquid water content. The loss of signal from transducer C towards the end of the flight was due to the slope of the ice/air interface at the edge of the accretion.

Flight 86-33

As a final illustration, the ice growth during flight 86-33 is presented in figure 10. Experimental difficulties with the oscilloscope display prevented ultrasonic thickness measurements from being recorded for the entire encounter; hence, there are no final ultrasonic measurements of the ice shape. However it is interesting to observe that although the final profile displays a deep depression near the stagnation region, the initial ultrasonically measured profiles do not show any depression developing early in the encounter. Dry ice growth was indicated by the ultrasonic echo characteristics for the first 18 minutes of the encounter, and the depression may have formed as a result of wet ice growth later in the flight.

A computer simulation of this encounter was performed using the LEWICE analytical icing code, and the predicted ice growth is shown in figure 11 along with the final ice profile from the stereo photograph analysis. The time-averaged icing conditions for the flight were again used as input for the code, and ice profiles were computed at one minute intervals.

The analytically predicted ice shape displays a similar depression in the stagnation region to that observed experimentally. However using the steady time-averaged icing conditions, the analytical model predicts wet ice growth throughout the encounter, while dry ice growth was initially observed from the ultrasonic echo characteristics. The analytical code also predicts significant ice accretion due to liquid runback over transducers G and H, although experimentally no runback accretion was observed over these transducers.

These discrepancies between experimentally observed ice growth in fluctuating icing conditions, and analytically predicted growth for steady icing conditons, highlight the need for more experimental measurements of the ice accretion process, particularly during wet or glaze ice growth.

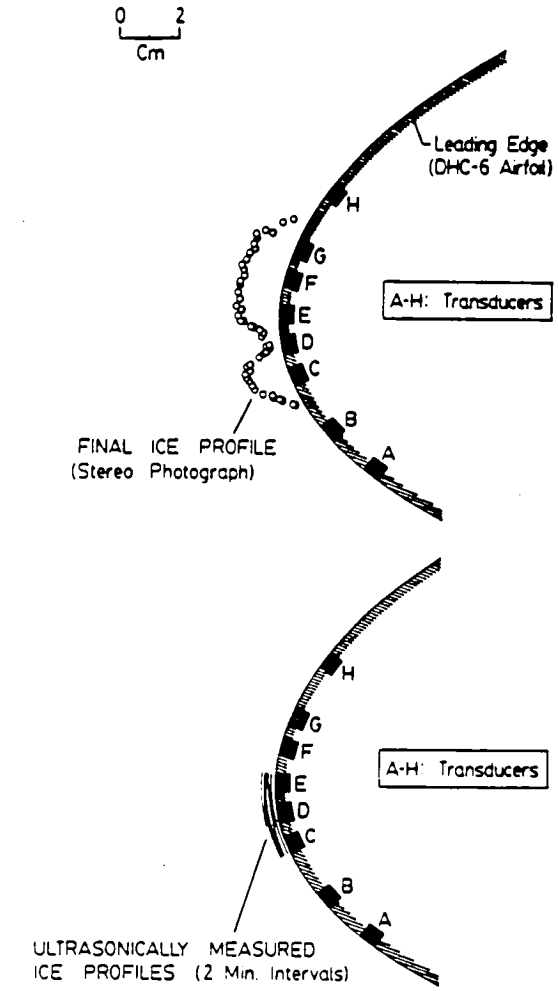

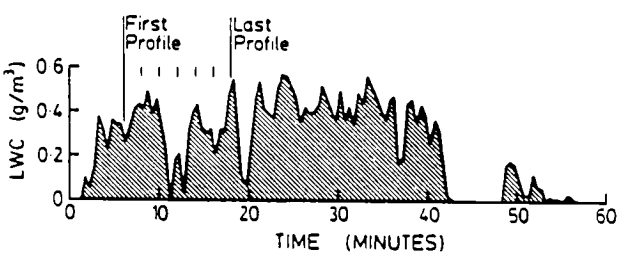

Fig. 10 Final ice profile and ultrasonically measured ice profiles (incomplete), for flight 86-33.

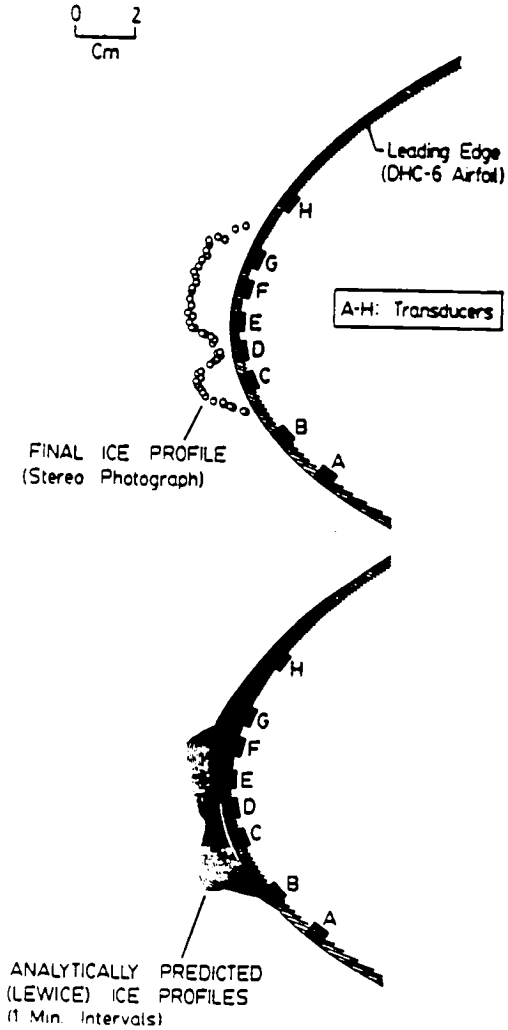

Fig. 11 Comparison of final ice profile from stereo photograph analysis with analytically predicted ice profiles (LEWICE), for flight 86-33.

Conclusions

Experimental measurements of ice growth as a function of time can provide a valuable tool for icing research. These measurements allow the evolution of the ice shape and the underlying physical processes to be studied, as well as permitting quantitative comparisons of flight and wind tunnel icing results. Initial tests using an array of ultrasonic transducers have shown the following:

Ultrasonic pulse-echo techniques may be used to measure ice thickness over a small area on a body to within 0.5 mm.

Thickness measurements from an array of ultrasonic transducers can be used to provide a profile of the ice shape. By repeatedly scanning the array, the ice profile can be measured as a function of time during the icing encounter.

Ice growth rates measured during flight icing conditions are typically not constant. For dry ice growth the accretion rate varies with the cloud liquid water content.

At the edges of the accretion, the ultrasonic echoes are significantly weakened due to the slope of the ice surface relative to the airfoil surface. Accurate ultrasonic thickness measurements are difficult in these cases and additional shape measurements, for example from stereo photographs of the ice accretion, can be used to provide good edge definition.

Differences between experimentally measured ice growth and analytically predicted growth underscore the need for a better understanding of the effects of varying ambient icing conditions, particularly when wet ice growth is involved.

Despite the preliminary nature of these tests, and the limited range of icing conditions encountered, the results presented illustrate the value of experimental measurements of ice growth. Further tests in both flight and wind tunnel icing conditions will aid the development of more detailed analytical icing models as well as documenting differences between flight and wind tunnel icing results.

Acknowledgments

This work was supported by the National Aeronautics and Space Administration and the Federal Aviation Administration under Grants NGL-22-009-640 and NAG3-666. Flight test facilities were provided by the NASA Lewis Research Center. The assistance of Patrick L. Cassady during the stereo photography analysis is gratefully acknowledged.

References

1. MacArthur, C.D., "Numerical Simulation of Airfoil Ice Accretion," AIAA 83-0112, January 1983.

2. Lozowski, E.P., Stallabrass, J.R., and Hearty, P.F., "The Icing of an Unheated Non-Rotating Cylinder in Liquid Water Droplet-Ice Crystal Clouds," National Research Council of Canada (NRC) Report LTR-LT-86, February 1979.

3. Bragg, M.B., Gregorek, G.M., and Shaw, R.J., "An Analytical Approach to Airfoil Icing," AIAA 81-0403, January 1981.

4. Ruff, G.A., "Development of an Analytical Ice Accretion Prediction Method (LEWICE)," Sverdrup Technology, Inc., LeRC Group Progress Report, February 1986.

5. Personal communication with W.A. Olsen, NASA Lewis Research Center, Cleveland, OH, March 1986.

6. Hansman, R.J., and Kirby, M.S., "Comparison of Wet and Dry Ice Growth in Artificial and Flight Icing Conditions," Journal of Thermophysics and Heat Transfer, to be published April 1987.

7. Hansman, R.J., and Kirby, M.S., "Measurement of Ice Accretion Using Ultrasonic Pulse-Echo Techniques," Journal of Aircraft, Vol. 22, June 1985, pp. 530-535.

8. Hansman, R.J., and Kirby, M.S., "Measurement of Ice Growth During Simulated and Natural Icing Conditions Using Ultrasonic Pulse-Echo Techniques," Journal of Aircraft, Vol. 23, June 1986, pp. 492-498.

9. Ide, R.F., and Richter, G.P., "Evaluation of Icing Cloud Instruments for 1982-83 Icing Season Flight Program," AIAA 84-0020, January 1984.

10. Mikkelsen, K.L., McKnight, R.C., Ranaudo, R.J., and Perkins, P.J., "Icing Flight Research: Aerodynamic Effects of Ice and Ice Shape Documentation With Stereo Photography," AIAA 85-0468, January 1985.

11. Personal communication with R.C. McKnight, NASA Lewis Research Center, Cleveland, OH, November 1985.

12. McKnight, R.C., Palko, R.L., and Humes, R.L., "In-Flight Photogrammetric Measurement of Wing Ice Accretions," NASA TM-87191, January 1986.

EXPERIMENTAL MEASUREMENTS OF HEAT TRANSFER FROM AN ICED SURFACE DURING ARTIFICIAL AND NATURAL CLOUD ICING CONDITIONS#

Mark S. Kirby + and R. John Hansman, Jr.*
Massachusetts Institute of Technology
Cambridge, Mass.

ABSTRACT

The heat transfer behavior of accreting ice surfaces in natural (flight test) and simulated (wind tunnel) cloud icing conditions have been studied. Observations of wet and dry ice growth regimes as measured by ultrasonic pulse-echo techniques were made. Observed wet and dry ice growth regimes at the stagnation point of a cylinder were compared with those predicted using a quasi steady-state heat balance model. A series of heat transfer coefficients were employed by the model to infer the local heat transfer behavior of the actual ice surfaces. The heat transfer in the stagnation region was generally inferred to be higher in wind tunnel icing tests than in natural, flight, icing conditions.

NOMENCLATURE

A,B	experimentally derived constants (-)
C_i	specific heat capacity of ice (J/kg K)
C_p	specific heat capacity of air (J/kg K)
C_w	specific heat capacity of water (J/kg K)
D_w	Diffusion coefficient of water vapor in air (m^2/s)
d	cylinder diameter (m)
h	local convective heat transfer coefficient (W/m^2 K)
k	thermal conductivity of air (W/m K)
L_f	latent heat of fusion of water (J/kg)
L_s	latent heat of sublimation of water (J/kg)
L_v	latent heat of vaporization of water (J/kg)
$\dot{M}''$	local mass flux/time (kg/m^2s)
Nu	Nusselt number (-)
$\dot{Q}''$	local heat flux/time (W/m^2)
Re	Reynolds number based on cylinder dia. and V_∞ (-)
r	recovery factor, 0.875 (-)
ΔT_∞	cloud supercooling = $-T_\infty$ (°C)
T_{surf}	equilibrium surface temperature (°C)
T_∞	cloud temperature (°C)
t	icing time (s)
V_∞	freestream velocity (m/s)
W_∞	cloud liquid water content (g/m^3)
β	local collection efficiency (-)
$\rho_{v,surf}$	saturated vapor density over surface (kg/m^3)
$\rho_{v,\infty}$	saturated vapor density in cloud (kg/m^3)

+ Research Assistant, Aeronautics and Astronautics
* Assistant Professor, Aeronautics and Astronautics.

AIAA Paper 86-1352.

INTRODUCTION

Whenever an aircraft encounters liquid moisture in the form of supercooled cloud droplets, or freezing rain, ice will form on the exposed surfaces. Typical cloud droplet diameters range from as large as 50 microns to less than 10 microns. In the case of freezing rain, droplets may be several mm in diameter. The shape of the accreted ice and its affect on the aircraft's aerodynamic performance[1] depend on several parameters - the cloud temperature, the average cloud droplet size and size spectrum, the amount of liquid water per unit volume, W, contained in the cloud and the size, shape and speed of the accreting surface.

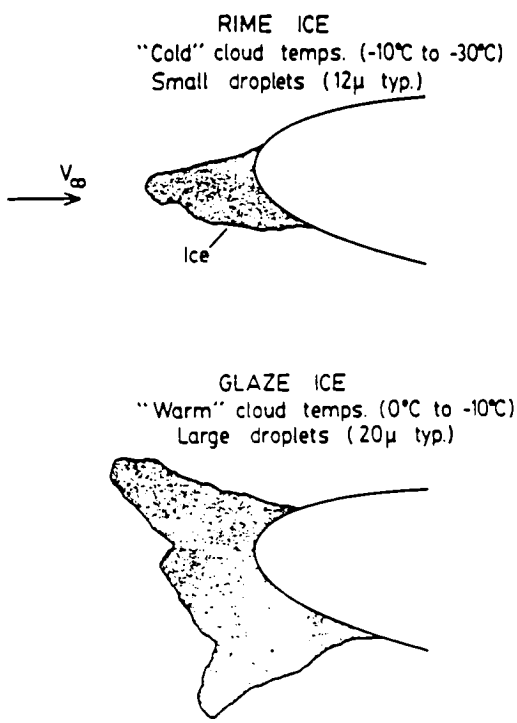

Figure 1. Typical "rime" and "glaze" ice shapes.

When all of the impinging droplets freeze on impact with the accreting surface the ice accretion is characterized as rime ice. The resulting ice shape typically protrudes forward into the airstream (see figure 1). Relatively cold cloud temperatures (below -10°C) and small droplet sizes promote rime ice formations. At warmer cloud temperatures and for the characteristically larger droplet sizes and liquid water contents present in these clouds, the impinging droplets do not freeze on impact and may run back over the accreting surface as

liquid water before freezing further downstream on the surface. This type of ice accretion is characterized as glaze ice and often the resulting ice shape displays two pronounced growth peaks, or horns, on either side of the stagnation line(see figure 1 also). The most severe aircraft performance degradation due to icing is typically associated with glaze ice formations[2].

Figure 2 illustrates schematically how recent attempts[3-5] to analytically model aircraft icing have decomposed the ice accretion process. First, the aerodynamic flowfield around the body of interest is calculated, usually by an inviscid panelling method. Droplet trajectories around the body are then calculated by integrating the droplet equations of motion within the body flowfield. From these trajectory calculations the mass flux of impinging droplets at a given location on the body can then be determined. The third, and crucial step, involves a thermodynamic analysis of the freezing process at the icing surface. A steady-state energy balance involving the impinging heat load from the droplets and the heat removed by convection, evaporation and sublimation is typically applied to small control volumes along the icing surface. The fourth step then calculates the amount of ice formed at each location on the body as a result of satisfying this energy balance and constructs the ice shape on the body. This entire process may then be repeated using the iced geometry as input for the flowfield calculation. Due to this form of time-stepped solution, any errors or inaccuracies in each of these four steps tend to propagate and may result in an unrealistic ice shape.

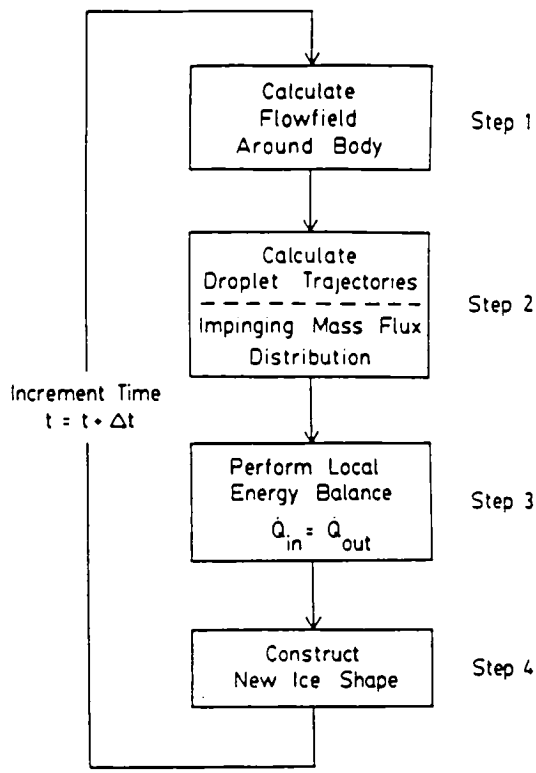

Figure 2. Schematic breakdown of analytical ice accretion modeling process.

Experimental results[6-8] have confirmed the accuracy of the flowfield and droplet trajectory calculations. For rime ice growth, where the droplets freeze at the point of impact, the predicted ice shapes are in good agreement with experimentally measured ice shapes. However, for glaze ice conditions the predicted ice shapes are extremely sensitive to the assumed convective heat transfer coefficient distribution over the body, and, to date, no analytic model has accurately predicted ice shapes throughout this important icing regime.

Because of the sensitivity to heat transfer, experimental measurements of the heat transfer coefficient distribution over an iced surface are critical for validating these analytic models. Due to experimental difficulties associated with these measurements on actual ice surfaces, local heat transfer coefficient measurements have only been made around wooden or foam models of typical ice shapes[9]. In addition, experimental measurements comparing local heat transfer coefficients obtained in icing wind tunnels and in flight are essential if natural icing conditions are to be accurately simulated in icing wind tunnels. Very little experimental data exists in this area.

This paper outlines the steady-state energy balance for the stagnation region of a body. From this energy balance the condition for transition from rime or "dry" ice growth to glaze or "wet" ice growth is determined in terms of the locally impinging mass flux and the local heat transfer coefficient. By measuring the locally impinging mass flux and whether the accreting ice surface is wet or dry, it is thus possible to infer limits on the magnitude of the heat transfer coefficient at the ice surface.

The detection of liquid water on an accreting ice surface is made by a unique application of an ultrasonic pulse-echo technique and is described. Results of tests employing this ultrasonic technique for cylinders exposed to artificial icing conditions in the NASA Lewis Icing Research Tunnel (IRT) and natural icing conditions in flight from the NASA Lewis Twin Otter Icing Research Aircraft are then presented. These experimental results are used to compare local heat transfer coefficients measured around a bare cylinder with different levels of freestream turbulence and surface roughness.

STEADY-STATE THERMODYNAMIC MODEL FOR AN ICING SURFACE

The thermodynamic analysis presented in this paper for a surface accreting ice follows the earlier work of Messinger[10] and others[11,12]. Figure 3 shows the principle modes of energy transfer associated with an icing surface. Heat is added to the surface primarily due to the latent heat of fusion released as the droplets freeze, but also from aerodynamic heating and, to an even smaller extent, from the kinetic energy of the droplets impacting the surface. Heat is removed from the surface primarily by convection, and to a lesser degree by sublimation (when the surface is dry) or evaporation (when the surface is wet). In addition, heat is absorbed from the surface as the supercooled droplets impinge and warm to 0°C.

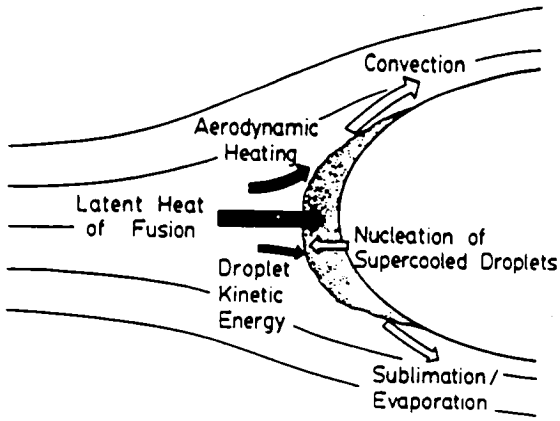

Figure 3. Modes of energy transfer for an accreting ice surface.

Figure 4 depicts the local control volume examined in this analysis. Since only the stagnation region of the body is considered in this paper, it is assumed that the only liquid entering the control volume is due to the impinging droplets. Liquid may, however, flow out of the control volume along the ice surface. Thus if the ice surface in the stagnation region is wet, insufficient heat is being removed to freeze all of the impinging liquid, and therefore the "freezing fraction", n, is less than unity, where n is given by

$$n = \frac{\dot{M}''_{frozen}}{\dot{M}''_{impinging}} \qquad (1)$$

When the ice surface is dry the freezing fraction is unity. The steady-state assumption requires that the rate at which energy is added to the control volume equals the rate at which it is removed, i.e.

$$Q''_{IN} = Q''_{OUT} \qquad (2)$$

At steady-state it is assumed that the ice surface achieves a locally uniform equilibrium temperature, T_{surf}. Conduction into the ice is assumed to be zero and chordwise conduction between adjacent control volume is neglected. With these assumptions eq. (1) may be written in terms of its component heat terms as

$$\left.\begin{aligned} \dot{Q}''_{freezing} &= \dot{M}''\{L_f + C_i(0^\circ C - T_{surf})\} \\ \dot{Q}''_{aero\ heating} &= \frac{rhV_\infty^2}{2C_p} \\ \dot{Q}''_{droplet\ K.E.} &= \frac{\dot{M}''V_\infty^2}{2} \end{aligned}\right\} \dot{Q}''_{IN}$$

$$\left.\begin{aligned} \dot{Q}''_{convection} &= h(T_{surf} - T_\infty) \\ \dot{Q}''_{subl/evap} &= \frac{hDL_{s/v}(\rho_{v,surf} - \rho_{v,\infty})}{k} \\ \dot{Q}''_{droplet\ warming} &= \dot{M}''C_w\,\Delta T_\infty \end{aligned}\right\} \dot{Q}''_{OUT} \qquad (3)$$

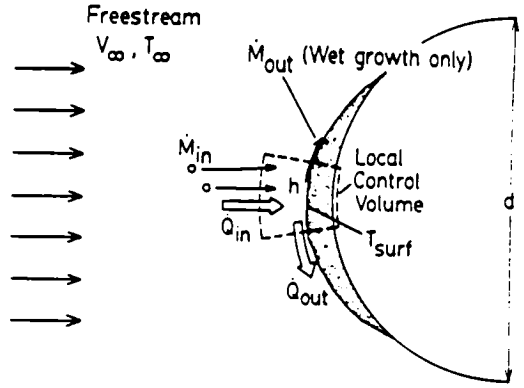

Figure 4. Stagnation region control volume used for steady state thermodynamic analysis.

$$\dot{M}''\{L_f + \frac{V_\infty^2}{2} + C_i(0^\circ C - T_{surf})\} + \frac{rhV_\infty^2}{2C_p} =$$

$$h\{(T_{surf} - T_\infty) + DL_s(\rho_{v,surf} - \rho_{v,\infty})\} + \dot{M}''C_w\Delta T_\infty \qquad (4)$$

Note that this equation (eq. 4) assumes all of the impinging mass flux, $\dot{M}''$, is frozen, thus the ice surface is dry and the latent heat of sublimation, L_s, is used in the mass transfer term from the surface.

The ice surface will first start to become wet when the equilibrium temperature of the surface rises to 0°C. The energy balance appropriate for the transition between dry and wet growth is thus

$$\dot{M}''\{L_f + \frac{V_\infty^2}{2}\} + \frac{rhV_\infty^2}{2C_p} = h\{(0^\circ C - T_\infty) + \frac{DL_v(\rho_{v,0^\circ C} - \rho_{v,\infty})}{k}\} + \dot{M}''C_w\,\Delta T_\infty \qquad (5)$$

In this case the freezing fraction must be very slightly less than unity, since the surface is now wet, although it has been taken to be unity for this transitional case. The latent heat of vaporization, L_v, is however used to represent the evaporative cooling term.

The local mass flux, $\dot{M}''$, of droplets impinging on a body is given by

$$\dot{M}'' = \beta WV_\infty \qquad (6)$$

Where β is the "local collection efficiency" and is defined as the ratio of the locally impinging mass flux to the freestream mass flux, i.e.

$$\beta = \frac{\text{Locally Impinging Droplet Flux}}{\text{Freestream Droplet Flux}} \qquad (7)$$

The local collection efficiency is governed by the ratio of the impinging droplets inertia to the aerodynamic drag on them due to the freestream flowfield disturbance created by the body. For most aircraft icing regimes the local collection efficiency is primarily a function of the cloud droplet median volume diameter, MVD, and the size

of the accreting body. Typical values for the local collection efficiency on the stagnation line of a 10cm diameter (4") cylinder at a freestream airspeed of 100m/s (230mph) are 0.6 for a cloud composed of droplets 20 microns in diameter and 0.4 for a cloud of 12 micron droplets. Thus a small body moving rapidly through a cloud of large droplets will have a much higher local collection efficiency than a large body moving slowly through a cloud of small droplets. Using eq. 6 allows the critical condition for transition between wet and dry ice growth to be expressed as

$$\beta W V_\infty \{L_f + \frac{V_\infty^2}{2}\} + \frac{rhV_\infty^2}{2C_p} = h\{(0^\circ C - T_\infty) + \frac{DL_v}{k}(\rho_{v,0^\circ C} - \rho_{v,\infty}) + \beta W V_\infty C_w \Delta T_\infty \qquad (8)$$

It is convenient to express the convective heat transfer coefficient, h, in terms of the dimensionless Nusselt number, Nu, where

$$Nu = \frac{hd}{k} \qquad (9)$$

With d being the uniced diameter or characteristic dimension of the body, and k the thermal conductivity of air. Experimental measurements of local heat transfer coefficient distributions are often presented in terms of a power law relationship between the Nusselt number and the Reynolds number,

$$Nu = ARe^B = A\left(\frac{\rho_\infty V_\infty d}{\mu_\infty}\right)^B \qquad (10)$$

Where A and B are experimentally derived constants. Using eqs. 9 and 10, equation 8 may be rewritten in terms of a "critical" impinging liquid water content, βW (eq(11) below). Here the product $(\beta W)_{crit}$ is the wet/dry threshold and represents the critical locally impinging liquid water content (gramms/meter^3) necessary to produce a wet ice surface. If βW is greater than this critical value the ice surface will be wet and the freezing fraction will be less than one, while if βW is less than this critical value the ice surface will be dry. From this equation it can be seen that $(\beta W)_{crit}$ depends on the assumed values of A and B in the heat transfer coefficient model. By measuring the locally impinging liquid water content, βW, and whether the resulting ice growth is wet or dry it is thus possible to compare different heat transfer models (different A and B constants in eq. 10) and determine which models best predict the observed wet or dry ice growth. The technique used to detect the presence or absence of liquid water on an accreting ice surface is described in the next section.

ULTRASONIC PULSE-ECHO ANALYSIS OF AN ACCRETING ICE SURFACE

Figure 5 illustrates the principle of the ultrasonic pulse-echo measurement technique applied for an icing surface.[13] A small transducer mounted flush with the accreting surface emits a brief compressional wave, the ultrasonic "pulse", that travels through the ice as shown. This wave is reflected at the ice surface and returns to the emitting transducer as an echo signal. By measuring the time elapsed between the emission of the pulse and the return of the echo, the ice thickness over the transducer may be calculated using the appropriate speed of sound for ice. By repeatedly emitting pulses the ice thickness can be constantly measured as ice accretes on the body; pulses are typically emitted several thousand times a second, while the time elapsed between pulse emission and echo return is on the order of microseconds for ice thicknesses less than 5 cm (2").

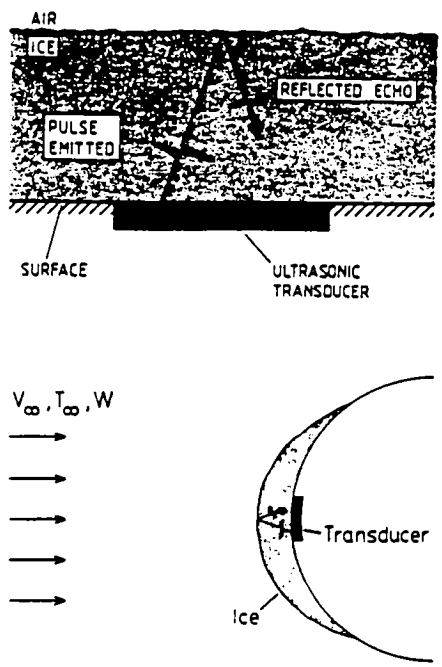

Figure 5. Ultrasonic pulse-echo measurement technique.

$$(\beta W)_{crit} = Ak\left(\frac{\rho_\infty}{\mu_\infty}\right)^B \frac{1}{(\overline{V}d)^{1-B}} \left\{ \frac{(0^\circ C - T_\infty) + \frac{DL_v}{k}(\rho_{v,0^\circ C} - \rho_{v,\infty}) - \frac{rV_\infty^2}{2C_p}}{L_f - C_w \Delta T_\infty + \frac{V_\infty^2}{2}} \right\} \qquad (11)$$

In addition to obtaining the ice thickness from the pulse-echo transit time, the condition of the ice surface may also be monitored via the characteristics of the ultrasonic echo pattern received from the ice surface. Specifically it has been found[14] that the echo patterns received from a dry ice surface and a wet ice surface are markedly different. A "single" echo, corresponding to the ice/air interface over the transducer, is received from a dry ice surface. However during wet ice growth the presence of liquid water on the ice surface creates a different, reflective interface, namely that between liquid and air. Thus during wet ice growth the received echo pattern contains an echo from the ice/water interface and further, rapidly varying echoes from the water/air interface. The presence of these echoes, which vary due to the distortion of the water by the impinging droplets and flowfield, is used to determine if the ice growth is wet. If only a single echo is received from the ice surface then the ice growth is determined to be dry.

EXPERIMENTAL FACILITIES AND TEST DESCRIPTION

Icing Research Tunnel Tests

The first series of tests was performed in the NASA Lewis Research Center Icing Research Tunnel. A 0.102m (4.0") diameter cylinder instrumented with ultrasonic transducers was suspended vertically from the icing tunnel roof as shown in figure 6. The transducers were located on the stagnation line of the cylinder. The echo signals received from these transducers were displayed on an oscilloscope. The oscilloscope screen was video-taped in order to provide a permanent record of the time-dependent echo patterns. The test procedure consisted of lowering the tunnel temperature to the desired icing cloud condition with the water spray off. Once the tunnel temperature had stabilized, the water spray system was turned on in order to produce a cloud of droplets of the desired size (median volume diameter). Typically the spray system was activated for a six minute period, after which it was turned off. Photographic and other measurements of the iced cylinder were then made and the cylinder was completely de-iced before the start of the next run. A total of 36 runs for 15 different icing conditions were performed.

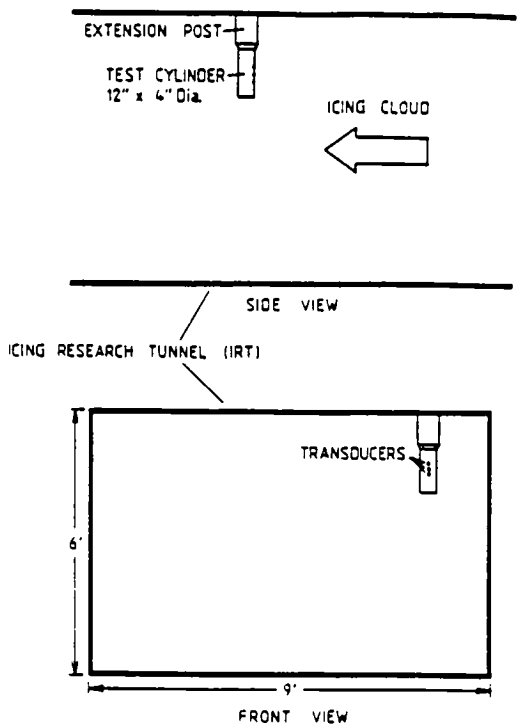

Figure 6. Test cylinder installation for icing wind tunnel (IRT) tests.

Natural Icing Tests

A second series of tests was performed in natural icing conditions using a 0.114m (4.5") diameter cylinder similarly instrumented with ultrasonic transducers on the stagnation line. An oscilloscope was again used to display the received echo signals and video-taped as before. The cylinder was exposed to the icing cloud via an experiment carrier mounted in the roof of the NASA Lewis Icing Research Aircraft, (De Havilland Twin Otter) shown in figure 8. When deployed, the cylinder was located 0.53m (21") into the freestream above the roof-line of the aircraft. The cylinder was exposed throughout the icing encounter, which typically lasted approximately 20 minutes. Throughout the exposure other instruments mounted on the research aircraft measured aircraft and icing cloud parameters. In particular a Johnson-Williams hot-wire probe was used to record cloud liquid water content and a forward scattering laser probe (FSSP) was used to measure the cloud droplet size distribution. Four separate exposures were conducted in this series of flight tests.

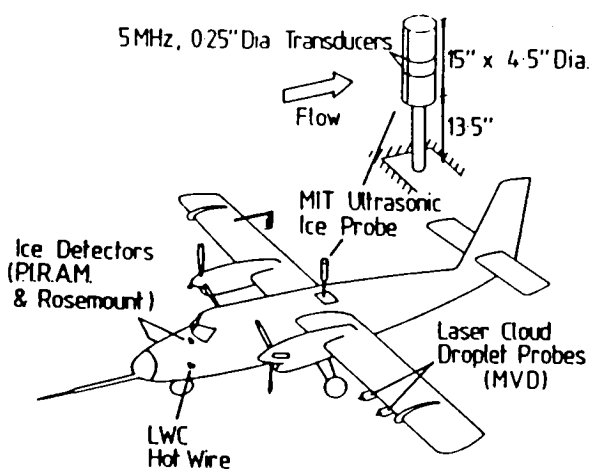

Figure 7. Test cylinder installation for natural icing flight tests on the NASA, Twin Otter, Icing Research Aircraft.

Experimental Results & Discussion

The limited time available for testing in the icing research tunnel and the research aircraft prevented a precise determination of the local heat transfer coefficient by means of the experimentally measured wet or dry ice growths alone. However, the wet/dry ice growth data obtained can be used to compare the ice growth predicted by different heat transfer coefficients in the form $Nu=A\ Re^{B}$ and the quasi steady-state icing model. Recent experimental heat transfer coefficient measurements about a bare cylinder by Van Fossen et al., in support of NASA Lewis' icing research programme are compared in this way. The bare cylinder is considered because most of the wet/dry measurements were obtained for relatively small ice thicknesses, and hence the geometry is essentially that of a bare cylinder. In the Van Fossen study heat transfer coefficients were measured for two different freestream turbulence levels, 0.5% and 3.5%, and for two different cylinder surface conditions, one smooth and one roughened with grains of sand with an average element height of 0.33mm. The 0.5% freestream turbulence level was the minimum turbulence level achievable in the Van Fossen tests. The 3.5% turbulence was chosen to characterize the higher turbulence level believed to exist in the icing research tunnel.

Icing Research Tunnel Results

Figure 8 shows the ultrasonically measured ice growth for six different icing conditions in the icing research tunnel. The freestream velocity was the same, 102.8m/s (230mph), for all six runs shown. The impinging liquid water content, βW, was determined from the ultrasonically measured dry ice growth accretion rate, since when the freezing fraction is unity the local ice accretion rate, $\dot{d}$, is given by

$$\dot{d} = \frac{\beta W V_\infty}{\rho_{ice}} \qquad (12)$$

In all cases the ice density, ρ_{ice}, was taken to be that of the pure substance.

Figure 8 also shows the four wet/dry threshold curves calculated using the Van Fossen heat transfer coefficients. These curves are plotted versus ambient temperature and were calculated for a freestream velocity of 102.8m/s (230mph), and a cylinder diameter of 0.102m (4"). The four curves shown thus represent the transition line between wet and dry ice growth calculated for the four different local heat transfer coefficients implied by the Van Fossen data. If the local impinging liquid water content exceeds this value of $(\beta W)_{crit}$ for a given ambient temperature then the ice growth is calculated to be wet, and if βW is less than $(\beta W)_{crit}$ the ice growth is predicted to be dry. From the figure, it can be seen that the heat transfer coefficient that best predicts the experimentally observed pattern of wet and dry ice growth is that measured for the cylinder roughened with sand and at a freestream turbulence level of 3.5%. While dry ice growth was observed at -23°C (-10°F) and an impinging liquid water content equal to $0.47 g/m^3$, the heat transfer coefficients for the 0.5% freestream turbulence level clearly imply wet growth for these conditions. Thus it appears that the 0.5% turbulence level heat transfer coefficients underpredict the actual heat transfer in the icing tunnel are therefore too low.

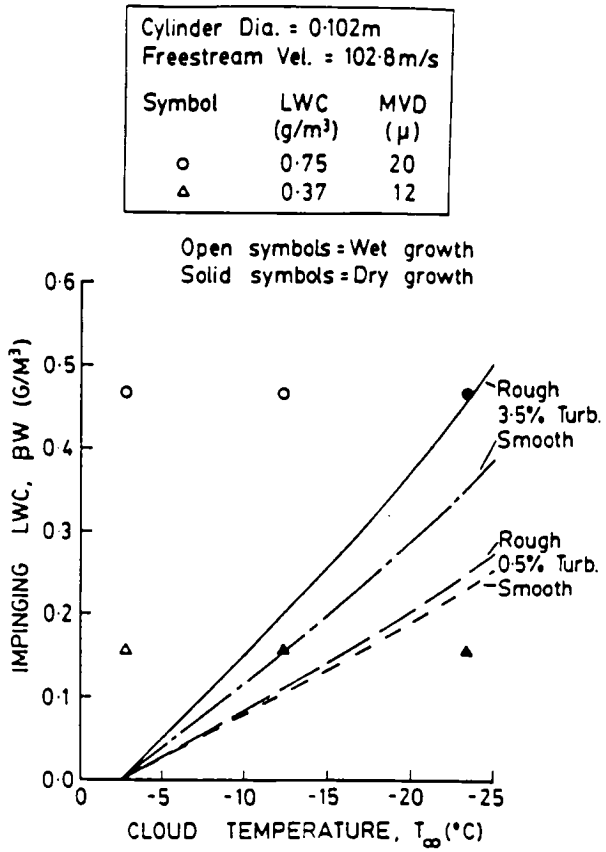

Figure 8. Plot of impinging liquid water content versus cloud temperature showing ultrasonically measured wet/dry ice growth and theoretical wet/dry threshold curves for four different heat transfer coefficients. (V_∞ = 102.8m/sec (230mph).

Since only the stagnation region of the cylinder is considered, the local heat transfer coefficient in this region is less sensitive to the surface roughness than to the freestream turbulence level, as can be seen from the four curves in figure 8. However local surface roughness does play a critical role in determining where boundary layer transition occurs, and this in turn significantly affects the heat transfer distribution around the body and therefore the resulting ice shape. Accurate analytic models of the local surface roughness on real iced surfaces have not yet been developed; however the local surface roughness has been found to vary with both position on the body and the icing conditions under which the ice was formed. For example, a surface roughness of 2mm has been measured at -8°C (+18°F) for ice accreted on a 0.53m chord NACA 0012 airfoil, while at -26°C (-15°F) the surface roughness was found to be less than 0.1mm[1]. Thus while the heat transfer coefficient implied by the "rough" surface, 3.5% turbulence level measurements appears to best predict the experimentally observed pattern of wet and dry ice growth, this heat transfer "model" may well only be applicable to the stagnation region and a different model may apply elsewhere on the cylinder.

A clear understanding of the stagnation region heat transfer is essential for ice shape prediction by current analytic icing models. Since these models assume that all the impinging liquid not frozen in the stagnation region flows downstream into the adjacent control volumes (see fig. 4), errors in the assumed stagnation region heat transfer coefficient will significantly change the mass flux distribution around the body during wet growth. If for example the stagnation region heat transfer coefficient used in such an icing model is less than the actual value, then during wet growth the model will overpredict the amount of liquid running out of the stagnation region into the adjacent control volume. This in turn may erroneously produce further liquid runback from this control volume, when in fact dry growth is the correct condition for this region. The ice shapes predicted in such a case will be in poor agreement with the actually observed shape, particularly when the feedback process inherent in the time-stepped flowfield and droplet trajectory calculations is taken into account (fig. 2).

Since the rough surface, 3.5% freestream turbulence heat transfer coefficient appeared to best approximate the actual heat transfer occurring in the icing research tunnel (based on the wet/dry ice surface date from the ultrasonic tests), this heat transfer power law model

$$Nu = 0.2460\ Re^{0.6444} \qquad (13)$$

was compared with other ultrasonic wet/dry ice growth data obtained at different tunnel icing cloud conditions. Figure 9 shows two plots similar to figure 8, with impinging liquid water content plotted versus ambient temperature. Ultrasonic wet/dry ice growth measurements are shown for two freestream velocities, 71.5m/s (160mph) and 49.2m/s (110mph). The impinging liquid water content, βW, was obtained from the dry growth accretion rate, where available, or by calculation of β for those cases where only wet or marginally wet ice growth was observed. The wet/dry threshold curves calculated using the 3.5% turbulence, rough surface heat transfer coefficient are plotted.

The 3.5% turbulence level, rough surface heat transfer coefficient correctly predicts all three observed dry ice growth cases. In addition, the two marginally wet cases observed suggest that the heat transfer over the ice surface may in fact be even greater than that implied by the 3.5% turbulence model. This would be consistent with the experimental results shown in figure 8 where dry growth was observed in one case while the 3.5% turbulence heat transfer coefficient predicted slightly wet growth.

Based on the results presented in figures 8 and 9 it appears that the heat transfer coefficient model that best approximates the actual heat transfer occuring in the icing research tunnel is the 3.5% turbulence level, rough surface model. The actual heat transfer coefficient is clearly greater than those applicable at the low (0.5%) turbulence level and may be even greater the high (3.5%) turbulence level value.

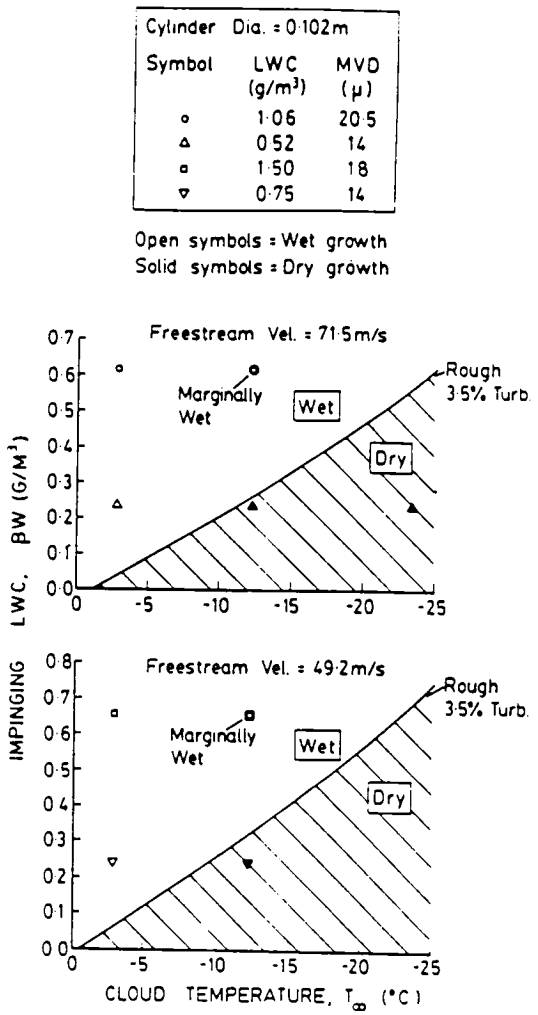

Figure 9. Plot of impinging liquid water content versus cloud temperature showing ultrasonically measured wet/dry ice growth at two additional free stream velocities and the theoretical wet/dry threshold curve for the 3.5% turbulence level, rough surface, heat transfer coefficient.

Natural Icing Cloud Test Results

While constant icing conditions were maintained throughout each exposure in the icing research tunnel, the natural icing cloud conditions, most noticeably the liquid water content, were not constant throughout each flight. Figure 10 shows a plot of cloud liquid water content versus exposure time for research flight 85-24. The liquid water content was measured by a Johnson-Williams hot-wire probe located near the nose of the aircraft (see figure 7). Also shown, are the experimentally observed periods of dry, wet and transitional ice growth, produced by the varying impinging liquid water content. The ultrasonic echo patterns received from the accreting ice surface were used to determine if the ice growth was wet, dry or transitional. Ice growth was characterized as transitional when the ultrasonic echoes received from the ice surface displayed neither predominantly dry nor wet echo patterns.

Since the thermodynamic model used to compare heat transfer coefficients assumes a quasi steady-state icing process, and since the cloud liquid water content varied significantly throughout each exposure, a simple, steady-state "time constant" was estimated. This time constant was then applied as a criteria for comparing the ultrasonic data with the wet/dry growth regimes predicted by the steady-state model. A time constant of ten seconds was selected based on the transient thermal response of a thin ice layer and on the time response of the Johnson-Williams liquid water content measurements. Therefore only liquid water content levels sustained for greater than ten seconds were used in the categorization of ice growth as wet, dry or transitional.

Figure 11 is a plot of impinging liquid water content versus cloud temperature. The experimentally observed ice growth regimes during the four research flights conducted are shown. Note that during flights 85-24 and 85-25 the full range of ice growth regimes was encountered with periods of dry, transitional and wet ice growth observed. No dry ice growth was observed during flights 85-22 and 85-23. Also shown are the four wet/dry threshold curves calculated using the four different Van Fossen heat transfer coefficients (0.5% turbulence, rough and smooth surface; 3.5% turbulence, rough and smooth surface). These curves were calculated for the test cylinder diameter of 0.114m (4.5%") and for the average (85-22 to 85-25) flight airspeed of 71.4m/s (160mph) and the average exposure altitude of 1613m (5292').

Figures 10 and 11 illustrate the considerable variations encountered in natural icing conditions, both during a particular flight and between flights conducted on different days. For example, the cloud temperature, liquid water content and droplet size were roughly comparable for flights 85-24 and 85-25. However, different ranges of wet and dry ice growth were observed, as indicated by the overlapping experimental wet and dry growth ranges at the same impinging liquid water content. The implication is that the heat transfer differed between the two flights, both at nominally similar icing conditions, but conducted on different days through different clouds.

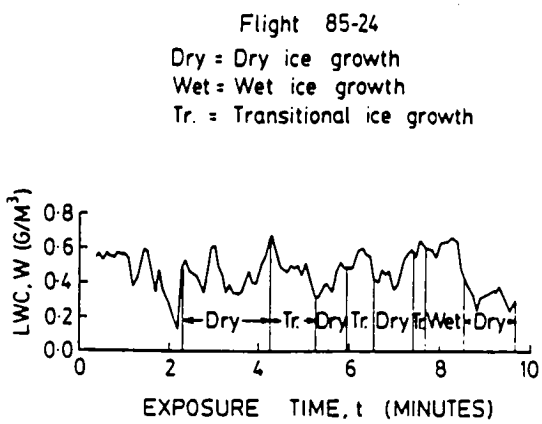

Figure 10. Plot of liquid water content (measured by the Johnson Williams probe) versus exposure time for flight 85-24 showing typical fluctuations observed in natural icing conditions. Also shown are ultrasonic measured periods of wet, dry, and transitional ice growth.

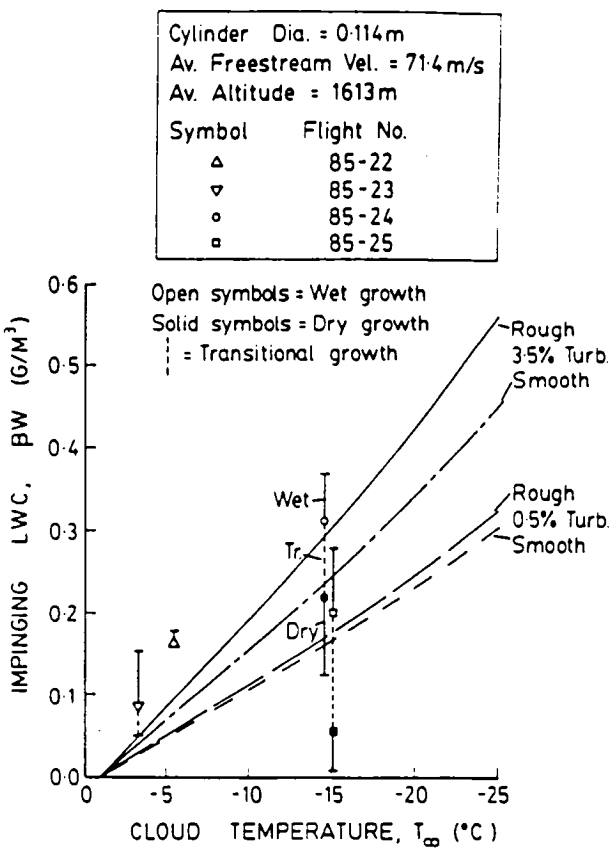

Figure 11. Plot of impinging liquid water content versus cloud temperature showing wet, dry and transitional ice growth regimes observed in flights and theoretical wet/dry threshold curves for four different heat transfer coefficients.

From the figure it can be seen that for flight 85-25 the high (3.5%) turbulence level heat transfer coefficients overpredict the observed heat transfer, based on the steady-state model analysis. For this flight the low (0.5%) turbulence level heat transfer coefficients appear appropriate since both of these coefficients correctly predict the observed wet and dry regimes. The actual turbulence level applicable could be even less than 0.5% based on the location of the observed wet and dry growth regimes.

The experimentally observed ice growth regimes during flight 85-24 are consistent with the wet/dry threshold predicted by the 3.5% turbulence level, rough surface heat transfer coefficient. For this flight the low (0.5%) turbulence level models incorrectly predict wet growth for impinging liquid water content levels where dry growth was experimentally observed. Thus, in contrast to flight 85-25, the low turbulence level appears to be too low, and the 3.5% turbulence level model gives acceptable results.

The results of these tests highlight the effect of variations in icing conditions which are inherent in all natural icing encounters. Ice growth may thus vary from wet to dry during a particular encounter as the impinging liquid water content fluctuates. The ice shapes formed during pure dry (rime ice) or pure wet (glaze ice) growth are markedly different (see fig. 1). Therefore the use of an average cloud liquid water content to represent a particular natural icing encounter will in general be inappropriate since this will imply either pure wet or pure dry growth, when in reality the ice growth (wet or dry) varies as a function of time.

The results of the natural icing tests also indicate the heat transfer occurring in natural icing conditions may vary from day to day despite similar icing conditions. One reason for this variation may be due to different icing cloud turbulence levels. Based on the limited amount of flight test data available it appears that in general the appropriate turbulence level for natural icing conditions is somewhat lower than the 3.5%+ level inferred for the icing research tunnel. This result is consistent with previous experimental comparisons between the icing research tunnel and flight.[15] For these reasons, care should be taken in extrapolating the results of icing wind tunnel tests to "similar" natural icing cloud conditions.

CONCLUSIONS

Results of tests conducted in artificial (icing research tunnel) and natural (flight) icing conditions have shown the following;

1. The presence of liquid water on an accreting surface may be detected using an ultrasonic pulse-echo technique.

2. The threshold between dry and wet ice growth can be theoretically determined if the local convective heat transfer coefficient is known.

3. By comparing experimentally measured wet or dry ice growth with wet/dry thresholds predicted by different heat transfer coefficients it is possible to infer heat transfer coefficient values for an iced surface in icing conditions.

4. The heat transfer occurring during initial ice growth in the icing research tunnel appears to be best modelled by Van Fossen's 3.5% freestream turbulence level, rought surface heat transfer model for a bare cylinder. The actual heat transfer coefficient may be slightly in excess of the values predicted by this model.

5. During natural icing cloud encounters conditions are not constant and as a result periods of wet, dry and transitional ice growth may be observed within a single encounter.

6. The heat transfer occuring during initial ice growth in natural icing conditions has been inferred to vary between that predicted at the 3.5% Freestream turbulence level and the 0.5% level, using Van Fossen's data.

7. Due to variations in natural icing cloud conditions care should be taken in extrapolating results from icing wind tunnels to "similar" natural icing cloud conditions.

ACKNOWLEDGEMENTS

This work was supported by the National Aeronautics and Space Administration and the Federal Aviation Administration under Grant NGL-22-009-640 and NAG3-666.

REFERENCES

1. Olsen, W., Shaw, R., and Newton, J. "Ice Shapes and the Resulting Drag Increase for an NACA 0012 Airfoil." NASA TN83556, 1984.

2. Ranaudo, R.J., Mikkelsen, K.L., McKnight, R.C., and Perkins, P.J., Jr., "Performance Degradation of a Typical Twin Engine Commuter Type Aircraft in Measured Natural Icing Conditions," NASA TM-83564, 1984.

3. MacArthur, C.D., Keller, J.L., and Leurs, J.K., "Mathematical Modeling of Ice Accretions on Airfoils." AIAA-82-0284, January 1982.

4. Lozowski, E.P., Stallabrass, J.R., and Hearty, P.F., "The Icing of an Unheated Non-Rotating Cylinder in Liquid Water Droplet-Ice Crystal Clouds." National Research Council of Canada (NRC) Report LTR-LT-86, February 1979.

5. Bragg, M.B., Gregorek, G.M., and Shaw, R.J. "Analytical Approach to Airfoil Icing." AIAA-81-0403, January 1981.

6. Brun, R.J. and Mergler, H.W., "Impingement of Water Droplets on a Cylinder in an Incompressible Flow Field and Evaluation of Rotating Multicylinder Method for Measurement of Droplet-Size Distribution, Volume-Median Droplet Size, and Liquid-Water Content in Clouds", NACA-TN-2904, March 1953.

7. Gelder, T.F., Smyers, W.H., Jr., and von Glahn, U., "Experimental Droplet Impingement on Several Two-Dimensional Airfoils with Thickness Ratios of 6 to 16 Percent," NACA TN3839, December 1956.

8. Hansman, R.J., "The Effect of the Atmospheric Droplet Size Distribution on Aircraft Ice Accretion," AIAA 84-0108, 1984.

9. Van Fossen, G.J., et.al. "Heat Transfer Distributions Around Nominal Ice Accretion Shapes Formed on a Cylinder in the NASA Lewis Icing Research Tunnel." AIAA-84-0017, January 1982.

10. Messinger, B.L. "Equilibrium Temperature of an Unheated Icing Surface as a Function of Airspeed." Journal of the Aeronautical Sciences, January 1953, pp 24-42.

11. Ludlam, F.H., "The Heat Economy of a Rimed Cylinder," Quarterly Journal of the Royal Meterological Society, Vol. 77, 1951, pp 663-666.

12. Macklin, W.C., and Payne, G.S., "A Theoretical Study of the Ice Accretion Process," Quarterly Journal of the Royal Meterological Society, Vol. 93, 1967, pp 195-213.

13. Hansman, R.J. and Kirby, M.S., "Measurement of Ice Accretion Using Ultrasonic Pulse-Echo Techniques," Journal of Aircraft, Vol. 22, June 1985, pp. 530-535.

14. Hansman, R.J., and Kirby, M.S., "Real-Time Measurement of Ice Growth During Simulated and Natural Icing Conditions Using Ultrasonic Pulse-Echo Techniques," AIAA 86-0410, 1986.

15. Gelder, T.F., and Lewis, J.P., "Comparison of Heat Transfer from Airfoil in Natural and Simulated Icing Conditions," NACA TN2480, September 1951.

OHIO UNIVERSITY

INVESTIGATION OF AIR TRANSPORTATION TECHNOLOGY AT OHIO UNIVERSITY, 1986

Richard H. McFarland
Avionics Engineering Center
Department of Electrical Engineering
Ohio University
Athens, Ohio

INTRODUCTORY REMARKS

Several important goals were achieved with the work supported by the Joint University Program during 1986. Among these goals is the first DC-3 flight with a Navstar Global Positioning System (GPS) receiver collecting positional data and allowing comparisons with simultaneous collected data from the Long Range Navigation system Loran-C. The principal purpose for this instrumentation was to learn of the detailed characteristics evident in the Doppler frequency shift from signals being received onboard an aircraft in flight (ref. 1).

This work was correlated with a thesis effort by a student who demonstrated the feasibility of using a despread spectrum technique to obtain positional information from GPS without knowledge of the code (ref. 1). By using Doppler information rather than range measurements one can also obtain positional information. The theory was mechanized by building a correlator and delay line which allowed a demonstration in the laboratory that the concept was indeed valid. The student has subsequently taken a position with an organization which is interested in extending this work.

Work with both GPS and Loran-C at Ohio University motivated the study of the use of Loran-C to augment the GPS capability. Especially in the present time frame when there are but a few satellites in orbit, additional navigational data are desirable, and these can come from a Loran-C station. This augmentation is expected to be useful for monitoring and integrity checking of GPS signals.

A completion of the Digital Autonomous Terminal Access Communications (DATAC) work has been achieved. This began with a student intern in residence at Langley Research Center. More systems in aircraft dictate more efficient and effective communications between units. The Airlines Electronic Engineering Committee of ARINC has evaluated comments concerning such a data bus which they consider as having the potential for improving integrity such that no single point terminal failure would significantly degrade the integrity of the data bus.

A continuing effort has been under way in collecting Loran-C data (ref. 2). The purpose of this is to learn of the variations in positional information as a function of the seasons and weather. Quantifying the grid shifts in the Ohio area has been achieved (ref. 3).

An investigation is beginning on the use of automatic data transfer from ground stations to an airplane. Particular emphasis is on handling weather data. A specific goal is for the system to be extremely efficient principally because of the limited radio frequency spectrum available for such use and the tremendous amounts of weather data that will soon become available with the central weather processor and Next-Generation Weather Radar (NEXRAD) systems that are now being developed.

Finally, work has begun on reliability assessment of avionics equipment. The need for high reliability is well known. Many current items used in aviation, general aviation in particular, are plagued by unacceptable high failure rates. The increase in the use of more complex avionics to achieve landings with lower and lower landing minima (Category III) makes it imperative to improve reliability. This will be stressed through design approaches (ref. 4).

This year has been fruitful and beneficial to the participants of the program. Ohio University continues to feel strongly that this Joint University Program and engineering investigation is extremely valuable to its students who have the opportunity to become thoroughly involved with contemporary engineering.

ANNOTATED REFERENCES

1. Laube, J. P.: An Investigative Study of Blind Despreading and Doppler Tracking Using Autocorrelation. Ohio University, Department of Electrical Engineering, Master's Thesis, June 1986.

   A simplified approach to detection of signals from an existing satellite navigation system is presented, which offers flexibility and possible use on several similar systems. A brief history and general overview are provided, developing the desirability of the technique described. The concept is presented analytically and experimentally verified. Results show conclusively that autocorrelation of a spread spectrum signal can occur, even when the signal is below the noise floor. The detection of this signal can provide Doppler information. This Doppler information can provide position data with low-complexity circuits. Knowledge of the signal spreading code is not necessary, which allows for inter system compatibility and freedom from losing code privileges due to government policy decisions.

2. Edwards, J. S.: FAA/OHIO University Loran-C Monitor. Ohio University, Avionics Engineering Center, Interim Data Reports No. 6 through 10, Report No. OU/AEC 1-86TM-TRIU104-108, April 1986.

   These reports contain Loran-C monitor data which are subject to further processing. The data are provided to interested parties as preliminary information only.

3. Lilley, R. W., and Edwards, J. S.: Loran-C Monitor Correlation Over a 92-Mile Baseline in Ohio. Proceedings of the WGA 15th Annual Technical Symposium, New Orleans, Louisiana, 21-24 October 1986.

Two Loran-C monitors, at Galion and Athens, Ohio, were operated over a one-year period, measuring chain 9960 Time differences (TD) and Signal to Noise Ratios (SNR). Analysis of data concentrated on correlation of short-term TD variations during the winter months of 1985-86, over the 92-nm baseline. Excellent correlation was found, with slight additional improvement possible if local temperature is also included in the analysis.

4. Alikiotis, D. M.: Discrete Markov Chain Compression Method. Ohio University, Avionics Engineering Center, Report No. OU/AEC 6-86TM TRIU109, June 1986.

This paper presents a method for dealing with the problem of the combinatorial explosion of the Discrete Markov Chains when a complex system is analyzed. A comparison between the standard Markov process or model and the Discrete Markov Chain Compression Method is also presented.

LORAN-C MONITOR CORRELATION OVER A 92-MILE BASELINE IN OHIO

Robert W. Lilley and Jamie S. Edwards
Avionics Engineering Center
Ohio University
Athens, Ohio

Abstract

Two Loran-C monitors, at Galion and Athens, Ohio, were operated over a one-year period, measuring chain 9960 TD and SNR. Analysis of data concentrated on correlation of short-term TD variations during the winter months of 1985-86, over the 92-nm baseline.

Excellent correlation was found, with slight additional improvement possible if local temperature is also included in the analysis. Although SNR and TD effects were suspected during the presence of thunderstorms near the monitors, the scope of the study did not permit storm-by-storm analysis. This is a necessary area for future work.

A computer tape data base of all measurements was produced, with measurements at both sites included. Data recording and analysis concentrated on the fall and winter months of September 1985 through mid-February 1986.

Background

Following a measurement study [1] to determine the suitability of Loran-C signals at Galion, Ohio, for instrument approach support, a ground monitor was installed to obtain data on signal variations at the site. The monitor consisted of a Northstar 6000 receiver linked to a small computer, driving a digital tape recorder [2]. An uninterruptible power supply was provided after discovery of frequent momentary power outages at the site. Subsequently, a monitor using an ARNAV AVA-1000 receiver was installed at Athens, Ohio, approximately 92 nm south of Galion.

Galion monitor coordinates were determined by theodolite and laser ranger measurement from the runway threshold benchmarks surveyed for the initial study [1]. At Athens, a survey combining trans-located TRANSIT measurements with conventional ground survey techniques was used. Expected TD values were then determined using the FAA Airport Screening Program [3, 4].

Various investigators have measured the long-term seasonal variation and have compared techniques for modeling the observed phenomena [see, for example, 5]. For the work reported here, shorter term

variations were emphasized, while the entire measurement data base was preserved for combination with others data for subsequent analysis as desired.*

Short-period variations may be caused by thunderstorms in the vicinity of the monitor, in which case SNR values fall due to increased local noise. The TD noise then also increases, reducing the reliability of the measure over a period of minutes or hours, but generally retaining the longer term mean value. Variations with weather system movement as the suspected cause occur over a period of hours or days, depending upon weather dynamics. For this study, the Loran-C sample period was extended to one hour by averaging to permit comparison of general weather effects. Raw data plots were inspected for evidence of storm-related variations.

Short-period TD variations are important, although generally smaller than seasonal variations. Refinement of Loran-C instrument approaches in the future through pseudo-differential use of monitor data will require knowledge of these TD movements. Storm-related SNR effects on TD quality are of concern both because of the resulting monitor output TD noise and because the storm is simultaneously affecting the airborne receiver. Differences between monitor and navigation receiver response to the impulse noise could well cause divergent TD values, accentuating position errors.

Data Collection

The two monitors were operated simultaneously during the winter of 1985-86. Each unit was designed to record all TDs and SNR values for Loran-C chain 9960 at approximately one-minute intervals. Tape recording limitations at the Athens site prompted a 5-minute interval for this monitor. Each measurement was time-tagged with date and time to one second. Initial results were reported in graphical form [4, for example], and computer tapes were aggregated into a complete data base for subsequent analysis.

At Galion, some 301,000 observations were recorded, most during the months of August 1985 through mid-February 1986. A subsequent recording session was performed during April 1986 to confirm that TD values had returned to warm-weather values observed in mid-1985.

At Athens, 29,000 measurements were recorded during a period bracketing the Galion monitor's operation.

Data Review

An overview of the data plots shows the anticipated seasonal variations, plus interesting short-term features. Thunderstorms in the Galion local area may have produced SNR reductions in all primary-triad (MYZ) measurements, but time and scope permitted only a partial analysis of these data. These local events were characterized by highly variable SNR in all three

*The tape data were delivered to the DOT Transportation Systems Center, Systems Evaluation Division, Cambridge, MA.

traces, with reductions of as much as -12 dB, lasting generally for 1-2 hours. The TD variations in both M-Y and M-Z were ± 0.25 to ± 0.5 μsec during strong events. Receiver cycle slips did not occur, likely due to the short-pulse nature of the noise. The TD effects were noisy in character, with the mean value remaining at the pre-event position.

Hurricane Gloria, moving up the U. S. east coast in late October 1985, apparently caused selective reduction in the Carolina Beach (Y) trace of up to 6 dB, leaving Dana (Z) and Seneca (M) unaffected.

It is evident from the data that local noise events can cause monitor data variations which would cause no-go approach indications. Such noise may originate with thunderstorms; this was not determined in all cases at Galion. The magnitude of such variation will be dependent upon the characteristics of the monitor receiver used. It is important to determine the effects of this type of interference on the receivers to be used in FAA approach monitors so that output data processing can minimize false no-go indications. If storms are the cause of these events, a single storm near the monitor could shut down approaches over a large area. A mosaic algorithm, using more than one monitor, may be necessary.

Effects of SNR on TD quality were considered for the MYZ triad at Galion (refer again to figure 1, at non-storm periods). The master SNR varied from +5 dB during the day, to +3 dB at night. The M-Z TD, with Dana signals at +5 dB day and +3 dB night, showed variations of generally less than ± 0.1 μsec., even at night, as expected for these high SNR values. No significant day/night bias is evident.

The Carolina Beach (Y) signal varied from +3 dB day to -6 dB night, and the TD varied approximately ± 0.05 μsec day and ± 0.1 μsec night.

These observations indicate TD position noise of less than 100 feet short-term, and are typical of the total observation period. It should be possible to relax the 0 dB SNR requirement for Loran-C approaches once experience is gained with the actual monitor receivers.

Non-primary TDs from Caribou and Nantucket evidenced position variations of from ± 1,200 to 2,400 feet at -12 dB, and of ± 400 feet at -8 dB, respectively. Poor geometry and low SNR combine to disqualify these TDs in Ohio.

Figure 2 shows an example of TD variation with movement of weather systems. This observation led to the temperature correlation discussed in the next section. A TD shift of nearly 0.25 μsec occurred, with the peak variation coincident in time with the passage of a strong cold front (temperature drop of > 30 degrees in approximately 12 hours). The lowest temperature of 20 degrees F occurred at 0000 on day 337. Temperatures then recovered to pre-frontal levels over the next nine days.

This weather-related effect is most pronounced during the winter and appears to introduce most of the short-to-medium term variation in the signal.

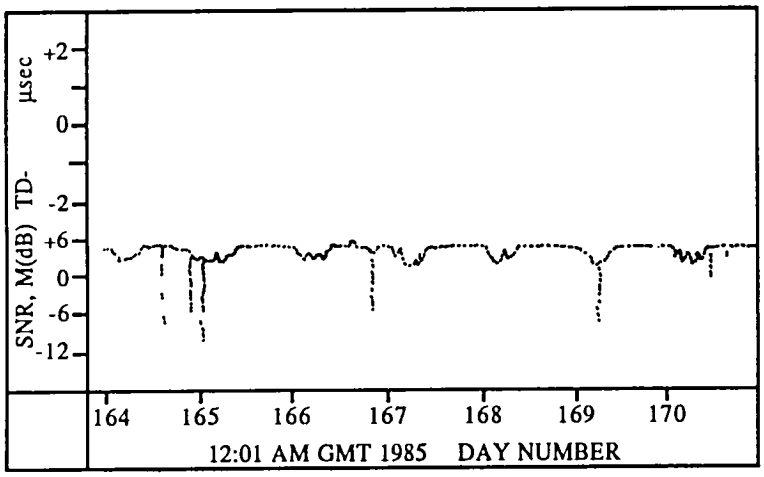

GALION, OH LORAN-C MONITOR
INTERIM DATA FOR 9960 TD M

Figure 1a.

Noise and diurnal events;
Ohio primary triad.

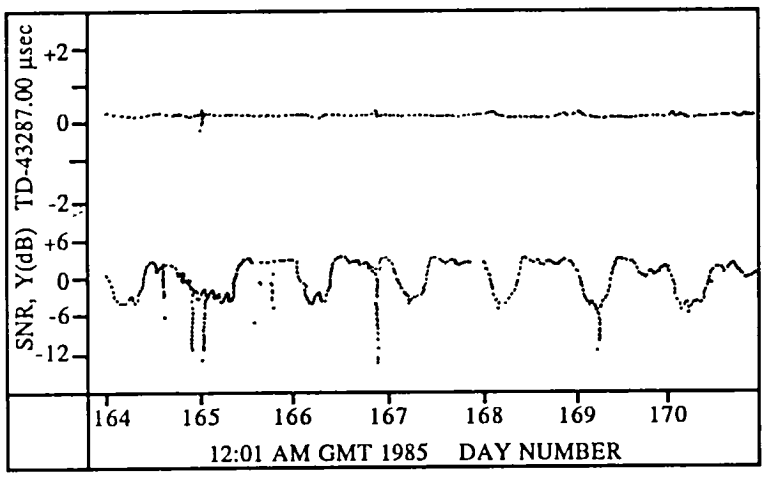

GALION, OH LORAN-C MONITOR
INTERIM DATA FOR 9960 TD MY

Figure 1b.

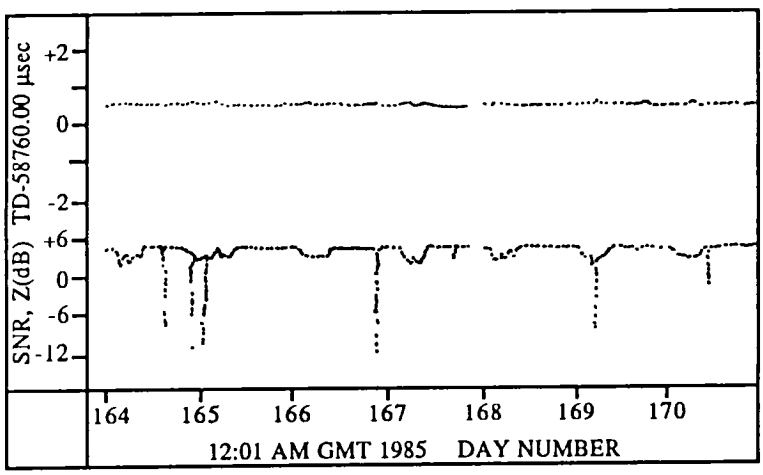

GALION, OH LORAN-C MONITOR
INTERIM DATA FOR 9960 TD MZ

Figure 1c.

Correlation of Monitor Data

Some insight into the range of validity of Loran-C monitor data may be obtained from the correlation of Athens and Galion monitors' output. Located 92 nm apart on essentially a north-south line, these two monitors produced highly correlated outputs, as may be seen in general from figure 3. Tables 1 and 2 give the comparisons in more detail.

CORRELATION

X_1 = Gallon TD or SNR

X_2 = Athens TD or SNR

X_4 = Athens Temperature

	r_{12}	$r_{12.4}$	$r_{14.2}$
MW	0.952	0.806	0.247
MX	0.954	0.802	0.341
MY	0.954	0.801	0.339
MZ	0.954	0.801	0.337
SNRM	0.954	-	-
SNRW	0.888	-	-
SNRX	0.937	-	-
SNRY	0.950	-	-
SNRZ	0.955	-	-
	n = 1072	n - 32	

Data is for January 15 through February 16, 1986

Table 1
Correlation and Partial Correlation

REGRESSION

Gallon TD =

Athens TD (A) + Athens Temperature (B)

	A	B
MW	0.819	0.153
MX	0.769	0.213
MY	0.769	0.213
MZ	0.769	0.213

MULTIPLE CORRELATION

Quality of Prediction Based on Actual Gallon TDs

	$R_{1.24}$	$R^2_{1.24}$	r^2_{12}
MW	0.955	0.913	0.906
MX	0.960	0.922	0.910
MY	0.960	0.922	0.910
MZ	0.960	0.922	0.910

Table 2
Regression and Prediction

Figure 3 is a plot of the 1-hour averaged data from Galion and Athens monitors from January 15 through February 16, 1986. The period was chosen to illustrate typical winter-months movement of a TD. A range of nearly 0.5 μsec is seen at both locations.

Table 1 shows results of simple correlation between Galion and Athens, on TD and SNR values. As shown, high positive correlation is shown in all cases, with a correlation coefficient r(12) above 0.95 for all TDs. Partial correlations r(12.4) and r(14.2) indicate the degree to which Athens TD and Athens temperature account for variance in Galion TD, with the third variable held constant. These partials are required for computation of the regression coefficients.

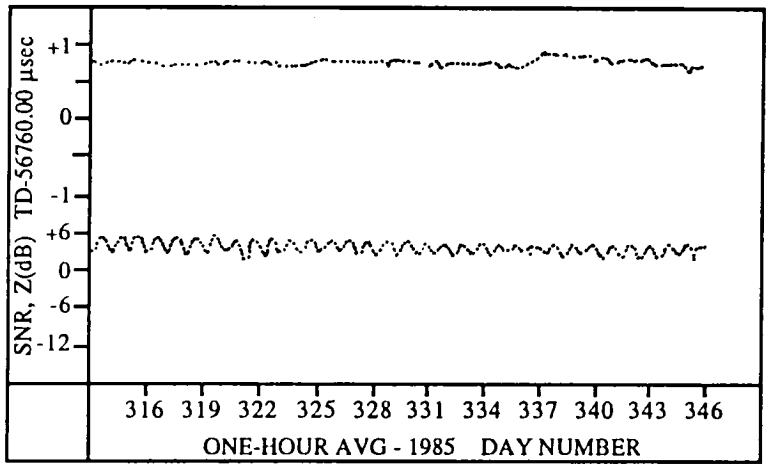

GALION, OH LORAN-C MONITOR
INTERIM DATA FOR 9960 TD MZ

Figure 2.

Cold-front passage.
(30° temperature shift)
December 3, 1985.

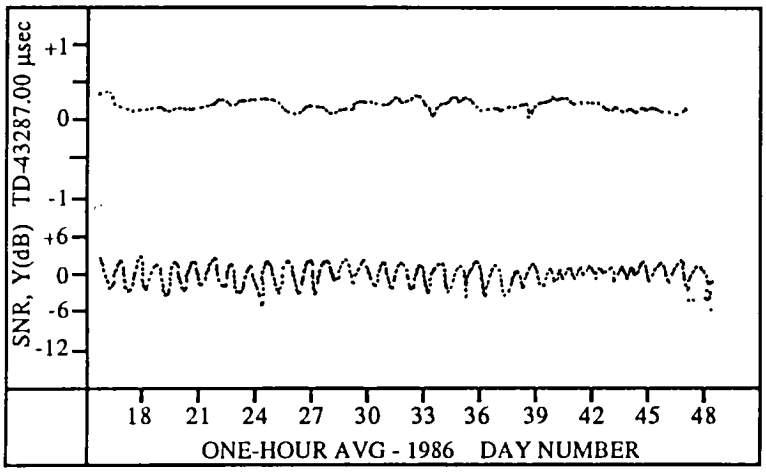

GALION, OH LORAN-C MONITOR
INTERIM DATA FOR 9960 TD MY

Figure 3a.

January-February data for
M-Y, averaged to 1-hour
intervals; Galion.

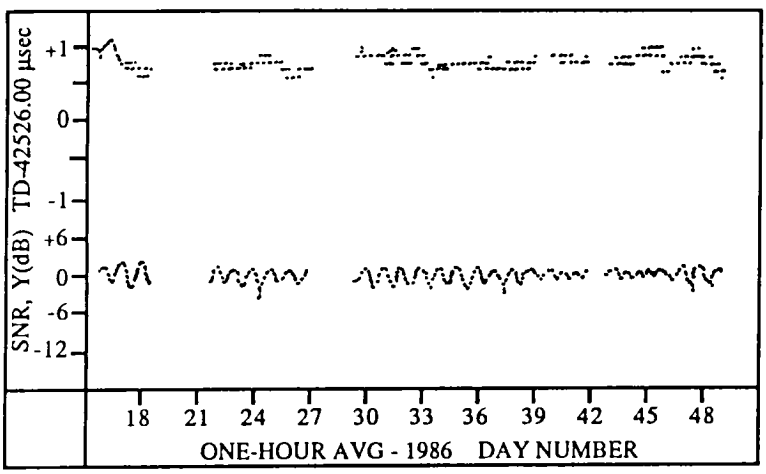

O.U. AIRPORT LORAN-C MONITOR
INTERIM DATA FOR 9960 TD MY

Figure 3b.

January-February data for
M-Y, averaged to 1-hour
intervals; Athens.

In Table 2, the linear prediction equation is developed. The Galion TD value is predicted from Athens TD and temperature, 92 nm away. Coefficients A and B indicate the weight given to each of the predictor variables. As expected, the Galion TD is much more closely related to the Athens TD than to the Athens temperature as indicated by the high A values and the low values for B.

Table 2 concludes with the multiple correlation, giving an index of quality for the prediction. The predicted TD values from the regression equation are compared with actual Galion data. R(1.24) indicates the coefficient of multiple correlation for each TD using the linear prediction equation A and B values. The square of this coefficient is the coefficient of determination, which can be interpreted as "... for TD M-W, 91.3% of the variation at Galion is accounted for by variations at Athens ...", for example. The degree to which temperature helps the prediction may be shown by the square of r(12), shown in the last column of Table 2. In the M-W case, 90.6% of the Galion variation is accounted for by simple correlation with Athens, ignoring temperature altogether. The result is an improvement of less than one percent when temperature is considered.

The fact that coefficients for M-X, M-Y and M-Z are identical is coincidental and flows from the fact that r(12) was the same in each case.

The data show good correlation over a baseline similar to that which has been proposed for FAA monitors. Note that the correlations performed here use approximately one month's data and thus will not be sensitive to longer term seasonal variations.

Conclusions

Local thunderstorms may have caused receiver-output variations. A single storm could shut down Loran-C approaches over a large area, unless overlapping monitor coverage permits alternate monitor consideration.

The data indicate minimal TD quality derogation with negative SNR as low as -6 dB at a secondary, with high positive SNR at the master. Further consideration to permitting approaches, even with monitor SNR values below zero, is warranted. The TD variations with SNR tend to be zero-mean noise, with minimal day/night bias present.

Over the 92-nm path tested in Ohio, correlation of short-term TD variations is good, and some additional improvement is obtained by including temperature in the computation. The increase is small and does not warrant instrumenting monitors for temperature measurement.

Recommendations

For the primary triad in Ohio, TD data show few ill effects of SNR as low as -6 dB. Consideration should be given to relaxation of the 0 dB monitor SNR requirement for Loran-C instrument approach initiation.

While TD data show excellent correlation over the 90-mile baseline, it should be noted that the north-south orientation may contribute to this positive correlation, since both monitors are affected by typical weather patterns at nearly the same times. A similar east-west baseline distance should be similarly measured and analyzed.

If weather effects are to be measured in subsequent tests, consideration should be given to humidity as a variable, rather than temperature. Also, this measurement should be automated and recorded at intervals similar to the Loran-C samples.

Specific measurements should be carried out to characterize short-term monitor effects caused by thunderstorm activity. Ground-based Stormscope and NWS weather radar data could be used as independent-variable measures.

References

[1] Lilley, R. W. and Brooks, N. K., "Evaluation of Loran-C for Instrument Approaches in Ohio," Proceedings of the WGA, Technical Symposium, October 1984, WGA, Bedford, MA.

[2] Edwards, J. S., "Loran-C Monitor Technical Manual," Technical Memorandum J-2, Avionics Engineering Center, Ohio University, May, 1985.

[3] El-Arini, M. B., "Airport Screening Model for Nonprecision Approaches Using LORAN-C Navigation," Report No. MTR-83W180, The MITRE Corporation, McLean, VA, May 1984.

[4] Lilley, R. W. and McCall, D. L., "Operational Considerations for Loran-C in the Non-Precision Approach Phase of Flight," Proceedings of the WGA, Fourteenth Annual Convention, October 1985, WGA, Bedford, MA.

[5] McCullough, J., et al., "A First Look at Loran-C Calibration Data in the Gulf of Mexico,", Woods Hole Oceanographic Institution, Woods Hole, MA.

Acknowledgements

This work was supported by DOT/TSC Contract DTRS-57-83-C-00097, TTD-6. Funding was also received from the Ohio Department of Development, through the Aviation Safety Institute of Columbus, Ohio; the FAA and NASA Langley through the Joint University Program in Air Transportation Systems; and the Ohio Department of Transportation, Division of Aviation. Columbus, Ohio consultant N. Kent Brooks assisted with Galion liaison and data-collection operations and with weather data capture.

DATAC BUS MONITOR

Stanley M. Novacki, III and Robert J. Thomas, Jr.
Ohio University
Athens, Ohio

INTRODUCTION

The Digital Autonomous Terminal Access Communications (DATAC) bus is a multiple transmitter data bus developed by the Boeing Company to interconnect various aircraft systems. Figure 1 shows a typical DATAC bus installation for the NASA B-737 aircraft. Essentially a local-area network for use aboard airliners, it uses Carrier-Sense, Multiple Access with Collision Detection (CSMA/CD) protocol. This means that operation of the bus relies on each system that uses a certain set of rules when it "broadcasts" a message via the bus. In the simplest mode of operation, each system listens to determine if the bus is currently in use. If no bus activity is detected, each system enables a counter with a unique value. The first counter to reach its terminal value assumes the right to broadcast over the bus and transmits its data. When the other terminals detect this bus activity, even if their respective timers are active, their timers are reset and are disabled until bus inactivity is again detected. When the current broadcasting system has concluded its transmission, its timer is disabled until all other systems have broadcast. This ensures that one system will not monopolize the bus. The system with the next shortest terminal count will expire next, and it will access the bus. The process is repeated until all systems have had the opportunity to transmit. After all stations have transmitted their messages, the process repeats itself.

A liability of this autonomous protocol is that it is not possible to interrogate a specific subsystem to determine its current operating condition. This would be particularly useful during bus development and testing. Should problems arise with a DATAC system, it would be useful to have a system which would enable an operator to identify which systems are using the bus and the data that they are transmitting. Having an independent means to monitor bus transactions would help in locating problem areas on the bus.

BUS MONITOR UNIT DEVELOPMENT

A bus monitor unit has been developed for the DATAC data bus. The bus monitor unit consists of two systems: a Zilog Z8002-based S100 bus microcomputer system that connects to a DATAC terminal and receives data appearing on the bus, and an IBM PC-compatible computer used to display and interpret that data. The bus monitor unit configuration is shown in figure 2. The Z8002 system receives data from the DATAC terminal by way of a ZBUS-to-S100 interface. The DATAC terminal presents data using the Zilog ZBUS component interconnect specification. The interface circuit translates the ZBUS data transfer signals to their S100 counterparts, allowing the bus terminal to deposit data into the Z8002 systems Random Access Memory (RAM) using a Direct Memory Access (DMA) type operation. Once the data has been received and identified by the Z8002 system, it is transmitted to via a 9600 bits-per-second RS-232C serial data link to the MS-DOS system, which can analyze, display, and store the data.

This bus monitor unit is able to process a maximum of 24 words of data during the 50 milliseconds data repetition rate of the Mode A operation and a maximum of four words during the 10 milliseconds repetition rate of Mode C. The total number of words possible during either the 50 or 10 milliseconds repetition rates is contingent upon the number of systems that are using the bus, but it is possible to estimate the maximum number of words appearing on the system by dividing the frame repetition rate by 20 microseconds to transmit a word across the bus. For example, 50 milliseconds per frame divided by 20 microseconds per word would yield 2,500 words per 50 milliseconds frame. This is a high estimate, since the label words used by each bus system take 24 microseconds themselves to transmit and be processed.

The limiting factor in processing the data is the relative slowness of the serial data link between the Z8002 and MS-DOS systems. The serial link was chosen because a CP/M computer with a closed architecture was originally chosen to serve as the console device for the S100 system. Because of its closed architecture, RS-232 was the only way to transmit data between the two systems. The CP/M system failed and was replaced by the MS-DOS system. Rather than redesign major parts of the system to accommodate a faster link between the two systems, the bus monitor unit was completed using RS-232 and then evaluated.

CONCLUSIONS AND RECOMMENDATIONS

Because of the general nature of the bus monitor unit, it is desirable to process large amounts of data in real time. Test results of the existing bus monitor have indicated areas for improvement. The most obvious improvement is to increase the speed of the data transfers between the S100 and MS-DOS systems. This could be achieved by using a bidirectional 16-bit port between the two computers. Such a port would improve the data transfer rate by nearly an order of magnitude. An expensive but more flexible approach would be to revise the design of the system to incorporate the Z8002 system into the MS-DOS system enclosure. The SS-62 bus used by most IBM PC-compatible computers provides several DMA channels which would be used for even higher-speed data transfers between the S100 and MS-DOS systems. This approach simplifies the overall system design by consolidating the entire unit into a single chassis with a single power supply and one set of support peripherals. The high throughput available with a DMA-type transfer could make real-time analysis and reconstitution of large amounts of data possible, a highly desirable feature for the bus monitor unit.

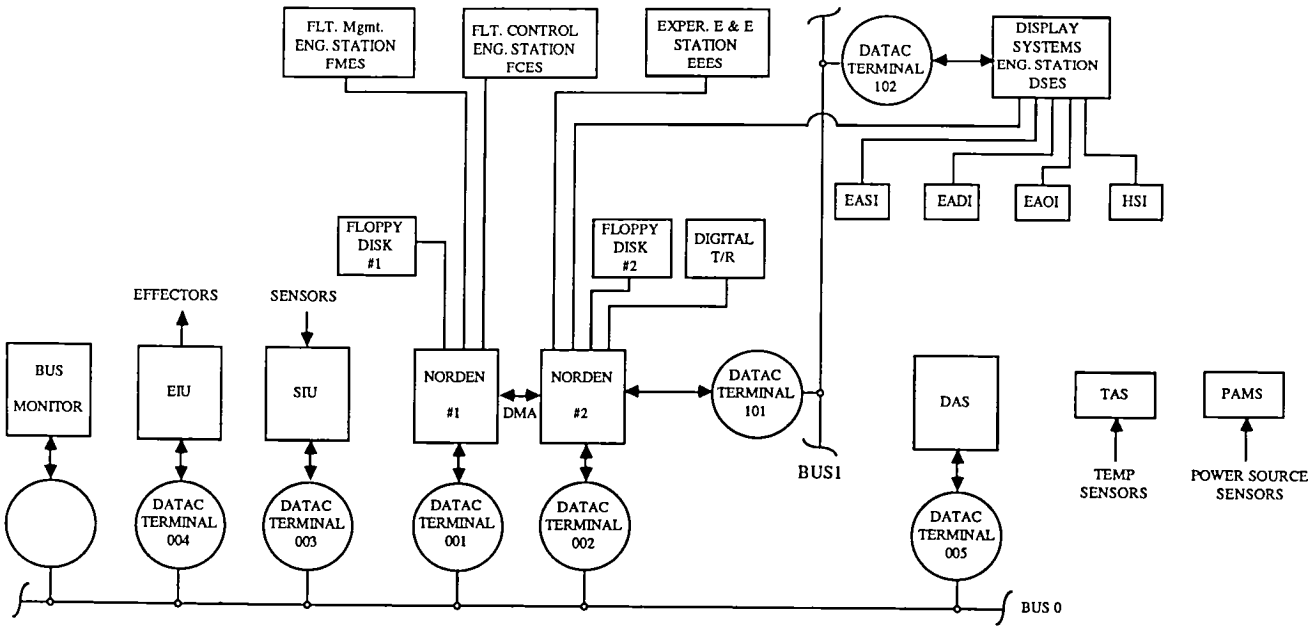

Figure 1. Typical DATAC bus installation for the NASA B-737 aircraft.

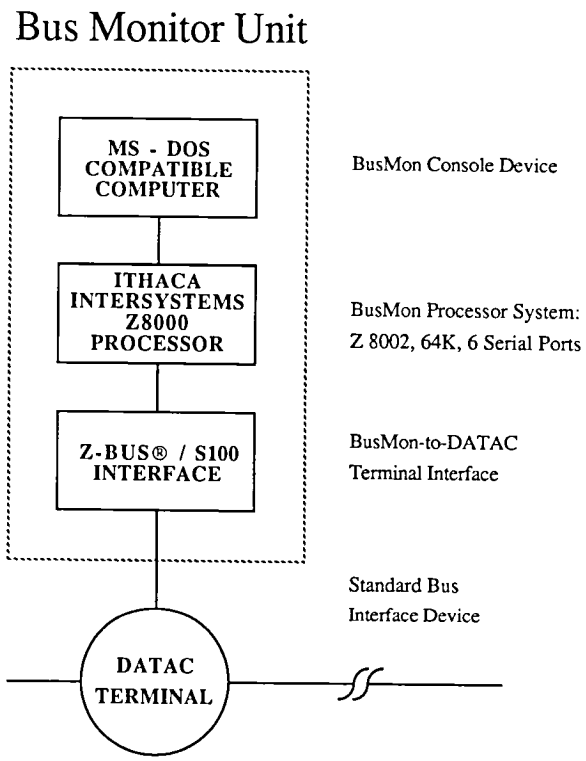

Figure 2. DATAC bus monitor unit configuration.

INTEGRATED MULTISENSOR NAVIGATION SYSTEMS

Frank van Graas
Ohio University
Athens, Ohio

BACKGROUND

The multisensor navigation systems research evolved from the availability of several stand-alone navigation systems and the growing concern for aircraft navigation reliability and safety. The intent is to develop a multisensor navigation system during the next decade that will be capable of providing reliable aircraft position data. These data will then be transmitted directly, or by satellite, to surveillance centers to aid the process of air traffic flow control. In order to satisfy the requirements for such a system, the following issues need to be examined:

- Performance
- Coverage
- Reliability
- Availability
- Integrity

The presence of a multisensor navigation system in all aircraft will improve safety for the aviation community and allow for more economical operation.

COMBINED GPS, LORAN-C, AND ALTIMETER

For the development of an integrated multisensor navigation system several navigation sensors were considered including the Long Range Navigation System (Loran-C), the Global Positioning System (GPS), an Inertial Navigation System (INS), and an altimeter. Based on system cost and complexity, signal characteristics and sensor accuracies, the inertial sensors are omitted from the initial design. Although the use of inexpensive inertial sensors can reduce the variance of the position solution error, the overall position accuracy still depends on the absolute position sensors such as Loran-C and GPS.

During last year, a GPS receiver (FAA Experimental Dual Channel GPS Receiver), a Loran-C receiver (Texas Instruments 9900), and an altimeter were installed in the DC-3 research aircraft. Figure 1 shows the functional block diagrams of the equipment. Data from the navigation sensors is stored on magnetic tape for post test analysis. The GPS receiver was initially installed to provide verification data for a codeless GPS tracking scheme developed under the FAA/NASA Joint University Program (JUP) (ref. 1). Loran-C receiver and application technology has been part of the JUP at Ohio University since 1976.

The navigation sensors were flight-tested during June 1986. The flight test results provide novel capabilities for a direct comparison between GPS and Loran-C. Figure 2 shows the ground track results for a typical data collection flight across southern and central Ohio on June 22, 1986. The duration of the flight was 24 minutes and contained two turns at an altitude of 12,000 feet.

Figure 3 shows the navigation solution differences between GPS and Loran-C in the East direction and figure 4 shows the differences in the North direction. The cause of the larger differences during the two turns is illustrated in figure 5. This figure shows the ground tracks for GPS and Loran-C during the second four-minute turn. From this figure it can be concluded that the Loran-C navigation solution lags in time due to a larger time constant used in the navigation filter. Even with the lag in the Loran-C solution, differences between GPS and Loran-C were typically less than 0.15 nmi during the flight. However, the stand-alone use of both systems does not provide optimal navigation and failure detection capabilities.

Original techniques were developed during the last year for a fully integrated GPS/Loran-C navigation system. Loran-C will be used in the ranging mode providing ranging accuracies on the same order of magnitude as GPS range measurements. In addition, the integrated system will have the following advantages compared to a combination of stand-alone GPS and Loran-C:

- Larger coverage area: degraded satellite observability can be compensated for by one or two range measurements to Loran-C stations.

- More measurements are available than necessary for the navigation solution allowing for user autonomous failure detection and system monitoring.

- The integrated system is expected to meet the requirements for sole means random navigation (RNAV) systems and nonprecision approaches.

FUTURE RESEARCH

Next year's multisensor navigation research will be focused on the following areas:

- Realize Loran-C direct ranging.

- Combine receiver clocks for GPS and Loran-C.

- Ground test Loran-C receiver.

- Integration of high-quality altimeter data.

- Computer simulations to predict the performance and coverage of the integrated GPS/Loran-C navigation system.

- Flight experiments with ground-referenced tracking.

The sensors involved in the flight experiments are GPS, Loran-C, and an altimeter. For this experiment, the hyperbolic Loran-C receiver will be replaced by a ranging receiver, most likely the Racal Megapulse Accufix 500.

Aircraft data will be referenced to measured positions obtained using the Ohio University ground tracking system. The data will then be post processed on the ground to prove the multisensor navigation concepts.

Successful flight tests of the integrated GPS, Loran-C, and altimeter system will be used as a basis for further multisensor navigation system research. Algorithms for efficient integrity checking will be developed and implemented. An inertial measurement unit will be added to the system to reduce position noise and also to aid failure detection algorithms.

REFERENCES

1. Laube, J.P.: An Investigative Study of Blind Despreading and Doppler Tracking Using Autocorrelation. Ohio University, Department of Electrical Engineering, Master's Thesis, June 1986.

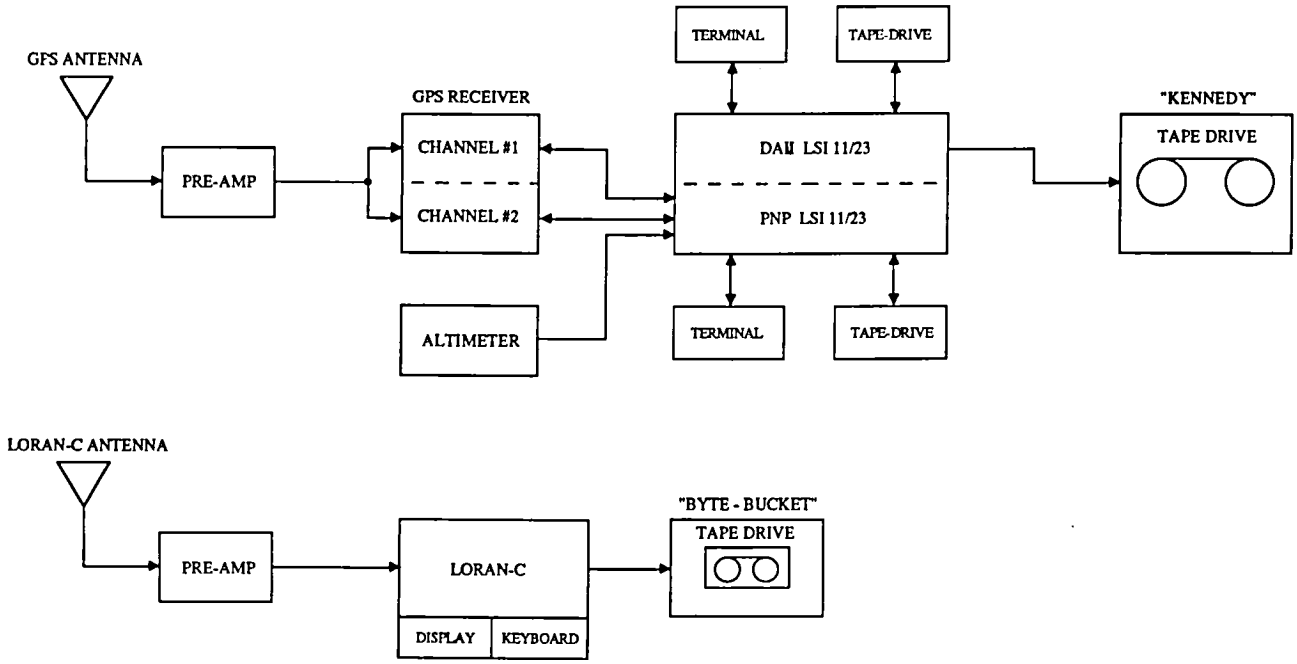

Figure 1. Functional block diagram of the navigation test bed in the Ohio University DC-3 research aircraft N7AP. The equipment consists of a dual channel GPS receiver, a Loran-C receiver, and an altimeter.

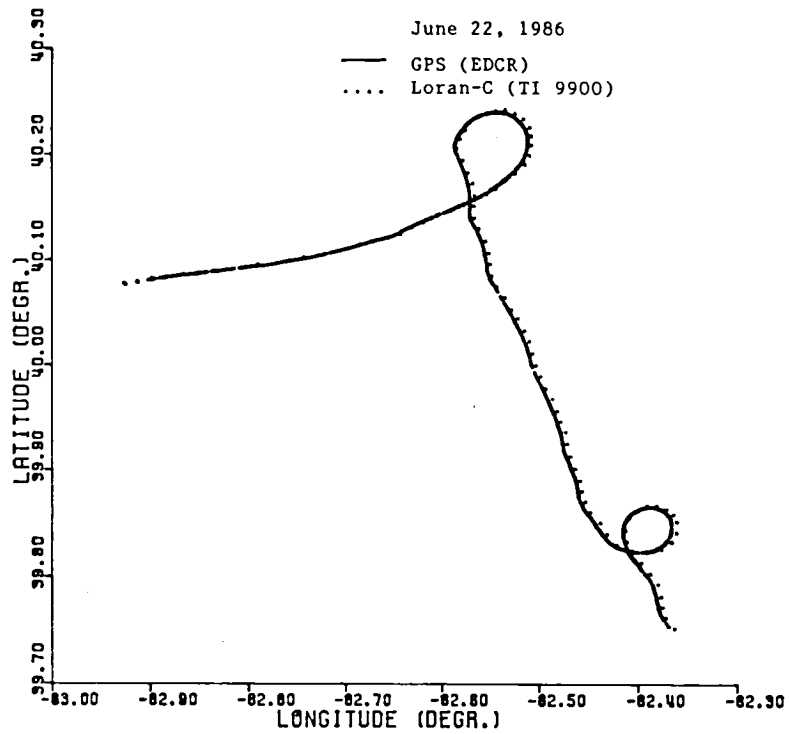

Figure 2. GPS and Loran-C ground tracks for a 24 minutes flight across southern and central Ohio on June 22, 1986.

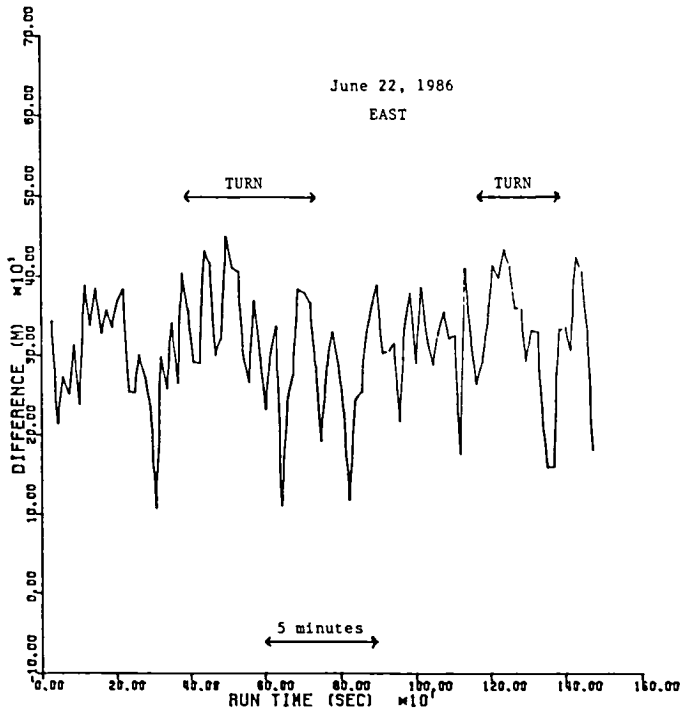

Figure 3. Navigation solution differences between GPS and Loran-C in the EAST direction.

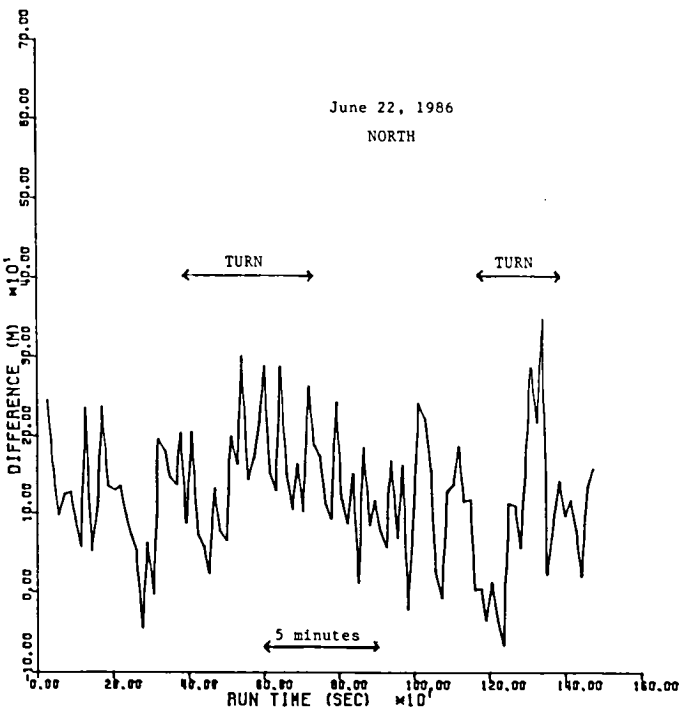

Figure 4. Navigation solution differences between GPS and Loran-C in the NORTH direction.

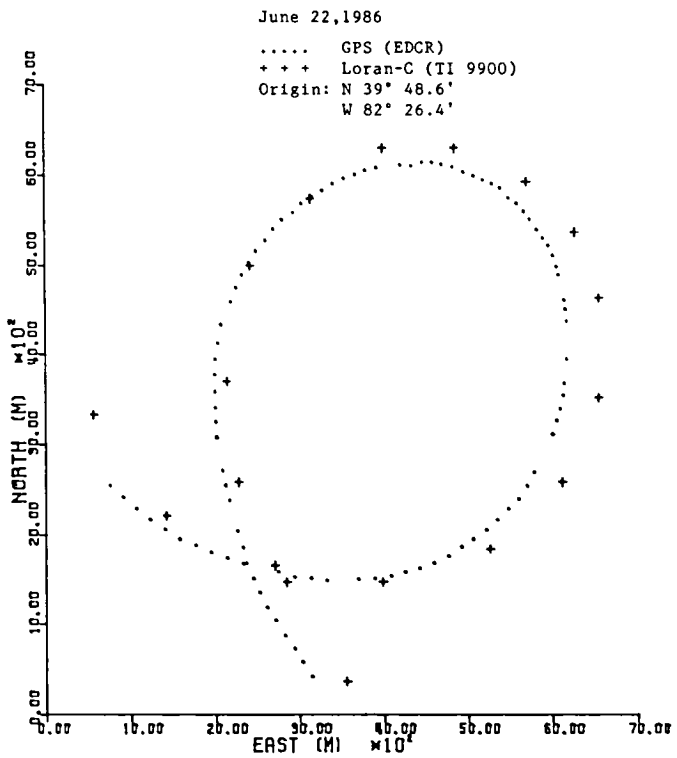

Figure 5. Ground tracks for the GPS and Loran-C navigation solutions during a four-minute turn.

INTEGRATED AVIONICS RELIABILITY

Dimitri Alikiotis
Ohio University
Athens, Ohio

INTRODUCTION

The integrated avionics reliability task is an effort to build credible reliability/performability models for multisensor integrated navigation and flight control. The 1986 research was initiated by the reliability analysis of a multisensor navigation system consisting of the Global Positioning System (GPS), the Long Range Navigation system (Loran-C), and an inertial measurement unit (IMU). Markov reliability models were developed based on system failure rates and mission time.

Figure 1 shows the mechanization of the multisensor navigation system based on GPS, Loran-C, and an IMU. Each sensor is implemented with triple redundancy. The decision making logic determines which sensors are to be used for navigation based on the Kalman filter residuals. Figure 2 depicts the state transition diagram for the multisensor system. The corresponding 16-state Markov model is shown in figure 3, with the assumption that no repairs are made during system operation.

In order to obtain position information from the IMU both the accelerometers and the gyros are needed. Using this information, the state transition diagram can be reduced to eight states as depicted in figure 4. The corresponding reduced Markov model is shown in figure 5. From the state transition matrix the stochastic probability matrix (SPM) can be obtained. The elements of the SPM represent the probabilities that the system will remain in a certain state (diagonal elements) and the probabilities that the system will make a transition to another state (off-diagonal elements). The SPM for the integrated navigation system is given in figure 6 along with the reliability formulas.

Starting the system from the initial state probability vector P(0), the state probabilities for some time later can be found by multiplying the state probability vector by the stochastic probability matrix. The number of multiplications is determined by the quotient of the mission time and the time interval between state updates.

As an example, consider the configuration as depicted in figure 1 and assume that the mean time between failure for each sensor is equal to 4,500 hours. It then follows that the probability of system failure during a mission with a duration of one hour is approximately one part in one hundred billion.

DISCRETE MARKOV CHAIN COMPRESSION METHOD

Markov analysis is based on the Stochastic Probability Matrix (SPM). The dimension of the SPM is determined by the nth power of two, where n is

the number of sensors in the system. For example, if a system consists of eight sensors, the dimension of the SPM is 256 by 256. Manipulation of matrices of this size is rather complicated.

A solution to the manipulation of large stochastic matrices was found by separating the sensors into statistically independent sets; i.e. the Discrete Markov Chain Compression Method (DMCCM). Figure 7 illustrates the DMCCM, the sensors are separated in sets and individual Markov models are made for the corresponding sets. The output of each smaller Markov model represents the failure probability for the given sensor set. All those outputs are merged into smaller size models again, until a single output is produced. The final (single) output represents the failure probability of the last system state for the specified mission time. This is also the probability that the system will have a total failure during the given mission time. A detailed description of the DMCCM can be found in reference 1.

FUTURE RESEARCH

Next year's reliability effort is defined with input from NASA Langley Research Center. This effort deals with the creation of a generic reliability tool for flight control systems operating in the terminal area. Figure 8 shows a multisensor flight control baseline system for terminal area guidance. The reliability model for this system is depicted in figure 9. The attitude, air data, and navigation aids are in series for the reliability evaluation since the system will fail if any of these three components fails.

In addition to the evaluation of a more complex avionics system, the system will also be allowed to incorporate fault detection and isolation (FDI) techniques (ref. 2). Adding FDI to the system increases the complexity of the reliability evaluation tremendously. This is illustrated in figures 10 and 11. Figure 10 shows the Markov model for a two-sensor system without FDI. Adding probabilities of fault detection, isolation, transient recovery, false alarm, and damage results in the Markov model shown in figure 11.

REFERENCES

1. Alikiotis, D. M.: Discrete Markov Chain Compression Method. Ohio University, Avionics Engineering Center, Report No. OU/AEC 6-86TM-TRIU109, June 1986.

2. Caglayan, A. K. and Lancraft, R. E.: An Aircraft Sensor Fault Tolerant System. NASA CR-165876, April 1982.

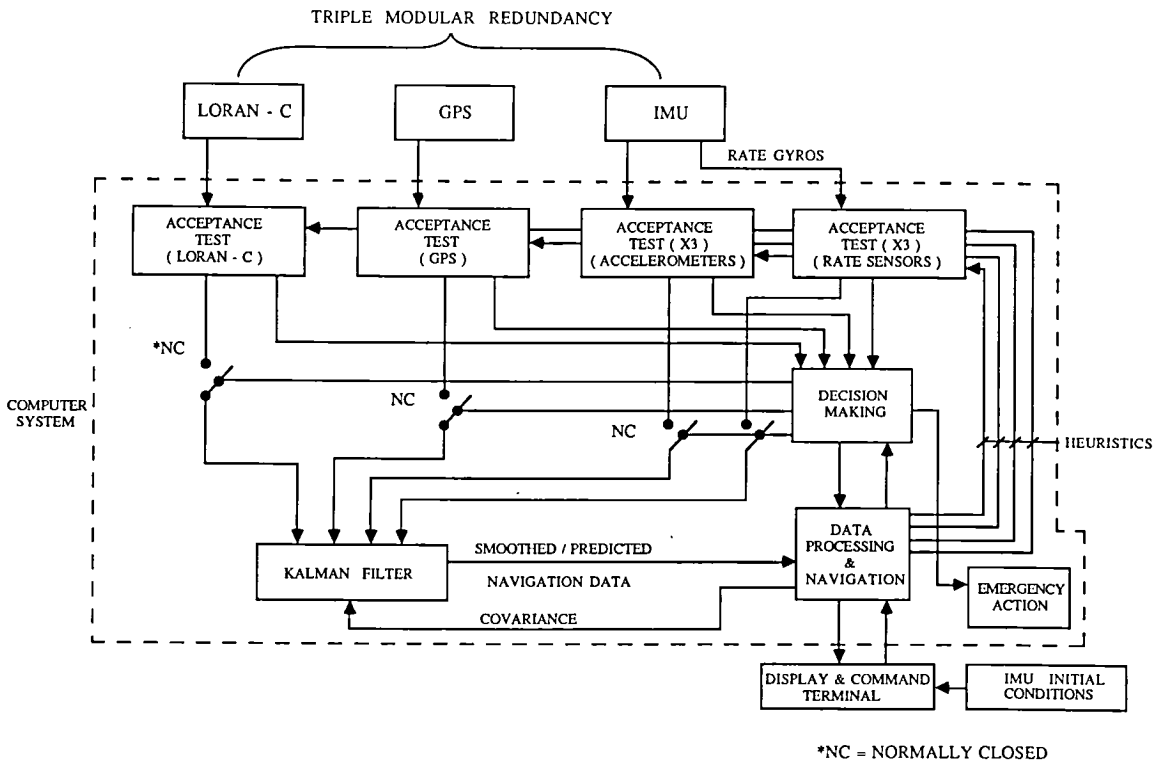

Figure 1. Multisensor navigation system mechanization for reliability analysis of an integrated GPS, Loran-C, and inertial measurement unit system.

STATE	DEFINITION
1	GYROS, ACCEL, GPS, LORAN
2	GYROS, ACCEL, GPS, $\overline{\text{LORAN}}$
3	GYROS, ACCEL, $\overline{\text{GPS}}$, LORAN
4	GYROS, $\overline{\text{ACCEL}}$, GPS, LORAN
5	$\overline{\text{GYROS}}$, ACCEL, GPS, LORAN
6	$\overline{\text{GYROS}}$, ACCEL, GPS, $\overline{\text{LORAN}}$
7	GYROS, ACCEL, $\overline{\text{GPS}}$, $\overline{\text{LORAN}}$
8	GYROS, $\overline{\text{ACCEL}}$, GPS, $\overline{\text{LORAN}}$
9	GYROS, $\overline{\text{ACCEL}}$, $\overline{\text{GPS}}$, LORAN
10	$\overline{\text{GYROS}}$, ACCEL, $\overline{\text{GPS}}$, LORAN
11	$\overline{\text{GYROS}}$, $\overline{\text{ACCEL}}$, GPS, LORAN
12	GYROS, $\overline{\text{ACCEL}}$, $\overline{\text{GPS}}$, $\overline{\text{LORAN}}$
13	$\overline{\text{GYROS}}$, ACCEL, $\overline{\text{GPS}}$, $\overline{\text{LORAN}}$
14	$\overline{\text{GYROS}}$, $\overline{\text{ACCEL}}$, GPS, $\overline{\text{LORAN}}$
15	$\overline{\text{GYROS}}$, $\overline{\text{ACCEL}}$, $\overline{\text{GPS}}$, LORAN
16	$\overline{\text{GYROS}}$, $\overline{\text{ACCEL}}$, $\overline{\text{GPS}}$, $\overline{\text{LORAN}}$

GYROS = GYROS GOOD
$\overline{\text{GYROS}}$ = GYROS FAILED
ACCEL = ACCELEROMETERS GOOD
$\overline{\text{ACCEL}}$ = ACCELEROMETERS FAILED
GPS = GPS GOOD
$\overline{\text{GPS}}$ = GPS FAILED
LORAN = LORAN-C GOOD
$\overline{\text{LORAN}}$ = LORAN-C FAILED

Figure 2. State transition diagram for the reliability analysis of a multisensor navigation system based on GPS, Loran-C, and and an inertial measurement unit.

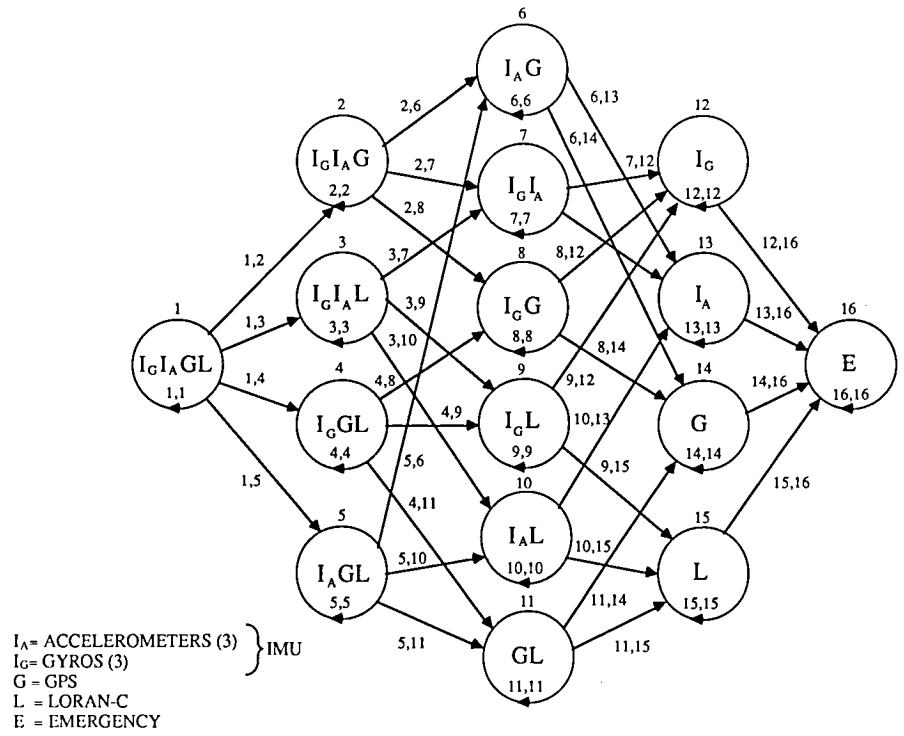

Figure 3. Sixteen-state Markov model for the reliability analysis of an integrated navigation system based on GPS, Loran-C, and and an inertial measurement unit.

STATE	DEFINITION
1	IMU, GPS, LORAN
2	IMU, GPS, $\overline{\text{LORAN}}$
3	$\overline{\text{IMU}}$, GPS, LORAN
4	IMU, $\overline{\text{GPS}}$, LORAN
5	IMU, $\overline{\text{GPS}}$, $\overline{\text{LORAN}}$
6	$\overline{\text{IMU}}$, GPS, $\overline{\text{LORAN}}$
7	$\overline{\text{IMU}}$, $\overline{\text{GPS}}$, LORAN
8	$\overline{\text{IMU}}$, $\overline{\text{GPS}}$, $\overline{\text{LORAN}}$

IMU = INERTIAL MEASUREMENT UNIT GOOD
$\overline{\text{IMU}}$ = INERTIAL MEASUREMENT UNIT FAILED
GPS = GPS GOOD
$\overline{\text{GPS}}$ = GPS FAILED
LORAN = LORAN - C GOOD
$\overline{\text{LORAN}}$ = LORAN - C FAILED

Figure 4. Reduced state transition diagram for the reliability analysis of an integrated navigation system based on GPS, Loran-C, and an inertial measurement unit.

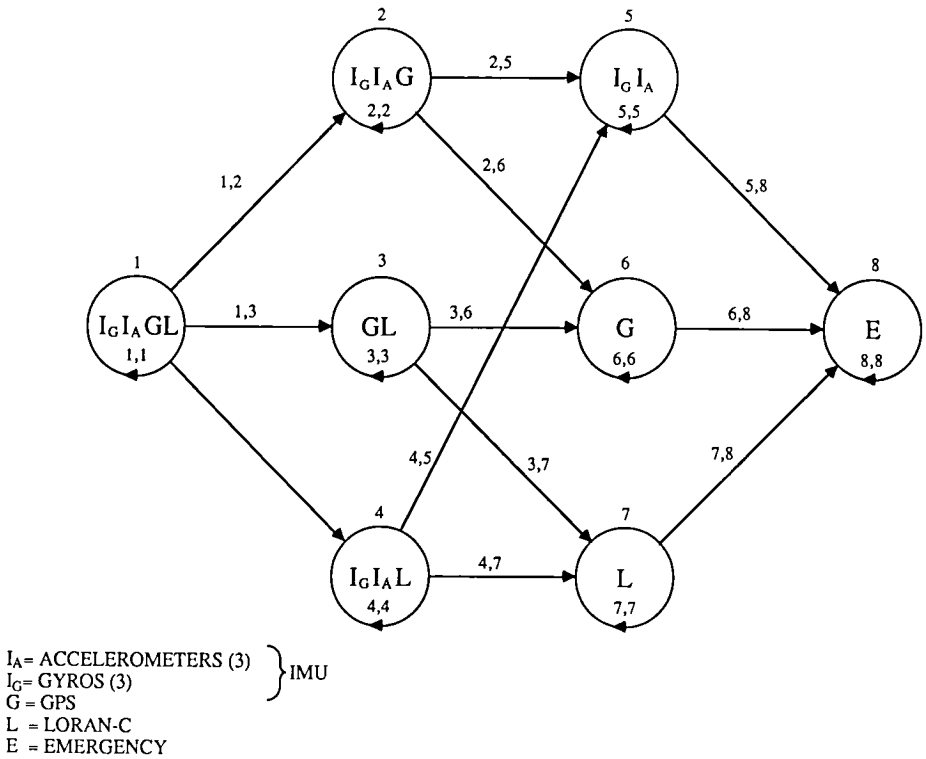

Figure 5. Reduced Markov model for the reliability analysis of an integrated navigation system based on GPS, Loran-C, and an inertial measurement unit.

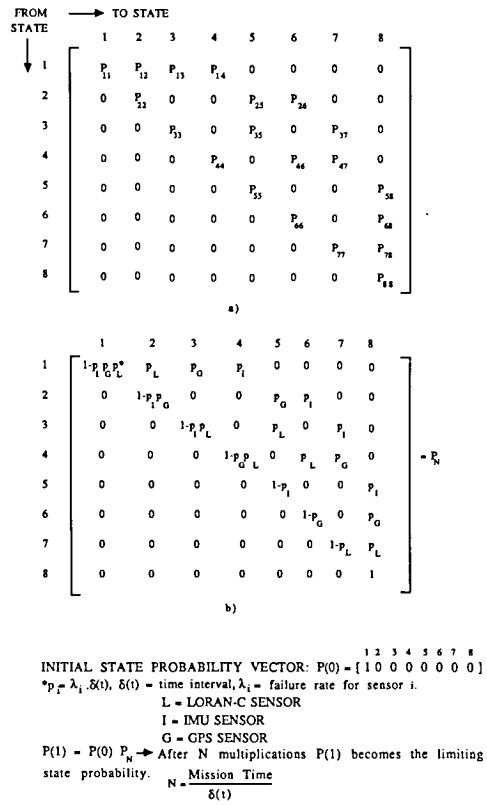

Figure 6. State transition matrix and reliability equations for the integrated navigation system.

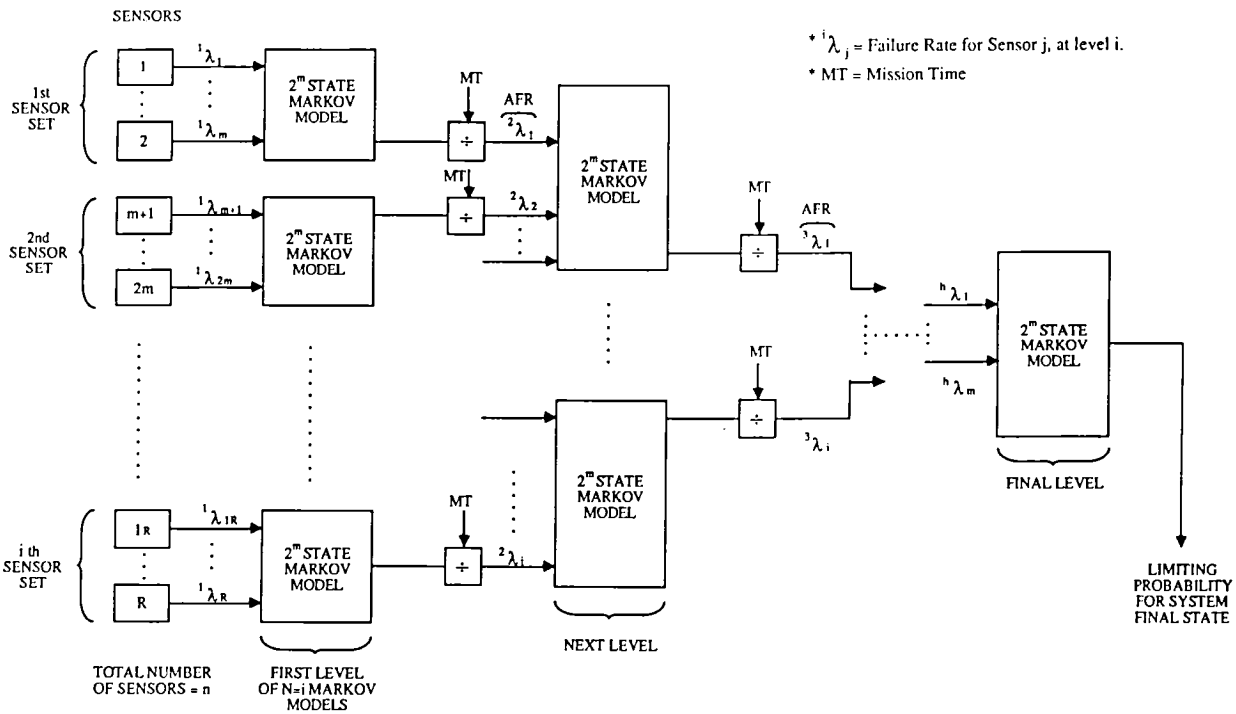

Figure 7. Functional block diagram representation of the Discrete Markov Chain Compression Method (DMCCM).

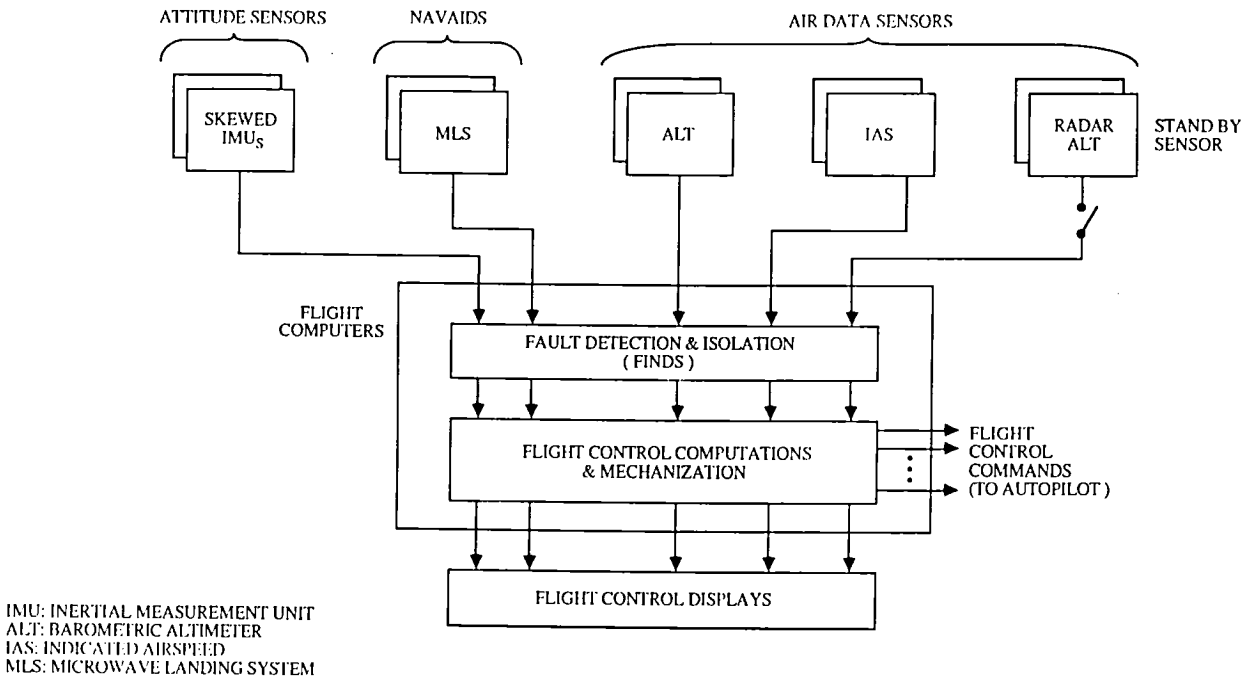

Figure 8. Multisensor flight control baseline system mechanization for terminal area guidance.

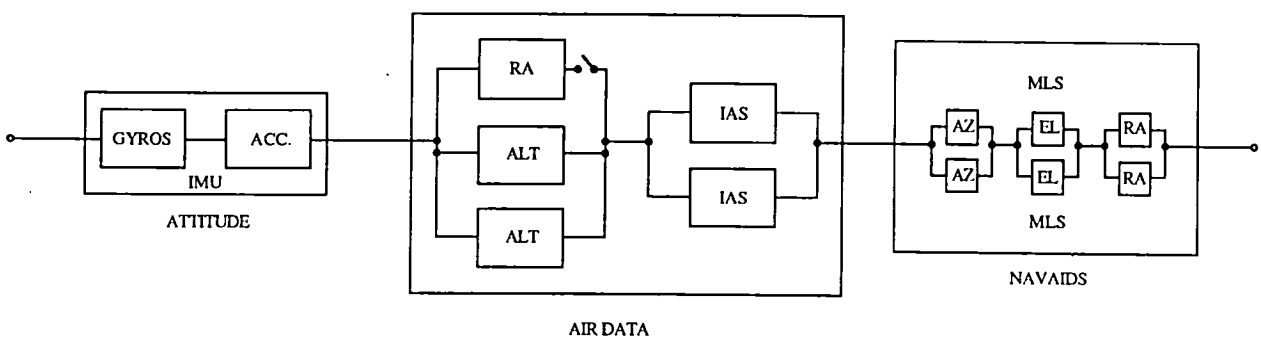

IMU: INERTIAL MEASUREMENT UNIT
ACC: ACCELEROMETERS
ALT: BAROMETRIC ALTIMETER
RA: RADAR ALTIMETER
IAS: INDICATED AIRSPEED
MLS: MICROWAVE LANDING SYSTEM

Figure 9. Reliability diagram for the multisensor flight control system.

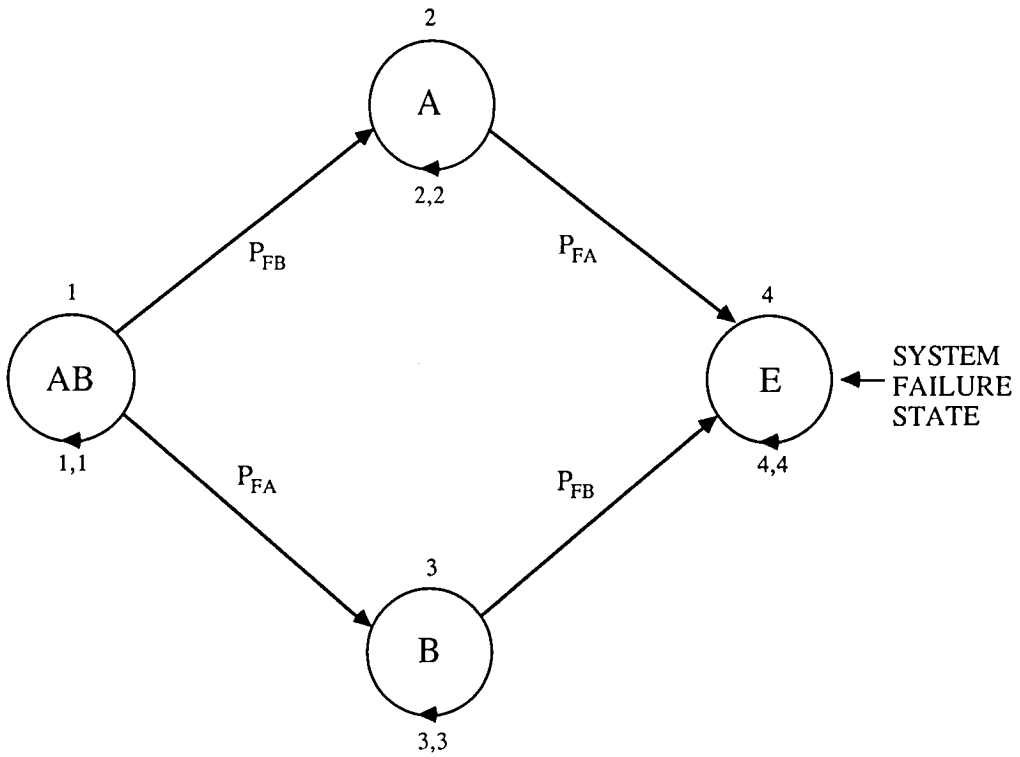

Figure 10. A two-sensor Markov model without fault detection and isolation.

P_{FA} = PROB. OF FAILURE FOR SENSOR A
P_D = PROB. OF DETECTION
P_I = PROB. OF ISOLATION
P_{DAM} = PROB. OF DAMAGE
P_{FAL} = PROB. OF FALSE ALARM
P_{TR} = PROB. OF TRANSIENT RECOVERY

$^{D}i_{F}$ = SENSOR i FAILED BUT WAS NOT DETECTED

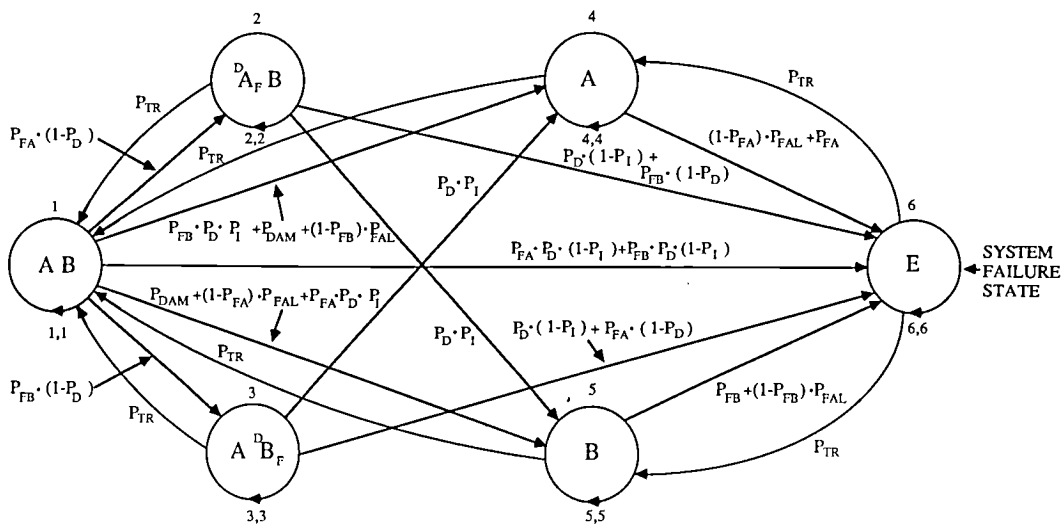

Figure 11. A two-sensor Markov model with fault detection and isolation including probabilities of failure detection, isolation, transient recovery, false alarm, and damage.

PRINCETON UNIVERSITY

INVESTIGATION OF AIR TRANSPORTATION TECHNOLOGY AT PRINCETON UNIVERSITY, 1986

Robert F. Stengel
Department of Mechanical and Aerospace Engineering
Princeton University
Princeton, New Jersey

SUMMARY OF RESEARCH

The Air Transportation Technology Program at Princeton University, a program emphasizing graduate and undergraduate student research, proceeded along four avenues during the past year:

- Guidance and Control Strategies for Penetration of Microbursts and Wind Shear
- Application of Artificial Intelligence in Flight Control Systems
- Computer-Aided Control System Design
- Effects of Control Saturation on Closed-Loop Stability and Response of Open-Loop-Unstable Aircraft

Areas of investigation relate to guidance and control of commercial transports as well as general aviation aircraft. Interaction between the flight crew and automatic systems is a subject of principal concern.

Recently, it has become apparent that severe downdrafts and resulting high velocity outflows present a significant hazard to aircraft on takeoff and final approach. This condition is called a microburst, and while it often is associated with thunderstorm activity, it also can occur in the vicinity of dissipating convective clouds that produce no rainfall at ground level. Microburst encounter is a rare but extremely dangerous phenomenon that accounts for one or two air carrier accidents and numerous general aviation accidents each year (on average). Conditions are such that an aircraft's performance envelope may be inadequate for safe penetration unless optimal control strategies are known and applied.

While a number of simulation studies have been directed at the problem, there are varied opinions in the flying community regarding the best piloting procedures, and optimal control strategies have only recently been defined. Graduate student Mark Psiaki has undertaken a study of guidance and control strategies for penetration of microbursts when encounter is unavoidable. His initial work shows that simple control laws could greatly reduce an aircraft's response to wind shear. Although the response mechanism is the same, jet transport and general aviation aircraft behave somewhat differently in microbursts; the larger, heavier aircraft are more adversely affected by variations in the

horizontal wind, while the smaller, lighter aircraft have greater difficulty with the downdraft. Our emphasis has shifted to the determination of optimal control strategies for the microburst encounter [1]. The study has begun with the computation of optimal control histories using steepest-descent and second-order gradient algorithms. An envelope of safe flight has been determined for typical jet transport and general aviation aircraft: these results will be documented shortly in Mr. Psiaki's doctoral thesis and in technical papers.

Attention is now being directed at optimal closed-loop control laws for wind shear encounter that could be executed in "real time." [2]. Graduate student Amit Joshi is working in this area. In addition, he will be developing a real-time fixed-based cockpit simulation as an adjunct to this research.

Undetected system failures and/or inadequately defined recovery procedures have contributed to numerous air carrier incidents and accidents. The infamous DC-10 accident at Chicago's O'Hare Airport, in which loss of an engine pod, subsequent loss of subsystems, and asymmetric wing stall led to disaster, provides a prototype for the kind of tragedy that could be averted by intelligent flight control systems. (An intelligent control system is one that uses artificial intelligence concepts, e.g., an expert systems program, to improve performance and fault tolerance.) Although many methods of modern control theory are applicable, the scope of the problem is such that none of the existing theories provides a complete and practical solution to the problem. At the same time, heuristic logic may be applicable, but it has yet to be stated in satisfactory format.

Graduate student David Handelman is developing a knowledge-based reconfigurable flight control system that will be implemented with the Pascal programming language using parallel microprocessors. This expert system could be considered a prototype for a fault-tolerant control system that could be constructed using existing hardware. The knowledge-based flight control system is specified initially and tested using the LISP programming language. When desired logic is determined, the corresponding Pascal code is generated automatically. Details of knowledge base development, expert system logic, and initial evaluations are contained in Ref. 3.

In a parallel effort, graduate student Chien Huang is using LISP to investigate the utility of a string-oriented, recursive logical system in the same role. A principal distinction between this and the previous approach is that flight control code will be modified in response to control system failures. As an adjunct to automatic restructuring of the control system, a tool for computer-aided control system design is being developed. The Control Equation Parser allows conventional state-space expressions to be translated to LISP code, and it executes complex design functions such as the solution of Riccati equations by

calling subroutines written in numerically efficient computer languages such as FORTRAN or Pascal [4].

Maintenance of flight control systems between flights also is a knowledge-intensive task, so it is likely that expert systems can be useful aids to aircraft mechanics. Senior Christopher Loh demonstrated the possibility of translating conventional maintenance and operations manuals for the hydraulic system of a tandem-rotor helicopter into an expert system using LISP [5]. The prototype expert system contains over 250 rules and 150 parameters in a MYCIN-like format, yet it describes only a fraction of the information contained in the manuals.

Whereas most expert system development tools are deductive, requiring the system designer to specify rules to be executed by a computer, inductive knowledge acquisition tools that generate rules from specified scenarios may be more useful in many applications. For example, a skilled pilot might well be able to explain what he or she would do in a given emergency, yet not recognize the rule structure that the actions represent. Graduate student Brenda Belkin has documented an exercise (performed under separate contract) in which an inductive tool was used to define procedures for an in-flight emergency [6].

One of the virtues of highly reliable electronic flight control systems is that an aircraft's stability and response, i.e., its closed-loop flying qualities, can be tailored to the pilot's needs. For reasons of performance and maneuverability, it may be desirable to design the aircraft so that its natural (unaugmented) modes of motion are unstable, with the understanding that the flight control system will provide the necessary stability by deflecting control surfaces to counter potentially divergent motions. Because control surfaces have limitations on their displacements and rates of travel, stability can be restored only within a bounded region about the trim point. If the aircraft's motions exceed the boundaries, the available control forces and moments will not be sufficient to prevent divergence.

Graduate student Prakash Shrivastava developed methods for determining the stability boundaries and control response for systems containing control saturation, and in the process, he was awarded the Ph.D. degree [7]. Analysis was carried out using state-space plots, in which saturation boundaries were represented by straight lines, stability boundaries were seen to be unstable limit cycles or straight lines, stable trajectories approach equilibrium points, and unstable trajectories diverge to infinity. The analysis pertained to systems containing unequal saturation boundaries, as well as those with multiple saturating controls.

In addition, a technical paper describing work completed in earlier years was published during 1986. Reference 8, which summarizes, in part, the Ph.D. research of Aharon Bar-Gill, describes the results of flight experiments to determine the effects of aircraft dynamic characteristics on flying qualities during single-pilot instrument flight.

The FAA/NASA grant supporting student research in air transportation technology has inestimable value in helping educate a new generation of engineers for the aerospace industry, and it is producing research results that are relevant to the continued excellence of aeronautical development in this country.

ANNOTATED BIBLIOGRAPHY OF 1986 PUBLICATIONS

1. Psiaki, M.L., and Stengel, R.F., "Optimal Flight Paths Through Microburst Wind Profiles", AIAA Journal of Aircraft, Vol. 23, No. 8, Aug 1986, pp. 629-635.

The problem of safe microburst wind shear encounter during the approach and climb-out flight phases was addressed using flight path optimization. The purpose was to investigate the physical limits of safe penetration and to determine control strategies that take full advantage of those limits. Optimal trajectories for both jet transport and general aviation aircraft were computed for encounters with idealized and actual microburst profiles. The results demonstrate that limits to control system design rather than to the aircraft's physical performance may be the deciding factor in an aircraft's capability for safe passage through a wide class of microbursts. The best control strategies responded to airspeed loss in an unconventional manner: by raising the nose to maintain lift.

2. Stengel, R.F., "Optimal Control Laws for Microburst Encounter," in Proceedings of the 15th Congress of the International Council of the Aeronautical Sciences, Paper No. ICAS-86-5.6.3, London, Sept 1986, pp. 870-878.

Simplified structures for longitudinal control laws that reduce an aircraft's response to the strong head-tailwind variations associated with microbursts are presented. They are based on non-zero-set-point linear-quadratic regulators that command throttle setting and angle of attack as functions of velocity and flight path angle, and they can incorporate direct measurements of the wind profile if available. Selection of cost functions to be minimized by feedback control has been aided by a prior study of classical control laws and exact nonlinear-optimal flight paths through realistic microburst wind profiles. The resulting optimal control laws have an adaptive, dual-mode structure that can be implemented either in flight-director logic or in an autopilot.

3. Handelman, D.A., and Stengel, R.F., "A Theory for Fault-Tolerant Flight Control Combining Expert System and Analytical Redundancy Concepts," in Proceedings of the 1986 AIAA Guidance, Navigation, and Control Conference, Williamsburg, AIAA Paper No. 86-2092-CP, Aug 1986, pp. 375-384.

This paper presents a theory for rule-based fault-tolerant flight control. The objective is to define methods for designing control systems capable of accommodating a wide range of aircraft failures, including sensor, control, and structural failures. A software architecture is described that integrates quantitative

analytical redundancy techniques and heuristic expert system concepts for the purpose of in-flight, real-time fault tolerance. The resultant controller uses a rule-based expert systems approach to transform the problem of failure accommodation task scheduling and selection into a problem of search. Control system performance under sensor and control failures is demonstrated using linear discrete-time deterministic simulations of a tandem-rotor helicopter's dynamics. It is found that the rule-based control theory can be used to enhance existing redundancy management systems. This approach to control system design also provides inherent parallelism for computational speed, smooth integration of algorithmic and heuristic computation, a search-based decision-making mechanism, straightforward system organization and debugging, and an incremental growth capability.

4. Huang, C.Y., and Stengel, R.F., "A Symbolic Parser for Control Equations," in Proceedings of the Institute of Measurement and Control 2nd Workshop on Computer-Aided Control System Design, Salford, England, July 1986, pp. 7-14.

A computer program for symbolic compilation and numerical simulation of control system design equations has been developed. The Control Equation Parser translates expressions written in standard state-space format into the LISP computer language for evaluation. Vectors and matrices are easily defined, and common operations of linear algebra are readily executed using this program. Numerical solutions can be obtained by executing LISP code or, as in the case of control calculations, by calling FORTRAN subroutines. In combination with a LISP workstation, the program provides a highly interactive tool for assisting in the design of multivariable control systems.

5. Loh, C.T., "A Prototype Maintenance Expert System for the CH-47 Flight Control Hydraulic System," Princeton Univerasity Technical Report No. MAE-1751, Apr 1986.

An investigation of the use of artificial intelligence techniques in the maintenance of hydraulic flight control systems was undertaken. A knowledge-based expert system employing situation-action rules (production systems) for diagnosing failures and subsequently identifying faulty devices was developed. The expert system's "inference engine" performs a backward-chaining process via a goal-driven control strategy. Its strategy involves finding rules that demonstrate a given hypothesis, then verify the facts used by the rule. The resulting LISP program, which emulates a small fraction of the procedures contained in maintenance and operations manuals for the CH-47 helicopter, contains over 250 rules for setting over 150 parameters.

6. Belkin, Brenda L., "A Demonstration Expert System for Implementing Emergency Procedures in a High-Performance Fighter Aircraft," Princeton University Report No. MAE-1749, Apr 1986.

A demonstration expert system was developed using a knowledge acquisition tool to simulate the operation of an electronic pilot's assistant. The task selected was the implementation of in-flight emergency procedures for a fighter aircraft. Two modes require the computer to help with routine flight tasks. Two others require the computer to plan and execute procedures for aircraft control autonomously, for instances in which the pilot is incapacitated or is subjected to high workload.

7. Shrivastava, P.C., "Stability Regions of Relaxed Static Stability Aircraft Under Control Saturation Constraints," Princeton University Report No. MAE-1747-T (Ph.D. Thesis), Oct 1986.

General characteristics of closed-loop stability regions for open-loop-unstable linear systems with bounded controls were determined. The shapes and sizes of stability regions were shown to depend on the types of singularities associated with system dynamics, feedback gains, control saturation limits, and command inputs. Analytical expressions were derived in normal-mode coordinates for the stability boundaries. Longitudinal static instability of the aircraft normally forces a single system root to become unstable, creating a saddle-point singularity, while directional static instability results in two unstable (real) roots with a focal point singularity. Stability regions can be characterized as hypercylinders in the state space surrounding the commanded closed-loop equilibrium point. Non-zero command inputs create asymmetry in the saturation effects, usually resulting in a net shrinkage of the stable region. Displacement saturation and rate saturation produce distinct effects, and a combination of the two can be particularly restrictive.

8. Bar-Gill, A., and Stengel, R.F., "Longitudinal Flying Qualities Criteria for Single-Pilot Instrument Flight Operations," AIAA Journal of Aircraft, Vol. 23, No. 2, Feb 1986, pp. 111-117.

Experiments to determine the flying qualities of more than a dozen dynamic configurations were conducted using the variable-stability Avionics Research Aircraft. Particular attention was paid to variations in long-period longitudinal characteristics and their effects on the performance of simulated IFR flights from takeoff through landing. Lift slope had the greatest effect on pilot opinion, workload, and tracking error. Bounds for satisfactory flying qualities were found for three parameters: phugoid mode damping, stick force gradient (with respect to trim airspeed), and pitch/airspeed gradient.

Wind Shear Guidance and Control Aircraft Applications of Machine Intelligence Fixed-Base Simulation

WIND SHEAR GUIDANCE and CONTROL

Classical Control System Design to Reduce Microburst Response

Flight-Path Optimization to Minimize Microburst Response

Linear-Quadratic Control System Design to Approximate Optimal Microburst Response

Significance of Control & Short-Period Lag

Application of Nonlinear Inverse Dynamics in Closed-Loop Control

AIRCRAFT APPLICATIONS of MACHINE INTELLIGENCE

Functions of a Knowledge-Based Control System

Fault-Tolerant Flight Control Systems

Real-Time Expert System Development

Signal Dependencies, Graphs and Frames

Computer-Aiding for the Pilot

Hydraulic System Failure Diagnosis

FIXED-BASE SIMULATION

Three Aircraft Simulations in Preparation:
Navion
Small Twin-Jet Transport
Twin-Jet Fighter/Attack Aircraft

Single-Person Crew Station

Computer-Generated "Out-the-Window" and Panel Displays

Silicon Graphics IRIS 3020 Workstation
(UNIX, 68020, Graphics Engine)
IBM PC-AT (PC-DOS, 80286/7)
3 - Multibus Single-Board Computers (80286/7)

"C" Programming Language

Verbex 4000 Voice Recognition System

Ethernet Connection to
Symbolics 3670 LISP Machine

RULE-BASED FAULT-TOLERANT FLIGHT CONTROL

Dave Handelman
Department of Mechanical and Aerospace Engineering
Princeton University
Princeton, New Jersey

APPLICATION VEHICLE: CH-47

Fault tolerance has always been a desirable characteristic of aircraft. The ability to withstand unexpected changes in aircraft configuration has a direct impact on the ability to complete a mission effectively and safely. The objective of this research was to investigate possible synergistic effects of combining techniques of modern control theory, statistical hypothesis testing, and artificial intelligence in the attempt to provide failure accommodation for aircraft. This effort has resulted in the definition of a theory for rule-based control and a system for development of such a rule-based controller. Although presented here in response to the goal of aircraft fault tolerance, the rule-based control technique is applicable to a wide range of complex control problems.

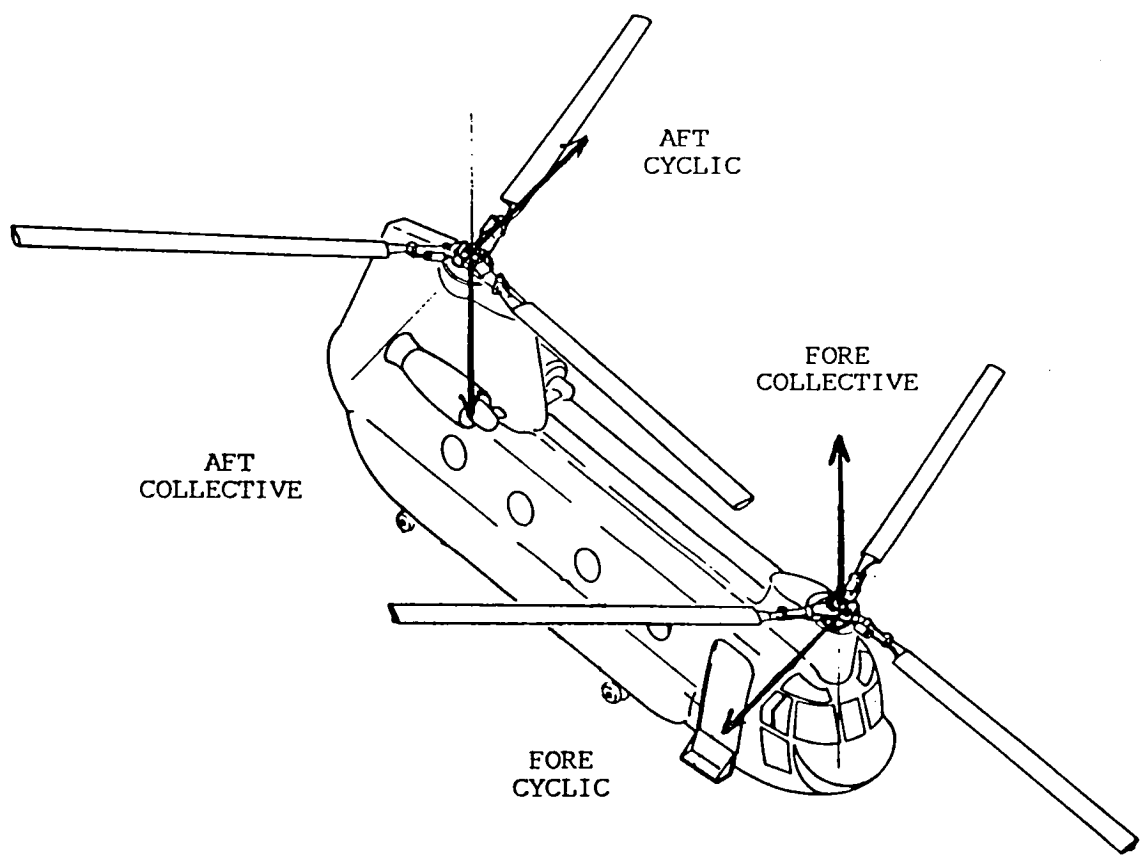

FAILURE MODES

The flight control system is expected to handle single abrupt and significant failures in aircraft sensors, controls, and structure. Biased, attenuated, and stuck sensors and controls, as well as structural failures in the form of center-of-gravity shifts, are to be detected, diagnosed, and accommodated automatically by the control system.

COMPONENT TYPE	ELEMENT	MODE
SENSOR	LONGITUDINAL VELOCITY	BIASED
	LATERAL VELOCITY	ATTENUATED
	VERTICAL VELOCITY	STUCK
	ROLL RATE	
	PITCH RATE	
	YAW RATE	
	PITCH ANGLE	
	ROLL ANGLE	
CONTROL	FORWARD CYCLIC PITCH	BIASED
	FORWARD COLLECTIVE PITCH	ATTENUATED
	AFT CYCLIC PITCH	STUCK
	AFT COLLECTIVE PITCH	
STRUCTURE	CENTER OF GRAVITY	SHIFTED

LINEAR MODEL OF AIRCRAFT DYNAMICS, ESTIMATOR, AND CONTROLLER
WITH FAILURE-MODEL VECTORS AND MATRICES

The fault-tolerant controller is designed to regulate aircraft motion about a constant flight condition. Assuming linearity within a neighborhood of this nominal operating point, a state-space mathematical model approximates the aircraft dynamics. Based on this no-failure model, a Kalman Filter is used for state estimation, and a Linear-Quadratic Regulator is used for feedback control calculations. A failure is assumed to change significantly the mathematical model representing the actual aircraft dynamics, prompting the need for estimator and regulator reconfiguration.

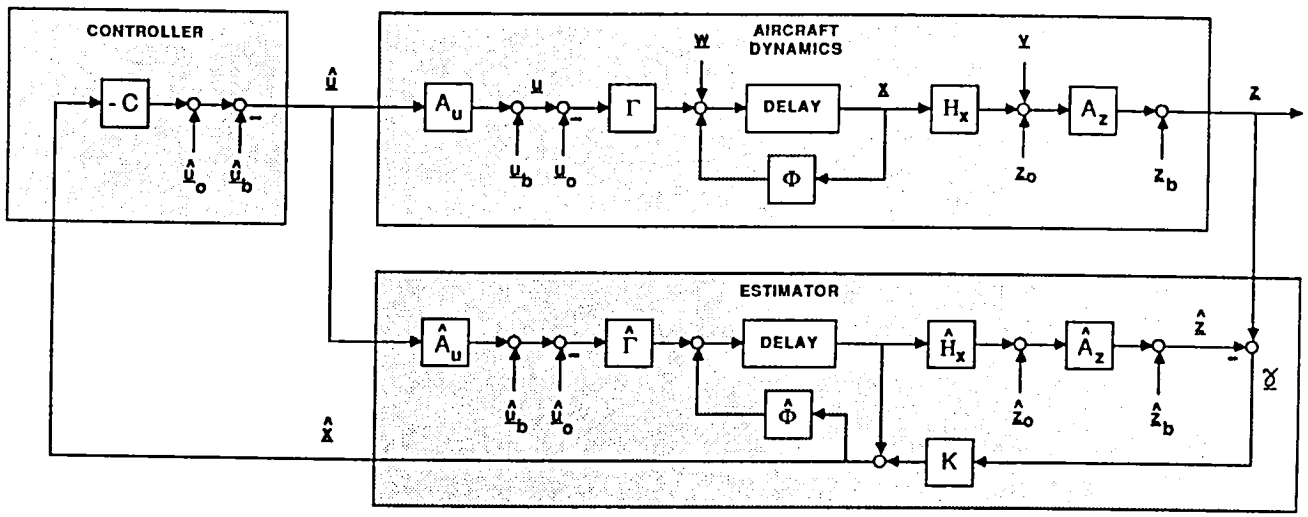

ORGANIZATION OF THE FAULT-TOLERANT FLIGHT CONTROL SYSTEM

The fault-tolerant flight controller breaks the overall job of failure accommodation into five main tasks. The executive control task provides continual dynamic state estimation, feedback control calculations, and synchronization of the remaining tasks. The failure detection task monitors aircraft behavior and detects significant abnormalities. The failure diagnosis task finds a set of probable causes and effects of the problem, while the failure model estimation task generates a mathematical model of the aircraft dynamics considered to reflect changes due to the failure. Finally, the reconfiguration task determines what action should be taken to correct the situation.

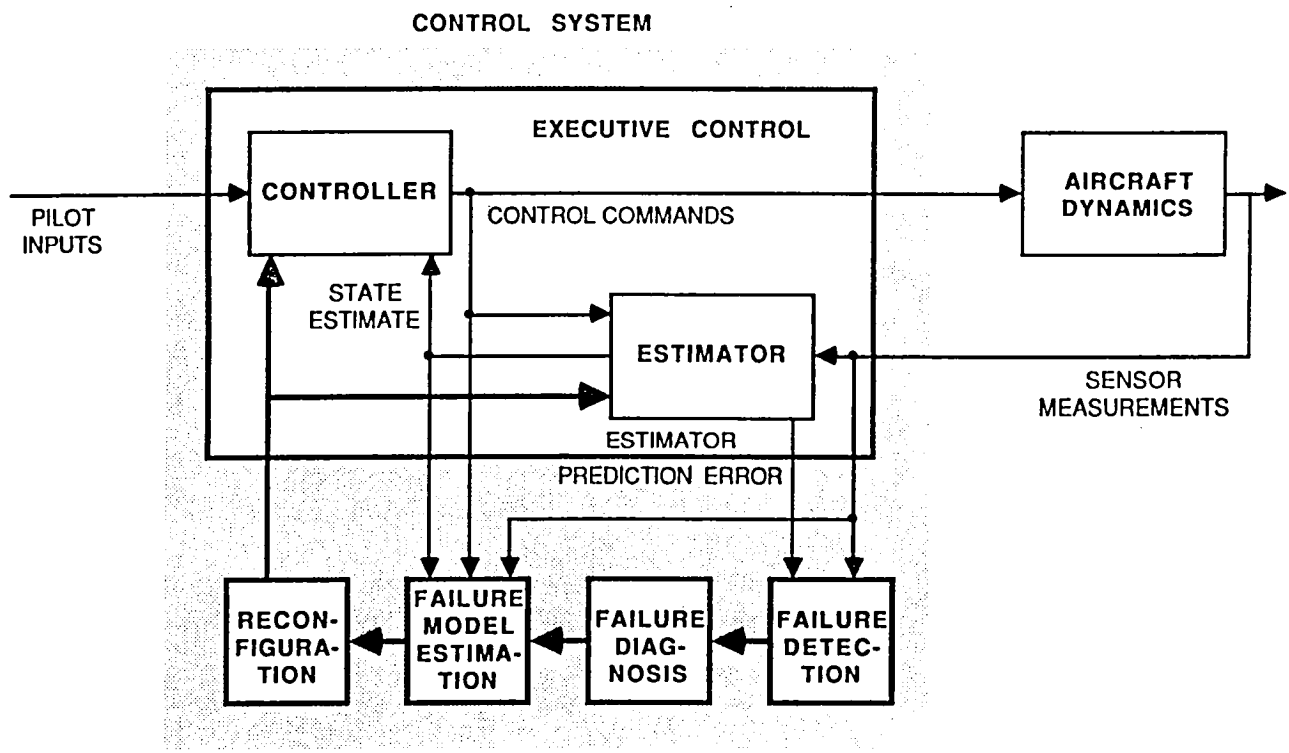

RULE-BASED CONTROL SYSTEM SOFTWARE ARCHITECTURE

The control system uses a rule-based search mechanism to perform control task scheduling and selection. Controller software development begins with the creation of a knowledge base for each task. Containing parameters, rules, and procedures, these knowledge bases perform intended task actions when properly searched. Tasks are grouped into processes, and each process knowledge base is translated automatically from LISP to Pascal. This code optimization, coupled with parallel processing, enables eventual real-time performance. The reduction of the overall control problem into tasks, followed by the grouping of tasks into processes, results in an organized hierarchical software structure resembling a set of cooperating expert systems using blackboard communications.

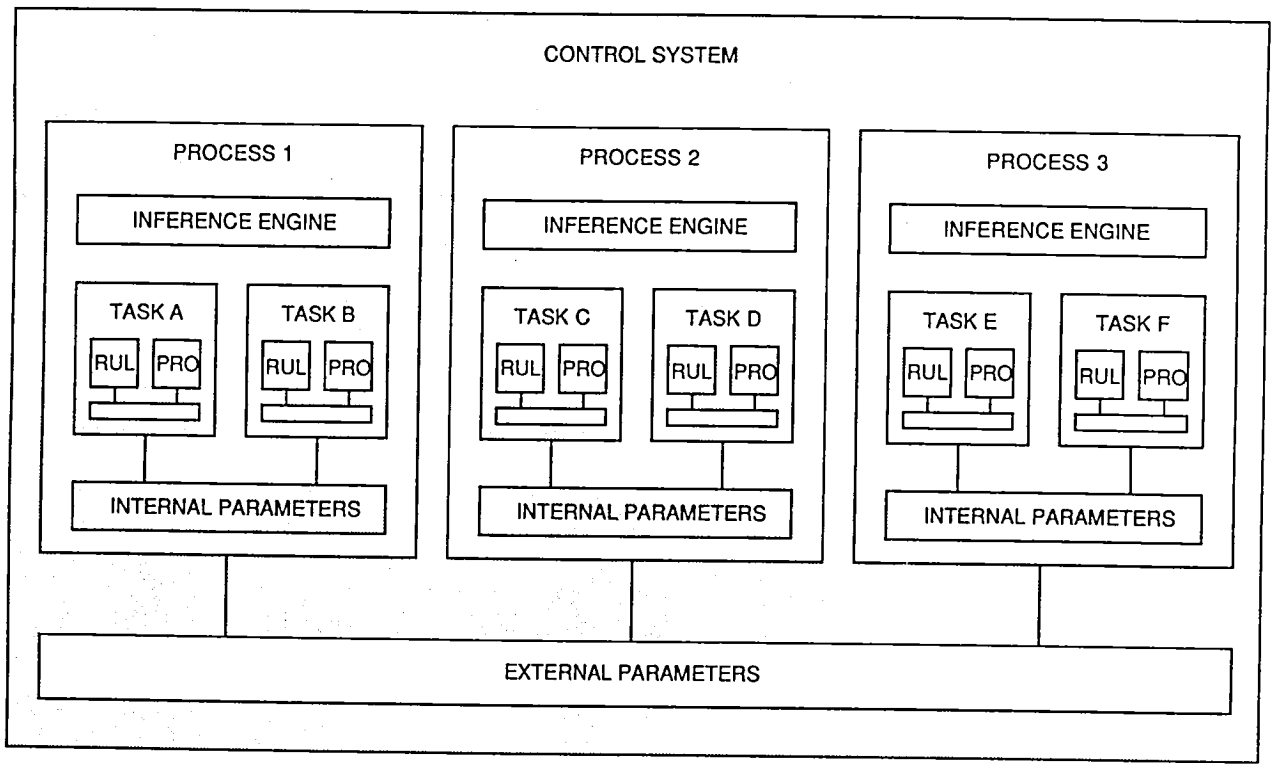

RULE-BASED FAULT-TOLERANT FLIGHT CONTROL SYSTEM SOFTWARE ARCHITECTURE

The fault-tolerant flight control system, presently capable of accommodating a significant bias or stuck failure in a sensor or control, implements the rule-based software architecture using 8 major tasks distributed among 3 processes. Each process contains a process control task responsible for intra-process task coordination and initialization. Process 1 contains the executive control task and a total of 19 parameters and 23 rules. Process 2 performs failure detection, failure model estimation, and reconfiguration using 51 parameters and 50 rules. Within process 3, 143 parameters and 247 rules perform failure diagnosis.

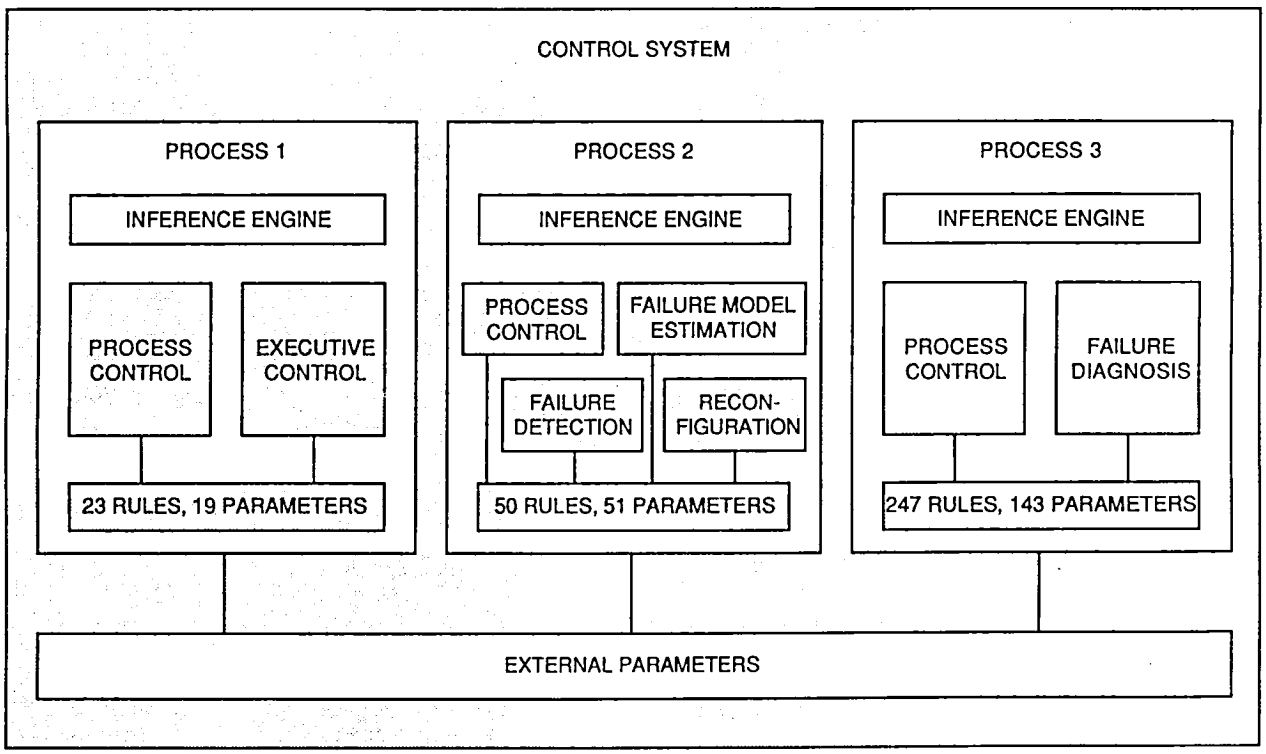

RULE-BASED CONTROL SYSTEM HARDWARE ARCHITECTURE

The controller is composed of single board computers embedded in a tightly coupled multi-microprocessor system. Each process is assigned to a processor, with inter-processor communications occurring through shared memory. During development, controller software is downloaded from a personal computer linked to the controller hardware through a memory-mapped bus interface.

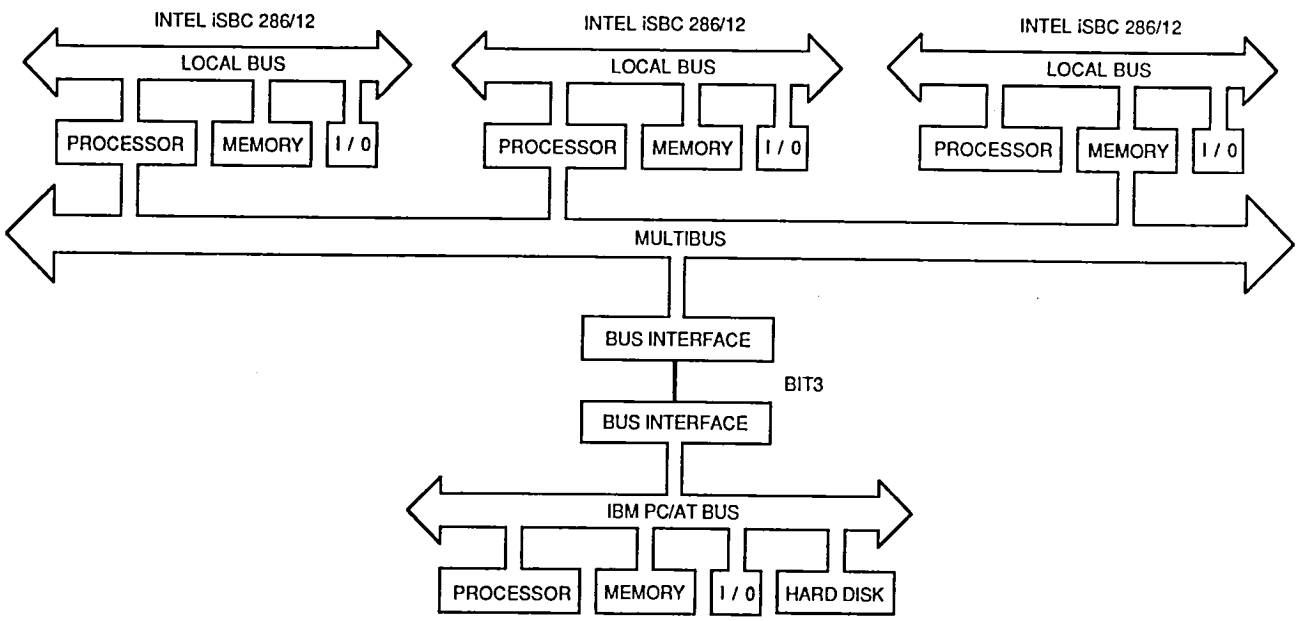

RULE-BASED FAULT-TOLERANT FLIGHT CONTROL SYSTEM
SEARCH EFFORT TIME HISTORIES

The rule-based control system uses search to schedule and select actions. During a search, rules are tested in the attempt to infer parameter values. The amount of effort expended by a control system processor during a search can be measured in an absolute sense by the total number of rules tested, and in a relative sense by the ratio of rules tested to parameters set. Performance measures such as search effort can be used to verify adequate balancing of work load between processors.

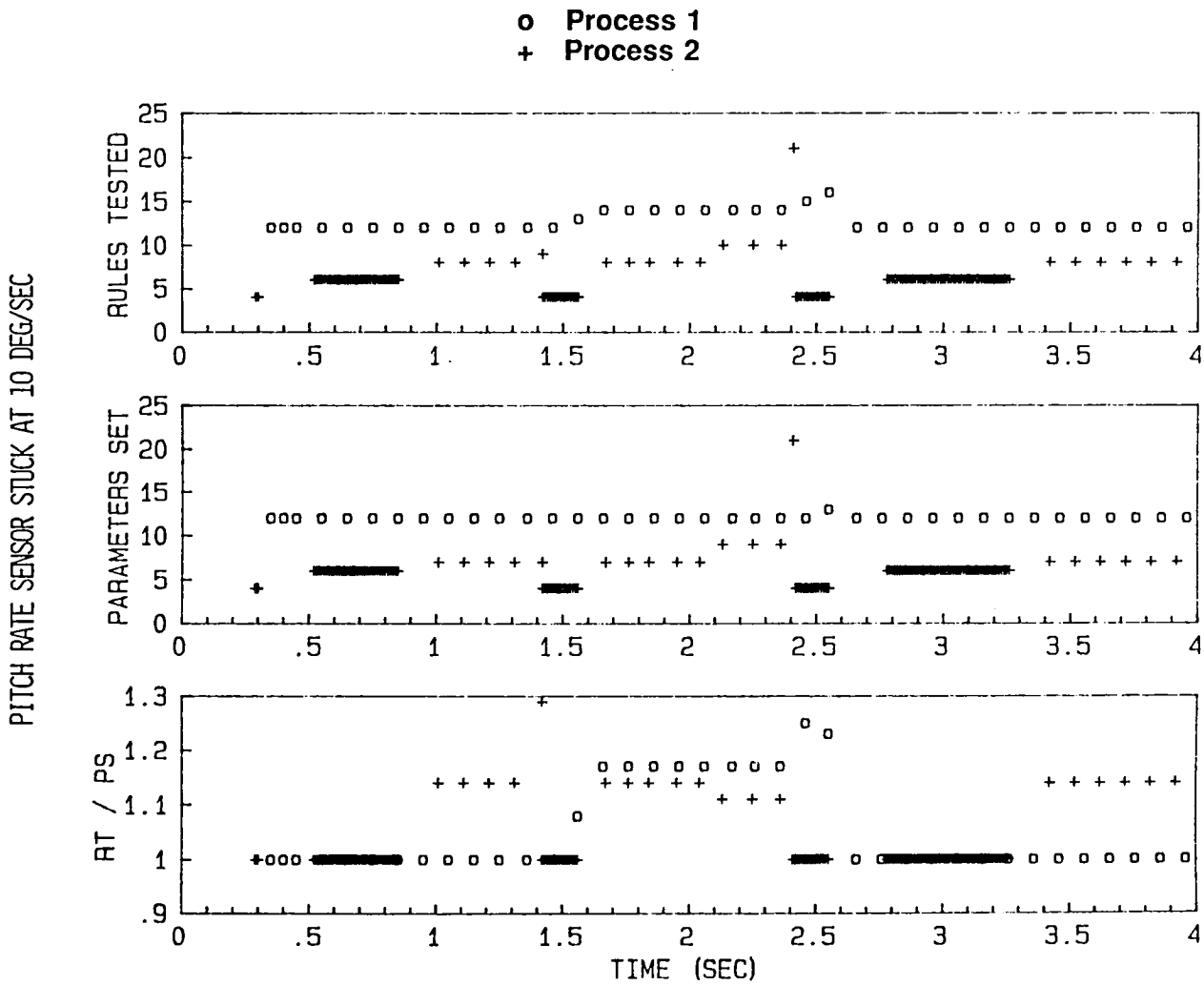

CONCLUSIONS

Based on experience gained through the design and implementation of a fault-tolerant flight control system, the proposed rule-based approach appears applicable to a large class of complex control problems. Its beneficial characteristics include a hierarchical system organization, high-level rule description, a search-based decision-making mechanism, smooth integration of numeric and symbolic computation, an incremental growth capability, inherent parallelism and automatic code optimization for real-time execution speed, simplified coordination of processor communications, simplified modification of code, and powerful debugging facilities. Additionally, the rule-based technique can deliver real-time performance using conventional, economical hardware.

- **RULE-BASED APPROACH FACILITATES COMPLEX CONTROL SYSTEM DESIGN**

- **REAL-TIME PERFORMANCE ACHIEVABLE USING CONVENTIONAL HARDWARE**

IT'S TIME TO REINVENT THE GENERAL AVIATION AIRPLANE

Robert Stengel
Princeton University

Current designs for general aviation airplanes have become obsolete, and avenues for major redesign must be considered. New designs should incorporate recent advances in electronics, aerodynamics, structures, materials, and propulsion. Future airplanes should be optimized to operate satisfactorily in a positive air traffic control environment, to afford safety and comfort for point-to-point transportation that is at least comparable to automotive travel, and to take advantage of automated manufacturing techniques and high production rates. These requirements have broad implications for airplane design and flying qualities, leading to a concept for the Modern Equipment General Aviation (MEGA) airplane. Synergistic improvements in design, production, and operation can provide a much-needed "fresh start" for the general aviation industry and the traveling public. Achieving these goals requires nothing less than the reinvention of the small airplane, providing new opportunities and requirements for research.

Although the term "general aviation" applies to a wide range of aircraft -- from single-engine, propeller-driven, single-seat planes to business jets -- the focus of this presentation is at the low end of the scale. Except as noted, a small four-place airplane is taken as a reference. Nevertheless, the proposed philosophy for new airplane design applies across the entire spectrum of general aviation.

IT'S TIME TO REINVENT THE GENERAL AVIATION AIRPLANE

Declining Practical Importance of Small General Aviation Airplanes

New Technologies for Airplane Systems

MEGA-Plane

Goals and Assumptions

Characteristics of a 4-Place MEGA-Plane

Opportunities for Research

DECLINING PRACTICAL IMPORTANCE OF SMALL GENERAL AVIATION AIRPLANES

For all practical purposes, the production of small general aviation (GA) airplanes in the United States has come to an end. The production rate for GA airplanes of all categories is about 1500 planes per year, less than 10 percent of what it was a decade ago. A thousand small GA airplanes were produced in 1986, but few of these were made by the manufacturers that formerly could be considered "The Big Three." Exports accounted for 30% of the US production; in the coming year, the General Aviation Manufacturers Association expects a comparable percentage of foreign imports, with a large concentration in the single-engine category. The average age of US small airplanes is 20 years old. The production of GA airplanes currently has minimal impact on the domestic economy. Although general aviation is said to be a $15 billion business, only $200 million of that can be attributed to the sale of small airplanes.

As fixed-base-operator income decreases, the idea of converting airfield real estate to condominiums and shopping centers becomes attractive, driving many small airports near major urban areas out of business. Small airports are losing the business of serious travelers, and an increasing number principally serve weekend pilots and flight schools. This trend is particularly detrimental to the national transportation system in view of the heavy congestion at most major airports, and it accelerates the decline in travel by GA airplane.

An ancillary point is that recent growth in commercial air travel has created a shortage of airline pilots. General aviation has long been a spawning ground for airline pilots, but it is not producing enough well-qualified pilots to meet the demand. One consequence is that relatively low-time pilots are flying in the right seats of many commercial aircraft cockpits.

Although important research continues in applicable technology areas such as stall/spin dynamics and aerodynamic flow control, neither the Federal Aviation Administration (FAA) nor the National Aeronautics and Space Administration (NASA) currently supports substantial research and development specifically directed at general aviation. If GA airplanes are no longer produced in the US or if GA flying must be perceived as the domain of the hobbyist and the well-to-do alone, it will be increasingly difficult to justify the expenditure of federal funds for its enhancement.

DECLINING PRACTICAL IMPORTANCE OF SMALL GENERAL AVIATION AIRPLANES

Large-Scale Production of Small Airplanes has Ended

GA Production Rates are Less Than 10% of What They Were a Decade Ago (about 1500 planes/yr)

Small Airplanes Production is Less Than a Thousand per Year

Three Major GA Manufacturers Currently Produce Few Small Airplanes

Small Airports are Closing

Neither FAA nor NASA has Any Substantial GA R&D Initiatives

REASONS FOR THE DECLINE

There are many reasons for the decline in production of small airplanes. While numerous evolutionary changes have been incorporated in GA airplanes, most examples trace their basic designs to the late 1940s, with technologies established a decade or more earlier. Manufacturers find certification costs higher than ever before, and production costs are in an unstable spiral as the number of produced aircraft decreases. Except in special cases, there is a large disparity between the cost of owning and using a GA airplane and the cost of traveling by competing modes. The GA airplane may well be cost-effective in a small-business setting, particularly where a large area must be covered quickly on a regular basis; lacking a business subsidy, few middle-income travelers consider GA transportation affordable.

GA manufacturers are being found liable for an increasing number of airplane accidents, and the cost of liability insurance or "self-insurance" has become a significant percentage of the total cost of each new airplane. This is a disincentive not only to the airplane producer but to the potential owner, who must pay the added costs. While gains have been made, the accident rate for GA aircraft still is substantially higher than that for competing modes. The hazard is comparable to motorcycle riding and somewhat greater than traveling by commercial aircraft, train, or automobile. Air traffic control procedures have become more complex with airline deregulation and increasing commercial air travel, and future GA travel is likely to be limited even more in view of productivity and fuel-use considerations. Flying an airplane in poor weather conditions demands a high level of IFR proficiency, something that relatively few GA pilots can achieve and maintain.

Finally, there is real confusion about the goals of general aviation. Should it be considered as a candidate mode for transporting large numbers of people? Should travel by small airplane be more like sailing to Bermuda or driving to Pittsburgh? Can general aviation have a major impact on the economy? Should particular classes of general aviation (e.g., air taxis and corporate aircraft vs. personally owned small planes) be singled out for special treatment? Without answers to these and similar questions, general aviation will decline even further.

REASONS FOR THE DECLINE

Slow Incorporation of New Technologies

High Costs of Certification, Production, and Operation

High Costs of Liability

High Accident Rates in Comparison to Other Modes of Transportation

Increasingly Complex Air Traffic Control Regulations

High Level of Piloting Proficiency Required for All-Weather Flying

Confusion About GA Goals

NEED FOR A RESURGENT GENERAL AVIATION INDUSTRY

General aviation provides unique capabilities for rapid point-to-point travel for small groups of people. It is complementary to the hub-to-hub and hub-spoke services of the major and feeder airlines. With area navigation and sufficient satellite airports, general aviation airplanes can be routed through under-utilized airspace, avoiding areas of congestion both in the air and on the ground. By diverting significant numbers of travelers from the public carriers, general aviation could actually reduce congestion in the terminal area. Just as automobile travel between two suburbs often is quicker, cheaper, and more efficient than public ground transportation into and out of a neighboring metropolis, general aviation offers a potentially attractive alternative for many trips between points not near large airports.

Improving reliability and safety are continuing issues in all modes of transportation. No matter what the current level, we always seek to lower the costs of operation, to simplify maintenance, to facilitate on-time performance, and to reduce the risks inherent in travel. In order for new GA airplanes to attract potential buyers, they must provide benefits in comparison to the competition -- used airplanes or new planes produced by other (possibly foreign) manufacturers.

The production of small airplanes could be a multi-billion-dollar business. The two most likely outcomes of not rebuilding the GA industry will be the *de facto* encouragement of foreign airframe and engine manufacturers to introduce their products to the US market and the loss of additional foreign markets for American products. Yet another business will be converted from a manufacturing to a service industry, with its attendant diminution of technical leadership and long-term economic security.

There is an opportunity -- if not an imperative -- to ask the question, "If we were unfettered by the need to adapt new technologies to old designs in piecemeal fashion, how would we design small airplanes?" Or put another way, "How would we invent the GA airplane to satisfy the needs of potential users while accounting for the realities of the National Airspace System and providing a reasonable incentive to prospective manufacturers to build such airplanes?"

NEED FOR A RESURGENT GENERAL AVIATION INDUSTRY

Transportation Requirements of the Public

Continuing Drive for Improved Reliability and Safety

Stimulation of Domestic Economy

Increasing Domestic Dependence on Foreign Suppliers

Lost Foreign Market Opportunities

NEW TECHNOLOGIES FOR GENERAL AVIATION AIRPLANE SYSTEMS

There is an exciting array of new technologies that, for the most part, have not been applied to the production of small airplanes. Some of them are listed here.

Electronics - In little more than a decade, the microprocessor has revolutionized many products and services, but it has done little for the GA airplane. It can provide the focal point for a host of major improvements. Together with concurrent advances in sensors, actuators, displays, and external systems, it can spearhead the drive for a new level of performance, reliability, and safety in GA production and operation. At the same time, flight-critical electronics introduce new concerns that must be addressed during design and operation, including guaranteed uninterupted power, lightning protection, mode switching, and complex control logic, all at a far lower cost than is normally associated with avionics equipment.

Modern Manufacturing Techniques - While it is unlikely that production rates would ever approach those of automobiles, much can be learned from advances being made in the automotive industry. Today's GA airplanes are essentially custom-made, deriving little benefit from common production-line concepts; however, modern manufacturing techniques emphasize flexibility, using computers, communication networks, and robotic devices (including numerically controlled machines) to perform a wide variety of functions from preliminary design to painting the end product. This flexibility is precisely what is needed in GA airplane production.

Structures and Materials - New materials not only promise direct benefits: they provide an opportunity for redesigning the basic airplane structure. Furthermore, modern objectives such as enhanced crash survivability and lightning protection can be combined with traditional design considerations like weight, air loads, and fatigue through the use of computational analysis. Composite materials offer strong and lightweight alternatives to aluminum components, although aluminum remains the cost-effective choice for most primary structures.

NEW TECHNOLOGIES FOR GENERAL AVIATION AIRPLANE SYSTEMS

Electronics

Microprocessors
Fiber Optics
Integrated Motion Sensors
High-Flux-Density Electric Motors
Electronic Displays
Weather Sensors
Precise Long-Range Navigation
Air Traffic Control Systems

Modern Manufacturing Techniques

Computer-Aided Design
Computer-Integrated Manufacturing
Robotics

Structures and Materials

Composites
Aluminum Alloys
Honeycomb
Integrated Structures

NEW TECHNOLOGIES FOR GENERAL AVIATION AIRPLANE SYSTEMS, continued

Aerodynamics - There is a widespread misconception that we have learned all we will ever know (or need to know) about subsonic aerodynamics. In fact, some rather dramatic breakthroughs have been made in recent years, and it is likely that there is much more to come. While seemingly redundant, three controllable horizontal surfaces for lift, stability, and control (canard, wing, and tail) provide a number of advantages, including reduced wing size, optimization of cruise condition to reduce trim drag, and stall/spin protection. Control surfaces need not be coupled mechanically as in the past; hence, there is a high level of redundancy that can be put to good use in improved safety margins. It is now realized that a combination of modern surface finishing techniques and shape selection can provide natural laminar flow over large segments of wings and fairings, reducing drag and improving overall performance. New perspectives on wing design suggest that significant gains in lift/drag ratio can be realized by reshaping the planform, particularly in the vicinity of the tips, as well as the airfoil.

Propulsion - Great strides have been made in automobile engines, suggesting avenues for improving the reciprocating engines of small airplanes. Computer-controlled electronic ignition, improved combustion chambers, multiport valving, and turbocharging all could contribute to increased safety, reliability, and efficiency. The new engines could be designed to use automobile gasoline with no loss in performance or economy, solving one of the more pernicious problems of operating small planes today. Computational fluid dynamics, new perspectives on laminar flow control, and recent developments in propeller design for human-powered airplanes, the world-circling *Voyager*, and wind turbines all can further advance propulsive efficiency.

NEW TECHNOLOGIES, continued

Aerodynamics

Three-Surface Longitudinal Control
Control Surface Redundancy
Natural Laminar Flow
Planform and Wingtip Design

Propulsion

Automotive Ignition and Combustion Technology
Propeller Design

THE MODERN EQUIPMENT GENERAL AVIATION AIRPLANE
(MEGA-Plane)

The principal objective for the "reinvented" GA airplane is to provide a viable alternate form of transportation for a large number of air travelers, in much the same way that automobiles provide a desirable alternative to public ground transportation. The goal is not to redefine our notions of existing GA concepts but to redefine the GA concepts themselves, to make general aviation something that it is not today. The goal is to design a new breed of airplanes that really do make private flying a constructive segment of the National Transportation System through the use of modern technology and manufacturing techniques.

Starting over in the design of small airplanes will result in synergistic benefits that would otherwise be unattainable. In effect, the whole design process is "rubberized", identifying desirable attributes in one system, evaluating the impacts of these attributes on other systems, and redefining the latter accordingly. For example, if independent, reconfigurable control surfaces are desirable (which they are) but they require uninterrupted electrical power with extremely low mean failure rates (which they do), existing systems for power supply and distribution are unacceptable. A new standard for power system design is mandatory, and such a system will, no doubt, contain redundancies that are not currently considered necessary. There is good reason to believe that the redesign can be achieved, given modern technology and no predetermined requirement to interface with traditional elements. Furthermore, by designing for the production process and reasonable production rates, costs will be minimized.

It is essential to take bold steps in planning for what amounts to a major overhaul of the National Transportation System. Clearly, the impact of a large increase in small airplane traffic would be great, and without a comprehensive approach that considers not only production and distribution but operation within the confines of the National Airspace System, that impact would be calamitous. There is a lot of unused airspace that could be used safely and efficiently, with virtually no infringement on airline operations. "Back-of-the-envelope" calculations suggest that a million GA airplanes (about five times the current number) would produce a volumetric density that is on the order of one hundred million times smaller than ground traffic density. Still, this space is unusable without positive assurances that airplanes will not interfere with each other. Consequently, the reinvented GA airplane must have a degree of autonomy and compatibility with other airplanes that is not realized in current designs.

THE MODERN EQUIPMENT GENERAL AVIATION AIRPLANE
(MEGA-Plane)

Objective:
Fast, Reliable, Safe, Comfortable, Cheap Transportation for Large Population of Travelers

Synergistic Use of New Technologies

No Need for Compatibility with Old Technology
Design for Low-Cost Automated Manufacturing
All-Electric Control Actuation
Reciprocating Engine(s)

Planning for GA to Become a Major Component of the National Transportation System

Production Rate of 50,000 Airplanes/yr by 2000

Equilibrium GA Population of 1,000,000 Airplanes by 2015

The reinvented GA airplane should be as simple as possible, containing few clever-but-failure-prone mechanisms. It is, for example, preferable to forego the extra aerodynamic efficiency of an intricate flap deployment mechanism in favor of a simply hinged flap with a single rotational degree of freedom. The latter device is less likely to fail, is easy to fix when it does, and provides a backup roll control device. Systems should contain line-replaceable units that are comprehensive in function, individually reliable, easily understood, and easily replaced. Redundancy should be provided where single-string reliability is inadequate; however, as automatic redundancy management in modern flight control systems often grows to dominate software specifications, the airplane should be designed to allow the pilot to do as much redundancy management as possible. This means that failure modes should be forgiving, allowing time for human decision making. In a similar vein, the airplane's flying qualities must be good enough to allow a relatively inexperienced (or not current) pilot to maintain safe control in a wide range of flight conditions, including those that generate high workload in existing airplanes (weather, traffic, etc.).

The reinvented GA airplane must be specifically designed for ATC system compatibility, or else none of the suggested improvements can be realized. The area navigation system is as important as the wings and engine of this airplane. It must be integrated with sufficient communication links to allow positive control at all times, and it must provide the pilot with the same sorts of cues that road signs, maps, and traffic lights provide the automobile driver.

There is an important caveat: positive air traffic control may not have the same meaning with this airplane that it has for current airplanes; it may be much less restrictive than the current ATC system. In the future, positive control for small planes operating outside major terminal areas could be more like positive control for today's automobiles, consisting of the equivalent of traffic lights and limited-access highways, with automated up- and down-link of important information, e.g., airplane identifier, location, destination, approved routing, and so on. Furthermore, by adhering to more stringent design and operational requirements, the reinvented GA airplane could be allowed to have preferential departure, routing, and arrival assignments without degrading safety or airline scheduling.

MEGA-PLANE, continued

Simplified Design for Certification and Operation

Improved Inherent Safety, Reliability, and Maintainability
Forgiving Failure Modes
"Video Game" Flying Qualities

Design for Air Traffic Control System Compatibility

Operation Under Positive Control 100% of the Time
Fail-Safe Area Navigation
Preferential Priorities for MEGA-Planes

CONCEPT FOR A TYPICAL 4-PLACE MEGA-PLANE

To provide a tangible idea of what a MEGA-Plane might be, a concept for a 4-place, single-engine design is discussed. This figure is a sketch, not a detailed drawing; it presents a concept for a MEGA-Plane, not the MEGA-Plane. The configuration appears similar to existing airplanes, and most of its characteristics have been suggested separately in earlier work. The most obvious difference is the addition of a controllable canard surface in addition to a conventional horizontal tail. More subtle visual characteristics include a split rudder, a "T" tail, small wing area, swept wing tips, large window area, fixed gear, and a sizable storage compartment.

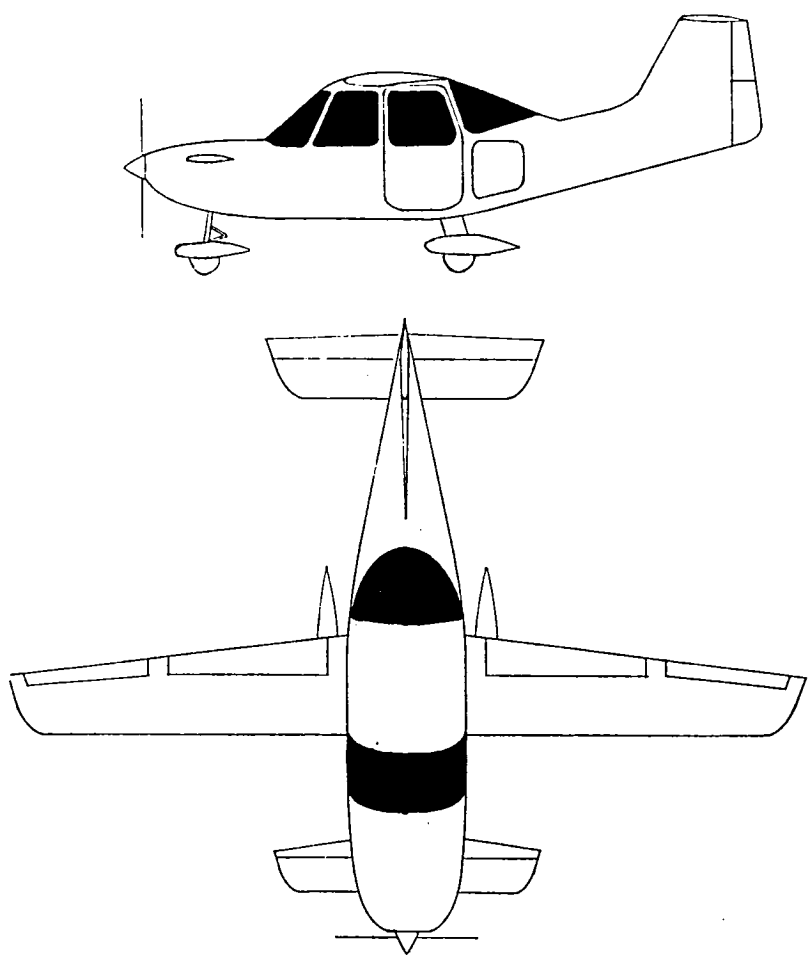

CONCEPT FOR A TYPICAL 4-PLACE MEGA-PLANE

AERODYNAMIC FEATURES

The principal control features of the airplane are its 3-surface longitudinal control, control redundancy, and simple flaps. Three-surface control provides a number of desirable attributes, including increased allowable center-of-gravity travel, pitch trim for minimum cruise drag, pitch control redundancy, and reduced wing area. (The latter comes about because the canard, unlike the rear tail, can provide positive angular rotation and positive lift for takeoff, eliminating the otherwise necessary download of the tailplane.) Because the canard control surfaces are immediately behind the propeller, they deflect the slipstream, providing strong forces and moments that can be used to reduce takeoff distance, to implement gust alleviation for improved ride qualities, and for stall/spin prevention (or recovery).

Each control surface is independent, i.e., not connected mechanically to any other surface; hence, there are 10 surfaces that can be used in numerous combinations to produce 3 forces and 3 moments for control. (Although not a primary requirement, it would be possible to produce side force for wings-level crosswind landings.) Consequently, ailerons could act like flaps and flaps like ailerons in the event of failure, within possibly reduced limits.

Recent flight research has shown that dramatic reductions in drag can be achieved by encouraging natural laminar flow over the airplane. Similarly, long-held notions of planform effects are being questioned; there is the possibility that swept tips and even more dramatic treatments such as sheared tips, crescent planforms, and serrated trailing edges may further reduce subsonic drag.

Although a redundant fly-by-wire/light control system is indicated, the MEGA-Plane should have inherent aerodynamic stability about all axes, allowing the "forgiving failure modes" mentioned earlier and eliminating the need for a stability augmentation system. (Closed-loop control may be desirable for a number of reasons; however, it should not be mandatory for safe flight.) While the airplane should never find itself in a spin, if it does enter the spin, it should have "honest" recovery characteristics, as implied by the unshadowed vertical tail and the full-length rudder.

CONCEPT FOR A TYPICAL 4-PLACE MEGA-PLANE

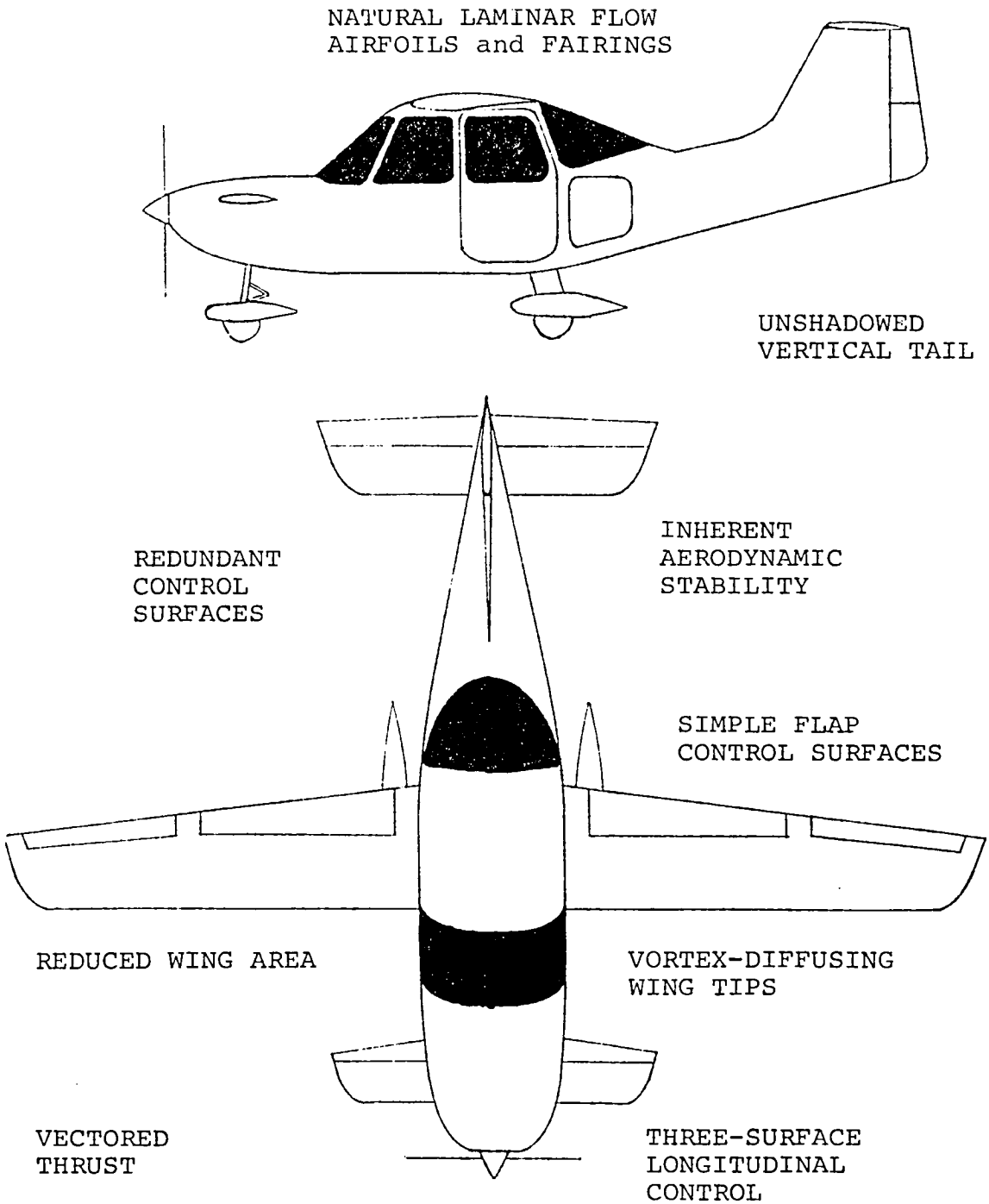

AERODYNAMIC FEATURES

CONCEPT FOR A TYPICAL 4-PLACE MEGA-PLANE

SYSTEM & STRUCTURAL FEATURES

The all-electric/fiber-optic control system provides redundant, direct commands and power to all control actuators with a reliability that is at least equivalent to current pushrod-and-cable systems. In overall use, control reliability would be considerably better than that of current mechanical systems because individual control surface failures will not have disasterous effects -- in fact, with one or two random failures, the changes in flying qualities would be barely discernable. Electric actuation is possible because the hinge moments for this small airplane need not be large. There would be considerable cost and reliability benefits from using identical actuators on all control surfaces. Fail-safe area navigation would be integrated with the flight control system; both systems would be aided by the use of solid-state motion sensors, as well as external navigation aids like LORAN. The integrated navigation, guidance, and control system would have artificial intelligence attributes as well as anti-wind shear/wake vortex features, which can be provided at minimal cost by existing microprocessors. Cockpit instruments also should be all electric, with a minimal complement of backup air-driven instruments to allow for display failure. Although the "see-and-avoid" approach to collision avoidance has been totally discredited over the years, optical aids that are visible in daylight should be mandatory.

While flight loads establish firm constraints, the airplane structure should be designed for inexpensive, automated fabrication and assembly. Common, "pre-fabricated" components should be used where appropriate, and major elements should be designed to minimize the need for labor-intensive operations. While much enthusiasm has been generated for composite materials lately, it is not clear that they present the minimum-cost solution to small airplane construction when labor and time costs are taken into account. There is a strong likelihood that large components would be made from aluminum, with small components and panels that can easily be molded into shape being made from composites.

For reasons mentioned earlier, advanced propulsion technology is warranted. With the increased importance of electrical power dictated by the control system, an auxiliary power unit and large batteries are appropriate. The APU should not only provide electrical power; it should be designed to support anti-icing capability for the primary aerodynamic surfaces.

CONCEPT FOR A TYPICAL 4-PLACE MEGA-PLANE

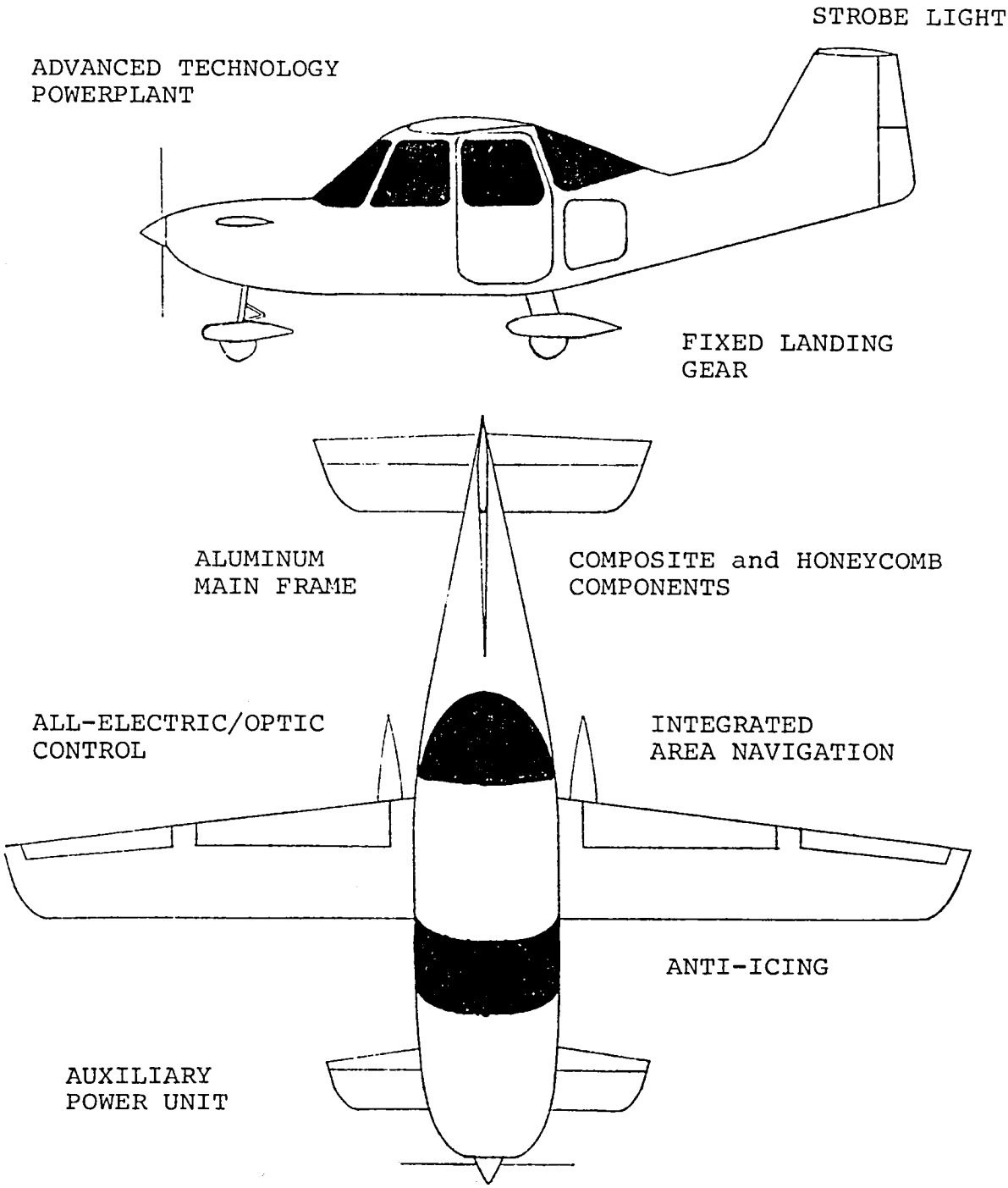

SYSTEM and STRUCTURAL FEATURES

CONCEPT FOR A TYPICAL 4-PLACE MEGA-PLANE

REDUNDANT CONTROL CHANNELS

Because the loss of control more often than once per some large number of flights (e.g., 10^9) is an unacceptable risk, it is likely that control system redundancy would be required. While the necessary level of redundancy is system-specific and should be the subject of intensive study, the sort of strategy that can be applied is suggested by this figure. The present objective is not to pre-design the system but merely to indicate that high reliability may be achievable in a fairly simple fashion.

There are two primary systems, each of which commands a different set of control surfaces and both of which operate in parallel in normal conditions. Both can command single units, such as the engine and auxiliary power unit, separately, and both accept the same pilot commands. In the event that either computer fails, a third computer (a "hot spare") would be brought on-line; in normal operation, the third computer would monitor the other two. If either primary string fails altogether, the other string can maintain control with the remaining control surfaces. The implication is that each string in a 2-string system must be individually quite reliable, with a mean-time-between-total-failures on the order of 40,000 hr (about $4\,1/2$ years of operation). Individual components could fail much more frequently; this large figure applies to all components in a single string failing simultaneously. Even in this case, the other 40,000-hr string would still be adequate to continue safe flight, and the spare computer would remain at the ready.

CONCEPT FOR A TYPICAL 4-PLACE MEGA-PLANE

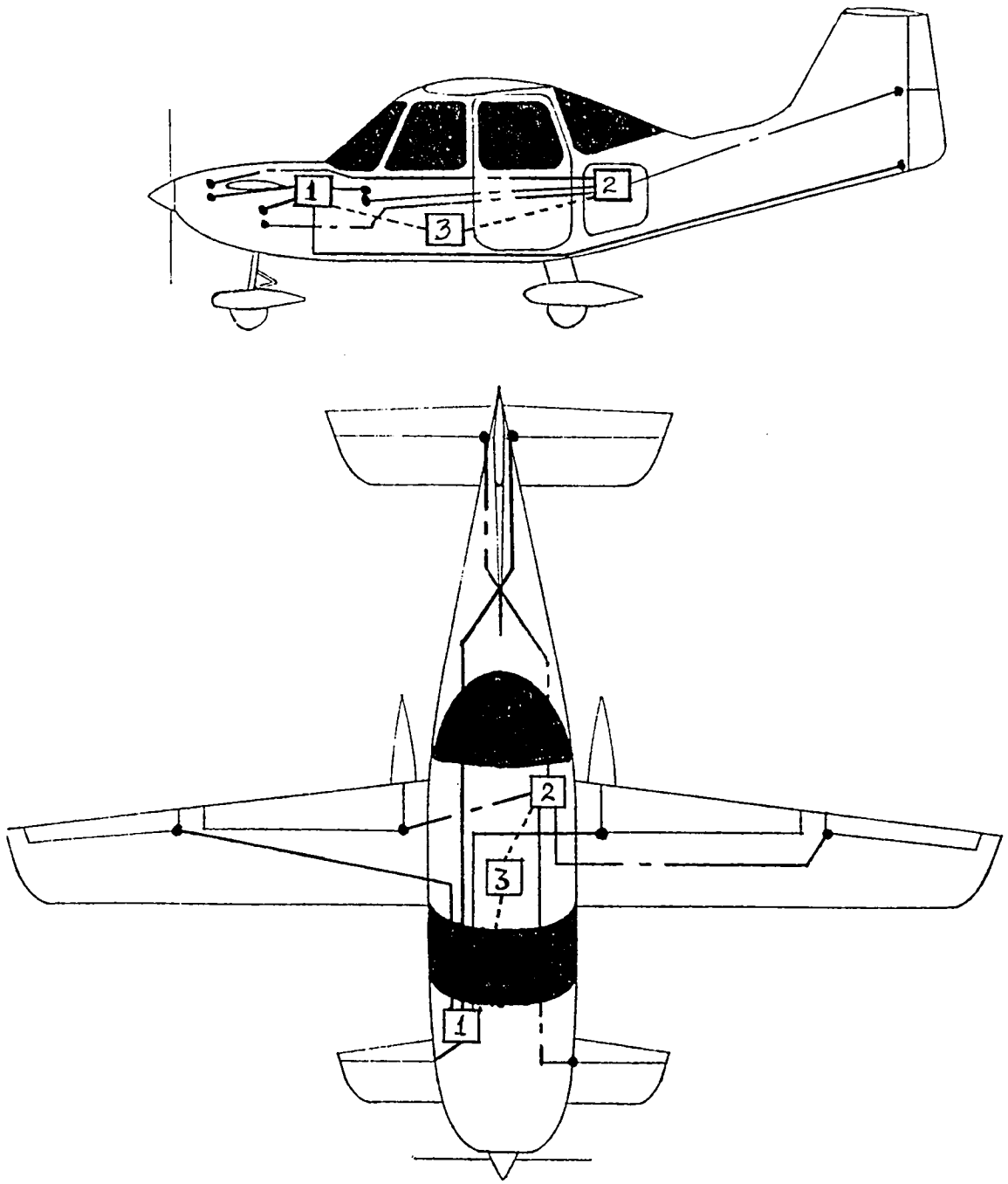

REDUNDANT CONTROL CHANNELS

OPPORTUNITIES FOR RESEARCH

Reinventing the small GA airplane is a systems problem, involving airplane design, human factors, and the air traffic control interface. This paper does not provide all the answers. It presents a concept and raises a challenge to the US aeronautical establishment, including government agencies, industry, and universities: conduct the research that is needed to make general aviation the vital contributor to economic, social, and transportation requirements that it can be.

Now in its fifteenth year, the FAA/NASA-sponsored Tri-University Program on Air Transportation Technology can play an important role in this research. Each of the participating universities -- Massachusetts Institute of Technology, Ohio University, and Princeton University -- provides unique perspectives and talents to be applied to the task. Together, we have demonstrated capabilities in literally all of the technologies that must be marshalled to produce this new generation of airplanes and the corresponding upgrade in the air traffic control system.

OPPORTUNITIES FOR RESEARCH

MEGA-Plane Development is a
Systems Problem, involving

Aircraft Design
Human Factors
Air Traffic Control Interface

Well-Defined Roles for FAA, NASA,
Industry, and University Participants

Candidate Focal Point for
Tri-University Program

FLIGHT PENETRATION OF WIND SHEAR : CONTROL STRATEGIES

AMIT S. JOSHI
PRINCETON UNIVERSITY

A Typical Microburst Encounter

Wind shear is a dangerous condition where there is a sharp change in the direction and magnitude of the wind velocity over a short distance or time.

This condition is especially dangerous to aircraft during landing and take off and can cause a sudden loss of lift and thereby height at a critical time.

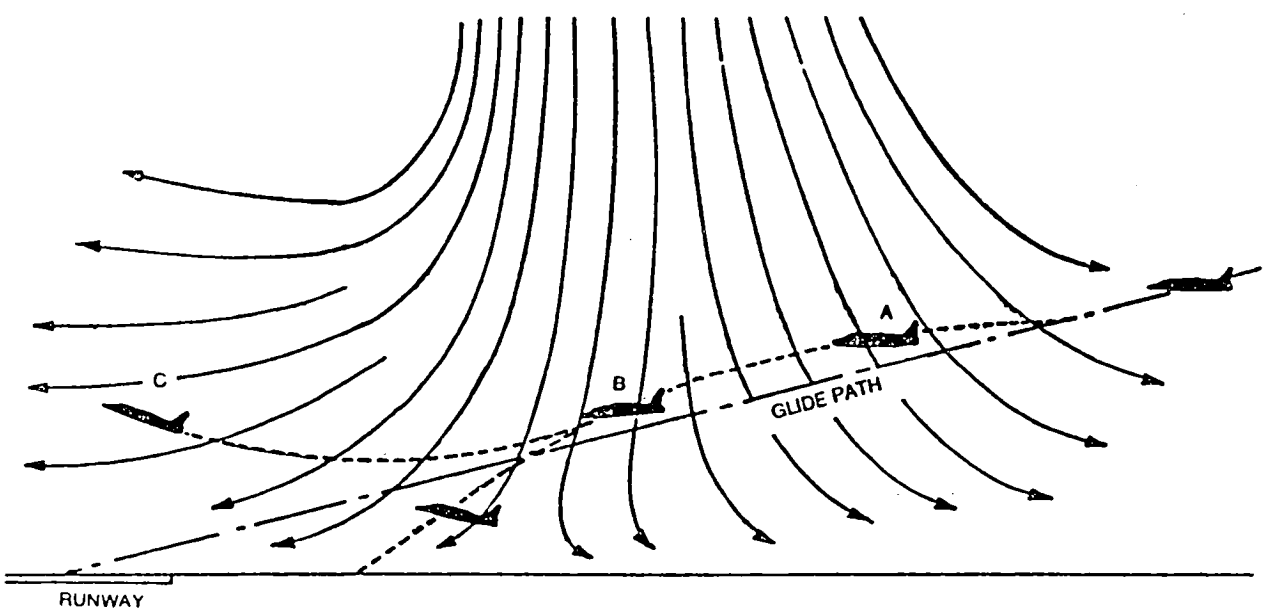

Problem Formulation

Wind shear is a condition of changing speed and/or direction of the wind rapidly over a short distance. A microburst is a special kind of a wind shear in which a downward blast of air hits the ground. Wind shears, especially microbursts, are very hazardous to aircraft manueuvering close to the ground. If unopposed by the pilot, there is a sudden gain in height and then an equally sudden loss in height which can lead to a crash. Microbursts have caused a number of crashes during take off and landing.

Wind Shear

A change in wind velocity in a brief time so as to cause a rapid change in the speed of the air flowing over the wing

Microburst

A downward blast of air which spreads on hitting the ground

Effects of Wind Shear

Loss in height and or position due to changes in lift causing severe hazard to the airplane

Problems

Could cause crashes during landing, take off or other maneuvers close to the ground

Linear Quadratic Regulator

An aircraft represents a nonlinear system; hence the general problem of its control is nonlinear. It is possible to linearize about the flight path to allow control strategies developed for linear systems to be applied. One approach is to use a Linear Quadratic Regulator, in which a control law that minimizes a quadratic cost function is found. Minimization leads to a linear state feedback strategy giving a stable closed-loop system.

x ==> states = { velocity flight-path-angle pitch-rate angle-of-attack
height thrust }

u ==> controls = { elevator throttle }

w ==> disturbances = { horizontal-wind vertical-wind }

Δ ( ) ==> perturbation about nominal

Q, M, R ==> cost weighting matrices

This approach hinges on choosing good cost weights. This is clear from the results. The choice can be difficult, and it is dependent on the aircraft; this is a major drawback of this method.

Given linear system

$$\Delta \dot{\underline{x}} = F \Delta \underline{x} + G \Delta \underline{u} + L \Delta \underline{w}$$

Define a " cost"

$$J = \frac{1}{2} \int_0^\infty [\Delta \underline{x}^T \; \Delta \underline{u}^T] \begin{bmatrix} Q & M \\ M^T & R \end{bmatrix} \begin{bmatrix} \Delta \underline{x} \\ \Delta \underline{u} \end{bmatrix} dt$$

Minimizing J leads to

$$\Delta \underline{u} = -R^{-1} (G^T S + M^T) \Delta \underline{x} = - C \Delta \underline{x}$$

Where S is the solution of the Riccati Equation

$$(F - GR^{-1}M^T)S + S(F - GR^{-1}M^T) - SGR^{-1}G^TS + Q - MR^{-1}M^T = 0$$

Variation of Cost Weights

The cost weights for the cost function were obtained by using a combination of state-rate and direct state and control weighting. No direct cross weighting between the states and the controls was used. The cost weights were varied by varying the direct cost weights on the controls.

A sinusoidal model of the microburst developed by Mark Psiaki was used.It had a maximum headwind/tailwind of 10.7 m/s and a maximum downdraft of 6 m/s.

State rate weighting used :

$$\begin{bmatrix} 100 & & & & & \\ & 10 & & & & \\ & & 10 & & & \\ & & & 1 & & \\ & & & & 100 & \\ & & & & & 1 \end{bmatrix}$$

Q0 (direct state cost weighting) = Identity

R0 (direct control weighting) =

$$\begin{bmatrix} 1000 & 0 \\ 0 & 10 \end{bmatrix} \qquad \begin{bmatrix} 10 & 0 \\ 0 & 10 \end{bmatrix} \qquad \begin{bmatrix} 10 & 0 \\ 0 & 1000 \end{bmatrix}$$

Microbursts :

Range : Headwind/tailwind begins 0 m and ends 3000 m

Strength : 10.7 m/s

Range : Downdraft begins 1050 m and ends 1950 m

Strength : 6 m/s

Gains with Varying Cost Weights

By varying the cost weight associated with the elevator, different gains were obtained for a Linear Quadratic Regulator. The aim of this figure is to show that different weights lead to very different control requirements.

Gains set #1 :

$$C = \begin{bmatrix} -3.407E\text{-}2 & -9.228 & -7.403 & -4.496 & -2.801E\text{-}2 & -8.644E\text{-}2 \\ 4.268E\text{-}1 & 3.260E+1 & 1.926E+1 & 1.299E+1 & 1.468E\text{-}2 & 1.983 \end{bmatrix}$$

Gains set #2 :

$$C = \begin{bmatrix} -1.662E\text{-}1 & -6.336E+1 & -2.581E+1 & -2.499E+1 & -3.081E\text{-}1 & -2.966E\text{-}1 \\ 3.372E\text{-}1 & 8.2 & 9.741E\text{-}1 & 1.104 & 7.082E\text{-}2 & 1.762 \end{bmatrix}$$

Gains set #3 :

$$C = \begin{bmatrix} -1.783E\text{-}1 & -6.367E+1 & -2.585E+1 & -2.503E+1 & -3.108E\text{-}1 & -3.309E\text{-}1 \\ 4.100E\text{-}2 & 6.429E\text{-}1 & 1.806E\text{-}3 & 8.513E\text{-}3 & 5.802E\text{-}3 & 3.414E\text{-}1 \end{bmatrix}$$

Effects of Cost Weighting

Variations on Altitude and Controls

Simulation results for a simplified model of a Boe727 (representing a typical jet aircraft) follow. All the simulations are for a take off condition. The nominal filght conditions are

Airspeed = 71.628 m / s		flight path angle = 0.0523 rad	
pitch rate = 0.0 rad / s		angle of attack = 0.0611 rad	
altitude = 3.0 m		thrust = 0.8713 * max thrust	
elevator = -0.0518 rad		throttle = 0.8713 * max thrust	

These conditions apply to all the simulation results. SI units are used on all the plots.

The altitude vs range plot shows the dramatic improvement due to the control law over the openloop performance. It also shows that a choice of high elevator cost weight leads to a poorer performance.

The difference between the throttle and the thrust plots is due to modelling of a lag between the generation of the thrust and the throttle command. The throttle vs range plot shows that as the cost weight of the throttle is increased, the throttle saturates later. The result is that the control activity of the elevator goes up. In general, though, the saturation of the throttle sooner or later means that the elevator is the main control remaining. This is seen from the similarity between all the elevator plots.

□ = open loop
▲ = gain set #2

Effects of Cost Weighting

Variations on Altitude and Controls

o = gain set #1
● = gain set #3

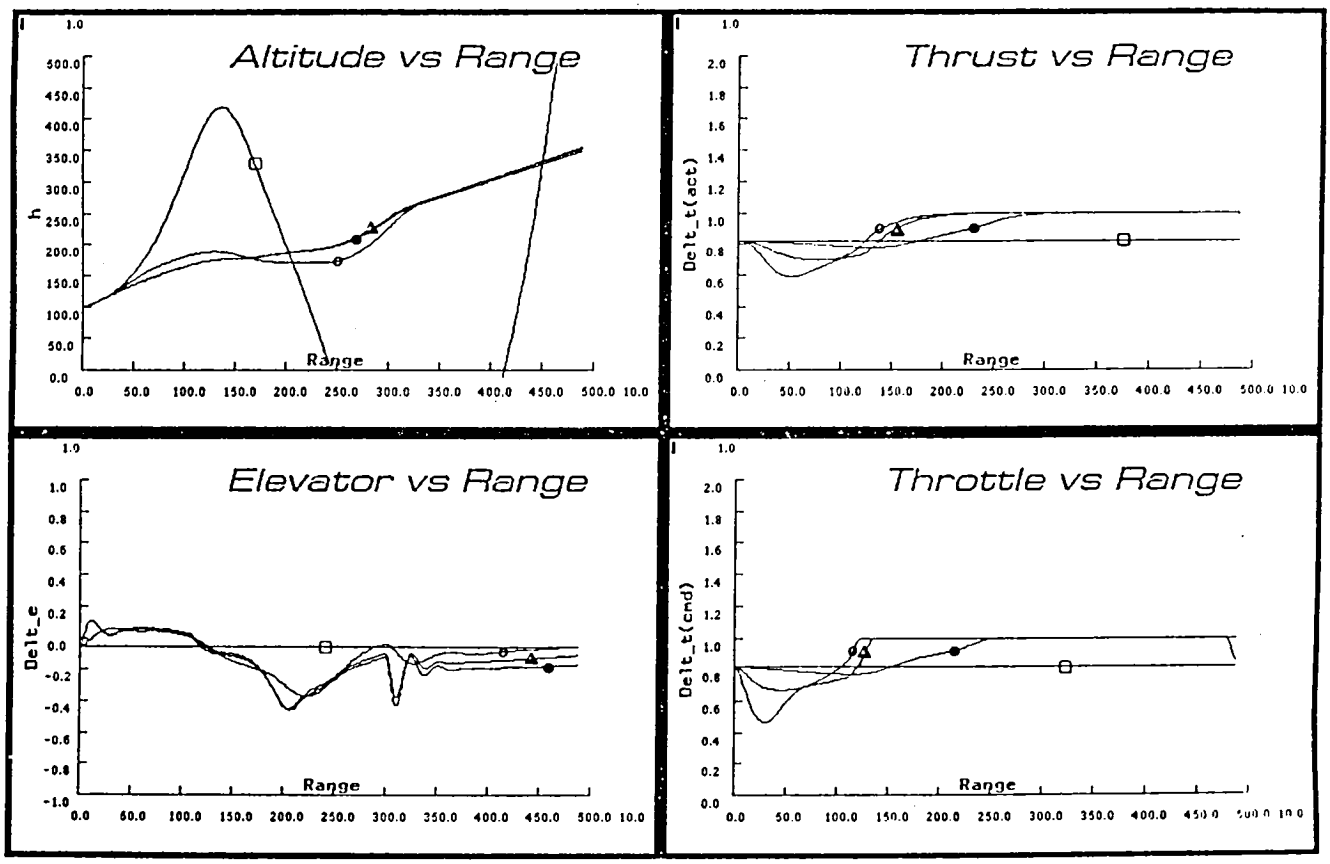

Effects of Cost Weights

Variations on Velocity and Angular Controls

These set of plots show the velocity, angle of attack (alpha), flight path angle (gamma), and the pitch rate as functions of the range. Again there is a dramatic improvement over the open-loop case. The flight path angle and velocity variations are reduced considerably, leading to the improvement in the altitude vs range seen earlier. The pitch rate and the angle of attack are affected much less. It can be seen that the angle of attack reaches quite high values.

□ = open loop
Δ = gain set #2

o = gain set #1
• = gain set #3

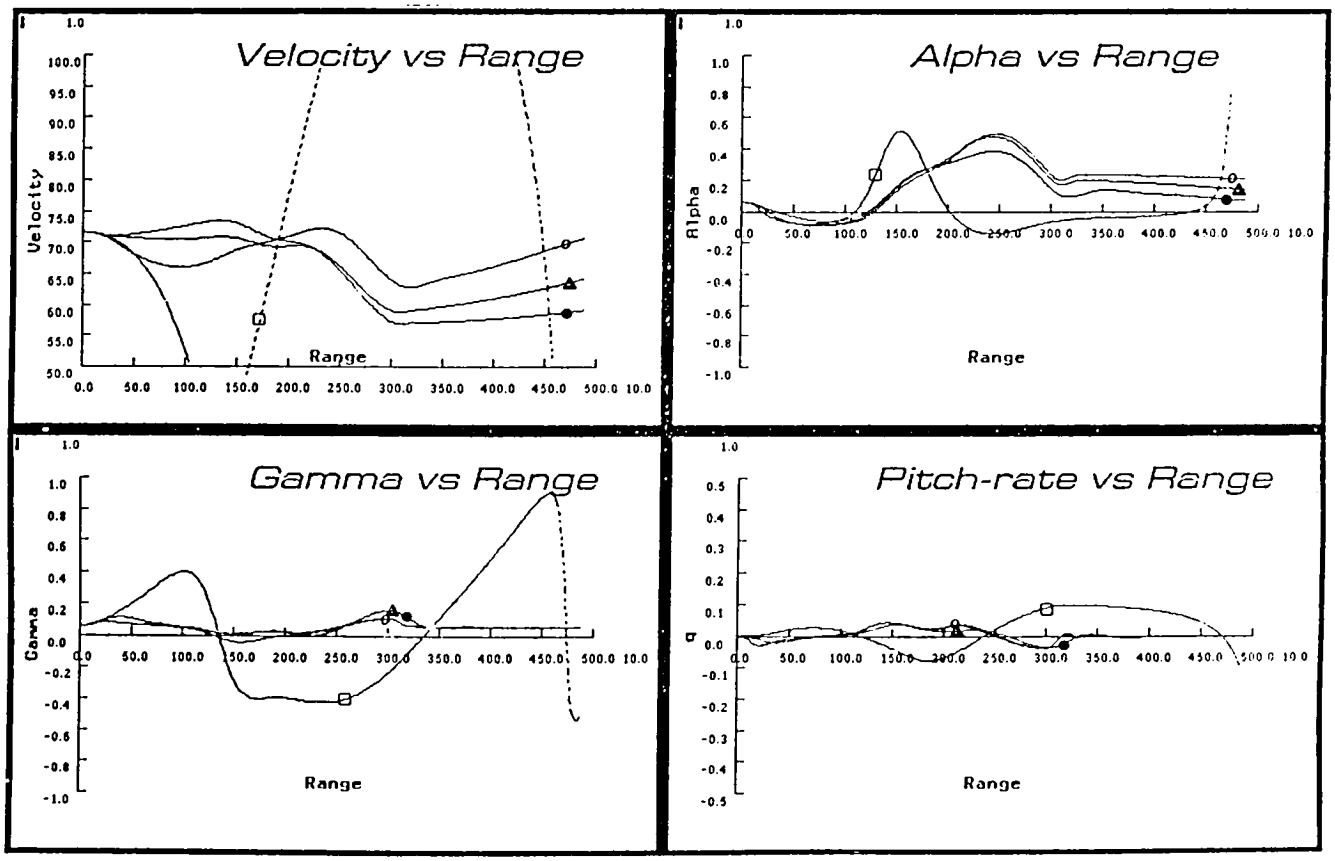

Nonlinear Inverse Dynamics

The aircraft is a nonlinear system, and we can tackle the nonlinear control problem directly using a nonlinear inverse dynamics (NID) approach.

In this approach we asume that we have a nonlinear system with $\underline{x}$, $\underline{u}$, $\underline{w}$ the states, controls, and the disturbances as for the LQR. Additionally we define an output $\underline{y}$ as linear combination of the states. Since an exact inverse of the nonlinear system cannot be found, we calculate an approximate one.

We differentiate the output 'd' times until some controls appear in each of the outputs. It is assumed that there is a function defining the desired output. Setting the derivatives of the output equal to those of the desired output gives us a set of nonlinear algebraic equations. When solved for the control with some simplifications, we get the set of controls giving the desired output behavior.

Given a nonlinear system

$$\dot{\underline{x}} = \underline{f}(\underline{x}, \underline{u}, \underline{w})$$

$$\underline{y} = C\underline{x}$$

Differentiate $\underline{y}$ 'd' times until the control appears in the output to get

$$\underline{y}^{[d]} = g(\underline{x}, \underline{v})$$

where $\underline{v}^T = (\underline{u}^T, \dot{\underline{u}}^T, \ddot{\underline{u}}^T, \dddot{\underline{u}}^T \cdots)$

Now let the desired output be $\underline{y}_{desired}$

Now set $\dot{\underline{u}} = \ddot{\underline{u}} = \ldots \underline{0}$ and solve

$$\underline{y}^{[d]} = g(\underline{x}, \underline{u}) = \underline{y}^{[d]}_{desired}$$

Nonlinear Inverse Dynamics

In the NID approach, we are free to choose either a functional form of the desired output or choose the d'th derivatives of the desired output and then specify a dynamics for the output.

Choosing $\underline{y}_{desired}$ we choose the desired dynamics for y

Alternatively choosing a dynamics for $\underline{y}^{[d]}_{desired}$ gives us the $\underline{y}^{[d]}$

Conclusions

* The results of the simulation show the effective performance of the LQR and the NID controllers. The major conclusions that one can draw from these results are

* The LQR seems to try to keep the variation in the velocity and the flight path angle to the minimum. This is obvious in hindsight when it is realized that these are the major factors controlling deviations from the desired flight trajectory.

* There is more variation in the angle of attack and the pitch rate from the nominal values.

* Thrust almost always saturates for the LQR type of control law and a reasonably large microburst. There is an initial reduction in the thrust as the aircraft enters the microburst ; then there is sharp increase until it saturates. Finally the thrust comes back to normal as the aircraft gets out of the region of the microburst.

* The elevator shows a very different behaviour. High cost weights associated with the elevator lead to lesser elevator use. However, with the thrust saturated, the elevator is effectively the only control and this shows in the elevator behaviour.

Linear Quadratic Regulators lead to a good performance with a good choice of costs.

LQR s can require very high feedback gains for a good performance.

Nonlinear Inverse Dynamics with complete solution of nonlinear equations promises to give excellent performance.
NID with complete solution of nonlinear equations would have the penalty of :

1) Time required
2) Possibility of none or multiple solutions.

ACRONYMS*

ARINC	Aeronautical Radio, Inc.
ASR	Automated speech recognition
ATC	Air traffic control
FLT	Flight Transportation Laboratory
GA	General aviation
GPS	Global positioning system
IFR	Instrument flight rules
IMU	Inertial measurement unit
INS	Inertial navigation system
IRT	Icing Research Tunnel
JUP	Joint University Program
LQR	Linear quadratic regulators
LWC	Liquid water content
MEGA	Modern equipment-general aviation
MVD	Median volume diameter
NEXRAD	Next-generation weather RADAR
NID	Nonlinear inverse dynamics
R-NAV	Random navigation
SNR	Signal-to-noise ratio
TD	Time delay

*Not previously defined in individual papers.

NASA
National Aeronautics and Space Administration

Report Documentation Page

1. Report No.	2. Government Accession No.	3. Recipient's Catalog No.
NASA CP-2502		

4. Title and Subtitle	5. Report Date
Joint University Program for Air Transportation Research - 1986	April 1988
	6. Performing Organization Code
7. Author(s)	8. Performing Organization Report No.
Frederick R. Morrell, Compiler	L-16406
	10. Work Unit No.
	505-66-01-50
9. Performing Organization Name and Address	11. Contract or Grant No.
NASA Langley Research Center Hampton, VA 23665-5225	
	13. Type of Report and Period Covered
12. Sponsoring Agency Name and Address	Conference Publication
National Aeronautics and Space Administration Washington, DC 20546-0001	14. Sponsoring Agency Code

15. Supplementary Notes

16. Abstract

This report summarizes the research conducted during 1986 under the NASA/FAA sponsored Joint University Program for Air Transportation Research. The material was presented at a meeting held at the NASA Langley Research Center, Hampton, Virginia, January 8-9, 1987. The Joint University Program is a coordinated set of three grants sponsored by NASA Langley Research Center and the Federal Aviation Administration, one each with the Massachusetts Institute of Technology, Ohio University, and Princeton University. Completed works, status reports, and bibliographies are presented for research topics, which include computer science, guidance and control theory and practice, aircraft performance, flight dynamics, and applied experimental psychology. An overview of the years activities is also presented.

17. Key Words (Suggested by Author(s))	18. Distribution Statement
Avionics Low-frequency terrestrial navigation Aircraft guidance navigation and control	Unclassified - Unlimited Subject Category 01

19. Security Classif. (of this report)	20. Security Classif. (of this page)	21. No. of pages	22. Price
Unclassified	Unclassified	122	A06

NASA FORM 1626 OCT 86

NASA-Langley, 1988

For sale by the National Technical Information Service, Springfield, Virginia 22161-2171

National Aeronautics and
Space Administration
Code NTT-4

Washington, D.C.
20546-0001

Official Business
Penalty for Private Use, $300

BULK RATE
POSTAGE & FEES PAID
NASA
Permit No. G-27

NASA

POSTMASTER: If Undeliverable (Section 158
Postal Manual) Do Not Return